Iranian Hydraulic Association

Shahid Chamran University of Ahvaz

Journal of
Hydraulic Structures

Scientific Professional Journal



January 2026
Volume 12, Issue 1

ISSN (Online): 2345-4156
https://jhs.scu.ac.ir/

Aims and Scope

Journal of Hydraulic Structures is an interdisciplinary journal which publishes high-quality peer-reviewed articles addressing the latest developments and applied methods in analysis and design, construction, maintenance, management, and operation policy of Hydraulic Structures.

The Journal aims at providing an efficient route to fast-track publication, within 10-12 weeks after manuscript submission.

The general areas covered by the Journal include:

- Advances in numerical and analytical methods applicable to hydraulic structures
- Hydro informatics and soft computing
- Hydraulic aspects of hydraulic structures
- Applied surface and subsurface hydrology and hydrometeorology
- Forecasting approaches in water resources engineering
- Economic and social aspects of hydraulic structures
- Uncertainty analysis and risk management in hydraulics and water resources engineering
- Application of Nanotechnology in hydraulic structures
- Geotechnics of hydraulic structures
- Damage detection techniques
- Technical and methodological advances in application, design/selection, production, construction materials of hydraulic structures.
- Application of Artificial Intelligence techniques in all aspects of hydraulic structures.

General Information:

Title: Journal of Hydraulic Structures

Publisher: Shahid Chamran University of Ahvaz

ISSN (Print): 2345-413X

ISSN (Online): 2345-4156

Website: https://jhs.scu.ac.ir/

Address: Faculty of Civil Engineering and Architecture, Shahid Chamran University of Ahvaz, Ahvaz, Iran

Email: jhs@scu.ac.ir

Journal of

Hydraulic Structures

Shahid Chamran University of Ahvaz

Director-in-Charge: Prof. Ali Haghighi

Editor-in-Chief: Prof. Hamid R. Ghafouri

Managing Editor: Dr. Amir H. Shafiee

Contents:

01

Investigation of discharge coefficient and energy dissipation in free-flowing Quarter-Circular Gates

Abbas Parsaie; AmirHamzeh Haghiabi

09

A Hybrid AHP-AI Framework for Assessing and Mitigating Tunneling Impacts on Confined Spring Discharge

Saeed Samiei; Ali Aalianvari

20

River Behavior and Morphological Analysis of a Meandering Channel in the Ganga River System, India

Kuldeep Pareta; Upasana Pareta

50

Effect of bed roughness shape on mitigating scour the downstream of parallel sluice gates

Iman Akbari; Mohammad Hemmati; Sung-Uk Choi; Yousef Ramezani; Babak Mahmoudi

69

Variation in Effluent Quality of Household Water Treatment Systems Over Time: A Case Study in Ahvaz

Hossein Sasani; Seyedeh Tooba Mirsalari; Mohammad Azizipour; Neematollah jaafarzadeh

84

Efficiency Improvement of Piano Key Weirs Using Numerical Simulation

Behnam Taheri; Ehsan Fadaei-Kermani; Mahnaz Ghaeini-Hessaroeyeh

Investigation of discharge coefficient and energy dissipation in free-flowing Quarter-Circular Gates

Abbas Parsaie [1], AmirHamzeh Haghiabi [2]

1. Faculty of Water and Environmental Engineering, Shahid Chamran University of Ahvaz, Ahvaz, Iran.
2. Department of Water Engineering, Lorestan University, Khorramabad, Iran.

***Corresponding Author:**
AmirHamzeh Haghiabi,

Email: haghiabi.a@lu.ac.ir
Received: 2025.04.16
Accepted: 2025.05.15
J. Hydraul. Struct., 2025; 12(1):1-8
DOI: 10.22055/jhs.2025.49153.1341

ABSTRACT

This study investigates the hydraulic performance of quarter-circular gates (QCGs) under free-flow conditions, with a focus on the discharge coefficient (Cd) and the energy dissipation rate (EDR). Results demonstrate that the C_d exhibits a logarithmic increase with the ratio of upstream flow depth to gate opening (y_1 / w), rising from approximately 0.9 to 1.1 as y_1 / w varies from 4 to 20, indicating that the gate's efficiency improves with increasing upstream flow depth. Notably, the C_d remains stable even when upstream load increases fivefold, reflecting the robustness of the QCG design. Additionally, the relationship between C_d and the ratio of flow depth to radius (y_1 / R) is nearly linear, with higher curvature and streamline compression resulting in increased C_d due to flow acceleration caused by geometric constraints. Regarding energy dissipation, the EDR ranges from 10% to 55%, growing logarithmically with $y1/w$ and being more pronounced with greater streamline curvature associated with larger y_1 / R ratios. Increased flow curvature causes more energy loss, so larger gate openings that reduce streamline compression consequently lower EDR. The findings reveal that despite increases in downstream loads, the QCG maintains high efficiency, with energy dissipation occurring at a diminishing rate. Compared to traditional sluice gates with sills, which typically have a discharge coefficient between 0.5 and 0.8, the QCG outperforms with coefficients ranging from 0.9 to 1.0. Overall, the results highlight the significance of geometric parameters, including gate opening, flow depth, and radius, in improving hydraulic performance. These insights highlight the potential of QCGs for high-capacity flow regulation, offering predictable and efficient behavior, which is valuable for hydraulic engineering applications.

KEYWORDS
Flow Measurement, Discharge Coefficient, Flow Energy Dissipation, Hydraulic Structures, Streamline Curvature.

1. Introduction

Flow measurement and water level control are crucial components in the design of hydraulic engineering projects, including irrigation and drainage networks, as well as dam construction. Various tools, such as weirs and gates, have been developed to achieve these objectives (1, 2). While weirs are primarily employed for flow measurement, their capacity for controlling water levels is somewhat limited. Corrective measures, such as labyrinthine the crest (1), piercing the lower part of the weir body in the form of gates or orifices (3–5), and utilizing devices like fuse-gates (6) and pivoting weirs (2), have been implemented to mitigate this limitation.

Gates are also extensively used for flow measurement and upstream water level control, with two predominant types: vertical (sluice) gates and radial gates (3). A different type of gate has been recently developed, known as Lopac gates (4–7), which have been extensively studied. Due to their superior performance in dam construction and primary water conveyance channels, where accurate flow control and high discharge measurement are essential, radial gates are generally favored. Over the past decade, numerous studies have investigated the hydraulic properties of radial gates (8,9). For instance, researchers have examined the effect of body slope and various geometric shapes of sills, including pyramidal, semi-cylindrical, cylindrical, and rectangular forms, on the performance of vertical sluice gates (8,9). Findings indicate that the shape and height of the sills significantly influence the discharge coefficient (Cd) of sluice gates, with the use of sills enhancing Cd by approximately 20% and markedly increasing energy dissipation by over 100%. Notably, the semi-cylindrical sill is particularly effective in increasing Cd, while the pyramidal sill enhances energy dissipation(10–13).

In recent years, in addition to laboratory studies, numerical investigations based on computational fluid dynamics (CFD) (12) and soft computing techniques(14)—including Gaussian process regression, generalized regression neural networks, support vector machines, and multi-genetic programming—have been utilized to predict the Cd of both radial and sluice gates (15,16). These studies indicate that soft computing models perform reasonably well compared to empirical formulas.

A literature review reveals that research on radial gates has predominantly focused on determining their Cd and methods for its enhancement, with comparatively less emphasis on energy dissipation. In contrast, quarter-circular gates (QCGs), a novel type of radial gate introduced by Babaei et al. (17), have not received the same level of attention. This study aims to investigate the Cd of these structures and the energy dissipation of the flow passing beneath them.

2. Material and methods

The QCG consists of a quarter-circle arch, as shown in Figure 1, which provides a sketch and its geometric and hydraulic parameters.

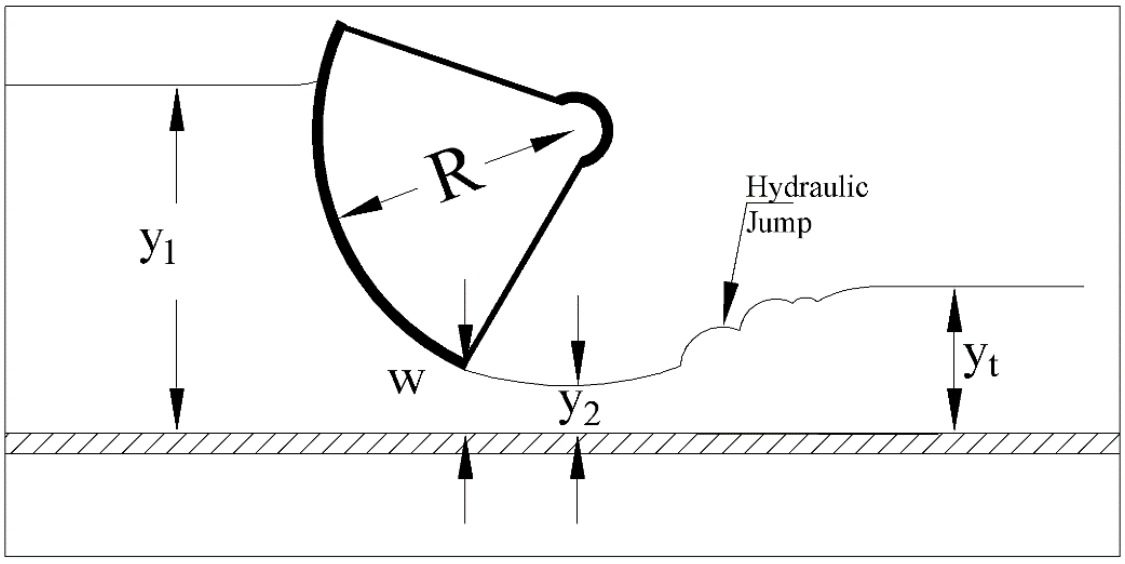


Figure 1. A Sketch of QCG

In Figure 1, R is the gate radius, $y_1$is the upstream flow depth, w is the gate opening, and y_2 is the downstream flow depth. Note that y_t is the tailwater and represents the submergence threshold. Equation (1) estimates the discharge capacity of the gates, which is a function of the upstream flow depth (y_1),C_d, and the gate opening (w)(5).

$$q = c_d w\sqrt{2gy_1} \quad (1)$$

To estimate the discharge capacity, $y_1$and w should be measured. However, for such structures, the $C_d$must be specified in advance. C_d is a function of geometric and hydraulic characteristics (Eq. 2).

$$Cd \text{ and } EDR = \varphi(y_1, y_2, y_t, R, W, g, \rho, \mu, \sigma) \quad (2)$$

Where g is the acceleration due to gravity, and ρ, μ, and σ are the water's density, viscosity, and surface tension, respectively. y_t is the maximum allowable downstream flow depth at which the flow condition is free-flowing. In addition to the C_d, the *EDR* should also be evaluated. Bernoulli's equation is used to calculate the *EDR* for upstream (Eq. 3) and downstream (Eq. 4), and then the *EDR* is computed using Equation (5).

$$H_1 = y_1 + \frac{{V_1}^2}{2g} = y_1 + \frac{q^2}{2g{y_1}^2} \quad (3)$$

$$H_2 = y_2 + \frac{V_2^2}{2g} = y_2 + \frac{q^2}{2g{y_2}^2} \quad (4)$$

$$\text{EDR}(\%) = \left(\frac{H_1 - H_2}{H_1}\right) \times 100 = \frac{\Delta H}{H_1} \times 100 \quad (5)$$

Where H_1 and H_2 represent the total upstream and downstream heads, respectively, the dimensionless parameters involved in $C_d$and *EDR* are obtained using dimensional analysis and are given by Equation (6).

$$Cd \text{ and } EDR = \varphi\left(\frac{y_1}{R}, \frac{y_1}{w}, \frac{y_t}{y_1}, \frac{w}{R}, Fr, Re, We\right) \quad (6)$$

Where Fr, Re, and We are the Froude, Reynolds, and Weber numbers, respectively. Note that y_t/y_1 is used in the submerged flow condition and does not affect the hydraulic properties of QCG in the free flow condition. It is noteworthy that due to the turbulent nature of the flow (Reynolds Number), merit the minimum flow depth in experiment (weber number) and also because the gate is installed in the flow path and the Froude (its range is very limit), these dimensionless number are neglected, To justify the relationship between Cd, EDR, and the independent parameters (y_1 / w, y_1 / R, and w / R), reference was made to the study conducted by Babaei et al. (18). The experiments were performed in a 10 m long, 0.6 m deep, and 0.4 m wide channel. The models were positioned 6 m from the start of the channel, and flow was measured with a volumetric flow meter. Flow depth was measured using a point gauge with a precision of ±1 mm upstream and downstream of the gate. The tailwater depth controlled the submergence threshold. The geometric and hydraulic characteristics of the models tested are detailed in Table 1.

Table 1. Geometrical and hydraulic specifications of the models

Range	W(m)	R(m)	q(m^3/s.m)	y_1	y_t
Min	0.01	0.2, 0.3, 0.5	0.0177	0.09	0.093
Max	0.06		0.124	0.505	0.236

3. Results and discussion

This section presents the results of the analysis and investigation of the $C_d$and *EDR* of the flow passing through the QCG under free-flow conditions. According to Equation 2, $C_d$and *EDR* depend on the ratio of upstream flow depth to gate opening (y_1 / w), the ratio of flow depth to the radius (y_1 / R: indicating the curvature of the streamlines), and the relative gate opening (ratio of opening area to radius of the gate: w/R). The C_d has been calculated (using Eq. 1), and the results are plotted against y_1/w in Figure 2. Examination of this figure shows that in the range of y_1 / w between 4 and 20, the C_d undergoes a logarithmic change, increasing from 0.9 to 1.0. An essential point of this figure is that the C_d does not decrease as the upstream flow depth increases. Figure 2 shows that even if the load behind the QCG is increased by about 5 times, its C_d not only decreases but also increases (even partially).

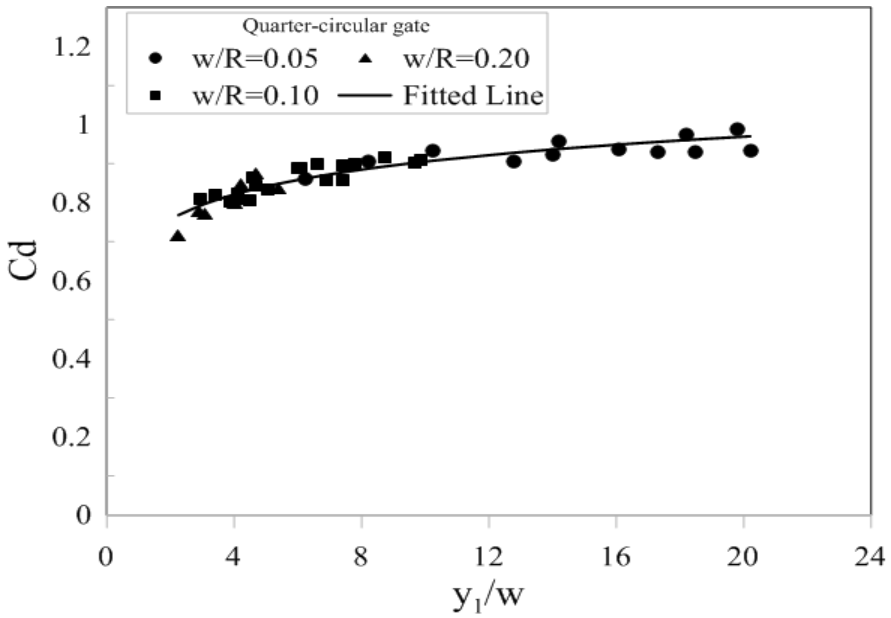


Figure 2. Variations of C_d of QCGs versus y_1/w

The changes in C_d with respect to the parameter y_1 / R are analyzed and presented in Figure 3. The analysis indicates that within the y_1 / R range of 0.25 to 1.5, the relationship between C_d and y_1 / R is almost linear. In other words, as the streamlines become more curved and compressed within the range of y_1 / R, the C_d also increases partially linearly. This is due to the acceleration of the flow caused by the curvature and compression of the streamlines. However, the deviation and curvature of the streamlines result in increased energy loss. In Figure 3, the legend also illustrates the effect of *w/R* on Cd. Examining Figure 3 reveals that at lower upstream flow depths, Cd decreases as *w/R* increases, which is attributed to the reduction in flow acceleration resulting from the curvature of the streamlines. The insignificance of the difference in the curvature and compression of the streamlines hydraulically explains this difference.

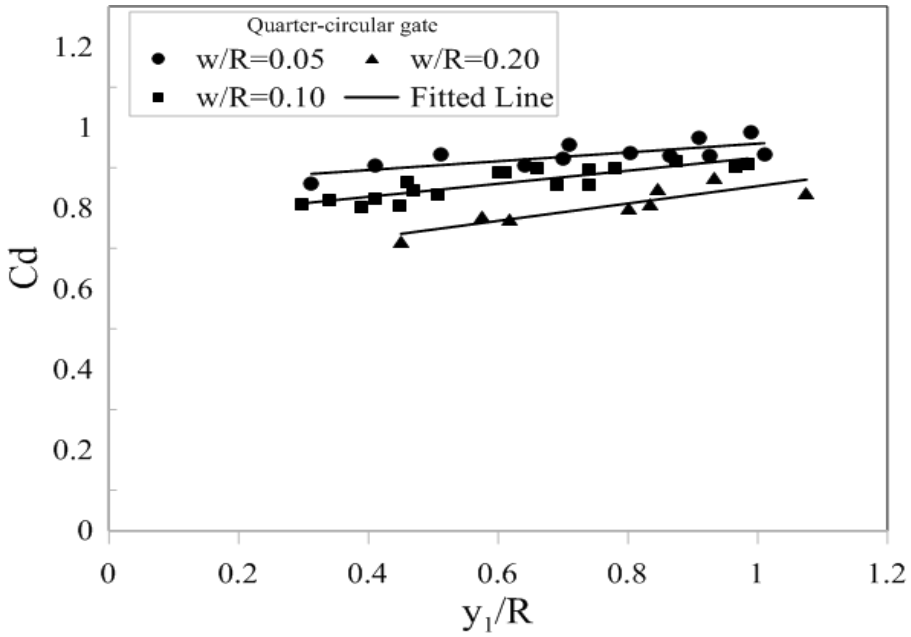


Figure 3. Variations of C_d of QCGs versus y_1/R

The *EDR* of the flow passing under the QCG was calculated using equations 3 to 5, as shown in Figure 4. Figure 4 shows the variation of *EDR* as a function of y_1/w. An essential point in estimating the *EDR* is the consideration of the maximum downstream flow depth (submergence threshold) in the calculation of the *EDR*. However, for values of downstream flow depths less than the submergence threshold, the *EDR* is less than the submergence threshold condition. As shown in Figure 4, the *EDR* varies between 10% and 55% for the same range of y_1 / w. As the value of y_1 / w increases, the EDR increases logarithmically. This is due to increased curvature, deviation, and compression of the streamlines as y_1 / w increases. The noteworthy point in this figure is that if the load behind this structure increases by 5 times, its energy dissipation is increased but much slower, indicating the efficiency of the QCG model.

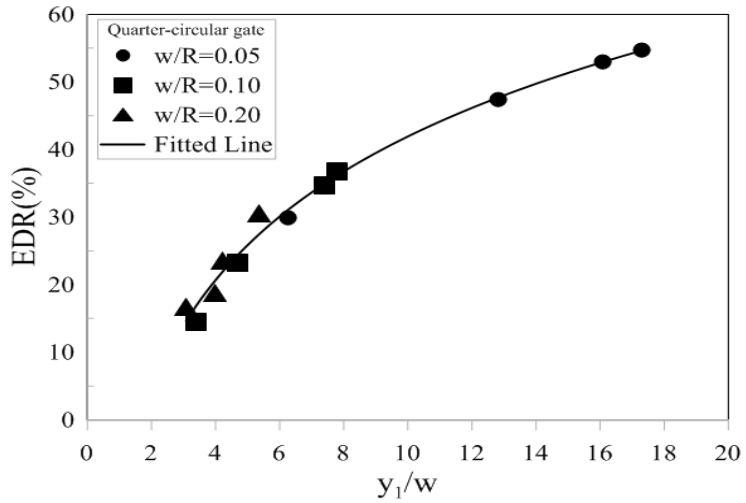


Figure 4. Variations of EDR of QCGs versus y_1/w

The effect of streamlined curvature and their compression on the *EDR* of flow passing under the *QCG* is shown in Figure 5. The graphs in Figure 5 show the relationship between *EDR* and y_1 / R for different values of w / R. It is clear from the graph that the relationship is nearly linear. As y_1 / R increases, the deflected streamlines become more curved and compressed, leading to an expected increase in flow energy loss. For example, when the gate opening was doubled and $y_1 / R \cong 0.6$, the *EDR* decreased by about 75%. Of course, the opposite analysis is correct, i.e., a 50% reduction in gate opening quadruples its energy dissipation. The decrease in EDR with increasing gate opening is logical from a hydraulic point of view. Thus, as the gate opening increases, the streamlines become less curved, resulting in less energy dissipation

.

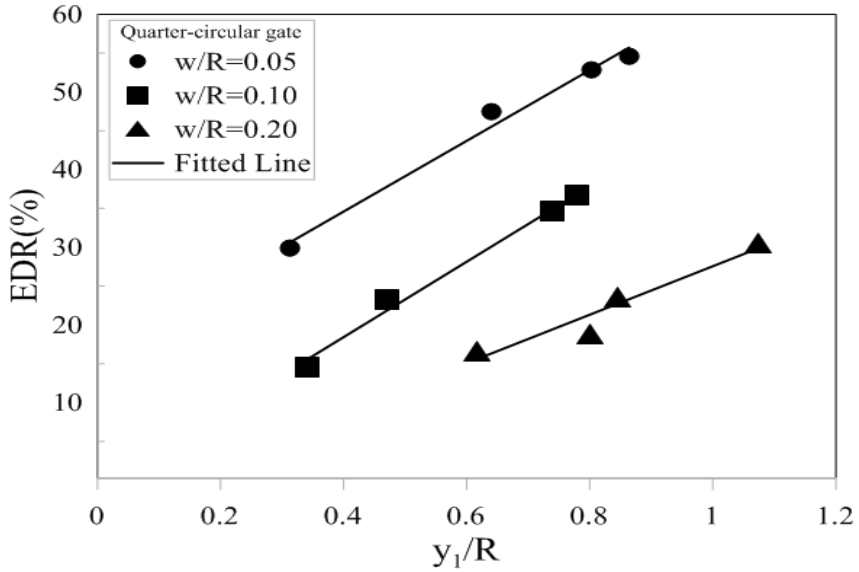


Figure 5. Variations of EDR of QCG versus y_1/R

4. Comparison with Previous Studies

Daneshfaraz et al. (19) investigated the effect of sills on the discharge coefficient of sluice gates. In this regard, they considered cubic sills in different dimensions, including length, height, and width, which ranged from the width of the sills to the width of the channel. They found that the discharge coefficient of sluice gates in the presence of sills ranges from 0.5 to 0.8, considering the range of upstream flow head to the gate opening between 0.1 to 50.

Heidari et al. (12) studied the effect of semicircular and rectangular sills on the discharge coefficient of sluice gates. They found that in rectangular sills, the discharge coefficient varied between 0.53 and 0.62, while the ratio of upstream head to gate opening varied between 2 and 6. In the same range of relative upstream head, the semicircular sill changes the discharge coefficient between 0.6 and 0.7.

Salmasi et al.. (13) studied the effect of different types of sills, such as rectangular and circular, on the discharge coefficient of radial gates. They found that in the presence of all the sills tested, the discharge coefficient varied between 0.55 and 0.75, while the relative upstream head varied between 5 and 30.

In total, through the tested relative upstream head, the discharge coefficient of the sluie and radial gates varies between 0.5 and 0.8. In contrast, the discharge coefficient of QCGs varies between 0.9 and 1.0 (without any sill).

5. Conclusion

This study provides a comprehensive analysis of the discharge coefficient (C_d) and energy dissipation rate (EDR) for flow passing through the quarter-circular gates (QCG) under free-flow conditions. The findings reveal that the C_d exhibits a logarithmic increase for the ratio of upstream flow depth to gate opening (y_1/w), demonstrating resilience to increased upstream loads. Specifically, C_d rose from 0.9 to 1.1 within the range of y_1/w from 4 to 20, indicating that the performance of the QCG improves with greater flow depth. The relationship between C_d and the ratio of flow depth to radius (y_1/R) was found to be approximately linear, suggesting that as flow streamlines become more curved and compressed, C_d also increases. Despite the associated energy losses, this linearity underscores the hydraulic implications of streamline curvature on flow acceleration. Additionally, the EDR analysis revealed that energy dissipation under varying conditions of y_1/w and y_1/R is significant, with EDR values ranging from 10% to 55%. The logarithmic increase in EDR with y_1/w further emphasizes the influence of streamline curvature on energy loss. Notably, the efficiency of the QCG model is highlighted by the observation that while increased downstream loads enhance energy dissipation, this occurs at a diminishing rate. Overall, the results highlight the crucial role of geometric parameters in enhancing the performance of QCGs. Future studies should explore the implications of these findings in practical applications and further investigate the effects of varying flow conditions (submerged flow condition) and gate geometries to refine the understanding of hydraulic efficiency in similar structures.

Notations

c_d	Discharge Coefficient
y_1	Upstream Flow Depth
y_2	Downstream Flow Depth
y_t	Tail Water
QCG	Quarter-Circular Gate
R	Gate Radius
w	Gate Opening
EDR	Energy Dissipation Ratio
g	Acceleration due to Gravity
q	Discharge Per Width
μ	Water Viscosity
ρ	Water Density
σ	Water Surface Tension
H_1	Total Upstream Head
H_2	Total Downstream Head

Funding

This research received no external funding.

Conflict of Interest

The authors declare that they have no conflict of interest.

AI Statement

The authors did not used AI in the context

Author Contributions

All authors contributed to the study conception and design. Material preparation, data collection, and analysis were performed by Abbas Parsaie. The first draft of the manuscript was written by AmirHamzeh Haghiabi and all authors commented on previous versions of the manuscript. All authors read and approved the final manuscript.

References

1. Parsaie A, Pili-Dezfouli M. Estimating the discharge coefficient of piano key weirs using soft computing models. Applied Researches in Water Engineering. 2025;2(2):239–48.
2. Bijankhan M, Ferro V. Experimental Modeling of Submerged Pivot Weir. J Irrig Drain Eng. 2020 Mar;146(3):04020001.
3. Akan AO, Iyer SS. Open channel hydraulics. Butterworth-Heinemann; 2021.
4. Fathi S, Sajjadi SM, Ahadiyan J, Parsaie A. Investigation of the effect of different submerging on the flow hydraulic parameters in multiple rectangular Lopac gates. Water and Irrigation Management. 2024;14(2):249–61.
5. Mobarak F, Sajjadi SM, Ahadiyan J, Zeynivand M. Numerical modeling of the effect of elliptical elongation on the hydraulic performance of an elliptical Lopac

gate. Water and Irrigation Management. 2022;12(2):263–75.
6. Sajjadi M. Numerical Hydraulic and Hydrodynamic Investigation of the Flow through Multiple Rectangular Lopac Gates with Flow 3D Software. JWSS-Isfahan University of Technology. 2024;28(1):51–64.
7. Taheri Talavari T, Sajjadi SM, Ahadiyan J, Azizi Nadian H. Numerical hydraulic and hydrodynamic investigation of flow passing through multiple elliptic lopac gates with Flow 3D software. Advanced Technologies in Water Efficiency. 2024;4(3):40–60.
8. Salmasi F, Abraham J. Expert System for Determining Discharge Coefficients for Inclined Slide Gates Using Genetic Programming. J Irrig Drain Eng. 2020 Dec;146(12):06020013.
9. Salmasi F, Shadkani S, Abraham J, Malekzadeh F. Experimental Investigation for Determination of Discharge Coefficients for Inclined Slide Gates and Comparison with Data-Driven Models. Iran J Sci Technol Trans Civ Eng. 2022 Jun;46(3):2495–509.
10. Daneshfaraz R, Norouzi R, Ebadzadeh P, Di Francesco S, Abraham JP. Experimental study of geometric shape and size of sill effects on the hydraulic performance of sluice gates. Water. 2023;15(2):314.
11. Daneshfaraz R, Norouzi R, Abbaszadeh H, Kuriqi A, Di Francesco S. Influence of sill on the hydraulic regime in sluice gates: an experimental and numerical analysis. Fluids. 2022;7(7):244.
12. Heidari MM, Karami S, Adibrad MH. Investigation of free flow under the radial gate with the sill. Journal of Civil and Environmental Engineering. 2020;50(100):9–19.
13. Salmasi F, Nouri M, Abraham J. Laboratory study of the effect of sills on radial gate discharge coefficient. KSCE Journal of Civil Engineering. 2019;23(5):2117–25.
14. Parsaie A, Najafian S. Mathematical Expression of Energy Dissipation of Flow over Stepped Spillways Using Genetic Programing. Applied Researches in Water Engineering. 2024;2(1):97–110.
15. Roushangar K, Alirezazadeh Sadaghiani A, Shahnazi S. Novel application of robust GWO-KELM model in predicting discharge coefficient of radial gates: a field data-based analysis. Journal of Hydroinformatics. 2023;25(2):275–99.
16. Salmasi F, Abraham J. Prediction of discharge coefficients for sluice gates equipped with different geometric sills under the gate using multiple non-linear regression (MNLR). Journal of Hydrology. 2021;597:125728.
17. Babaei SS, Mohammadzadeh-Habili J, Zomorodian SM. Experimental and theoretical modeling of a quarter-circular gate flow. 2021;80:101983.
18. Babaei SS, Mohammadzadeh-Habili J, Zomorodian SM. Experimental and theoretical modeling of a quarter-circular gate flow [Internet]. Vol. 80, Flow Measurement and Instrumentation. Elsevier; 2021 [cited 2025 Feb 5]. p. 101983. Available from: https://www.sciencedirect.com/science/article/pii/S0955598621000923
19. Salmasi F, Nouri M, Sihag P, Abraham J. Application of SVM, ANN, GRNN, RF, GP and RT models for predicting discharge coefficients of oblique sluice gates using experimental data. Water Supply. 2021;21(1):232–48.

© 2025 by the authors. Licensee SCU, Ahvaz, Iran. This article is an open access article distributed under the terms and conditions of the Creative Commons Attribution 4.0 International (CC BY 4.0 license) (http://creativecommons.org/licenses/by/4.0/).

A Hybrid AHP-AI Framework for Assessing and Mitigating Tunneling Impacts on Confined Spring Discharge

Saeed Samiei [1], Ali Aalianvari[*, 1]

1. Department of Mining Engineering, University of Kashan, Kashan,Iran.

***Corresponding Author:**
Ali Aalianvari,

Email: ali_aalianvari@kashanu.ac.ir
Received: 2025.02.20
Accepted: 2025.05.09
J. Hydraul. Struct., 2026; 12(1):9-19
DOI: 10.22055/jhs.2025.49054.1338

ABSTRACT

Tunnel excavation poses a significant threat to groundwater systems, particularly impacting confined tunnel springs and jeopardizing hydrological balance and water resource sustainability. This study tackles the challenges of tunnel-induced groundwater changes by introducing a novel hybrid framework. This framework combines expert qualitative insights with advanced quantitative modeling, leveraging the Analytic Hierarchy Process (AHP) and artificial intelligence. Building upon existing research that uses numerical and empirical models to assess tunneling impacts on aquifers and spring discharge, our approach integrates multi-criteria decision-making to identify and prioritize factors driving groundwater loss. We evaluate parameters impacting spring discharge, highlighting the importance of karst cavities, rock mass permeability, fracture aperture, and rock mass type. The proposed model categorizes excavation sites into six impact levels, from harmless to completely hazardous. Key findings underscore the influence of tunnel depth, excavation method, and geological conditions on groundwater drawdown and spring depletion. This framework offers an improved decision model for predicting hydrological consequences, bridging research gaps, and providing practical guidance for mitigating environmental impacts, ensuring sustainable groundwater management, and optimizing tunnel construction.

KEYWORDS

Tunnel Excavation, Confined Tunnel Springs, Groundwater Modeling, Analytic Hierarchy Process, Artificial Intelligence, Environmental Sustainability.

1. Introduction

Tunnel excavation is crucial for modern infrastructure development, supporting transportation networks, utilities, and urban expansion. However, this process poses significant challenges to groundwater systems, particularly impacting the flow and sustainability of springs and other underground water sources. Excavation can induce substantial alterations in the hydrological characteristics of the surrounding environment, potentially leading to water loss, ecological damage, and the depletion of vital groundwater resources. Recognizing and understanding the factors contributing to these impacts is essential for developing strategies to mitigate adverse environmental effects and optimize tunnel construction practices.

Several studies have examined the relationship between tunnel construction and groundwater behavior. For example, research by Yoo. [1] and Jiang et al. [2] has highlighted tunnel-induced groundwater drawdown, illustrating the consequent risks to nearby aquifers through the use of various numerical modeling techniques to predict changes in water flow and identify high-risk areas. Additionally, Zhang et al. [3] explored how tunnel excavation affects spring flow, revealing the critical role of structural characteristics, such as depth and construction methods, in influencing water loss dynamics. While existing research has identified several key factors, a comprehensive model integrating their combined influence remains lacking.

To address this gap, this study proposes a hybrid methodology combining qualitative expert assessments with statistical modeling and multi-criteria decision-making, including the Analytic Hierarchy Process (AHP). A structured survey collected qualitative data from experts, which was then used to quantitatively rank influencing factors, facilitating the development of a robust decision model aimed at understanding and predicting tunnel-induced water loss. This integration allows for a more refined assessment of key parameters, leading to more precise predictions of tunnel-induced water loss.

Earlier methodologies employed various approaches, such as finite element modeling and empirical analysis, to simulate these effects. This study refines these methods by incorporating both qualitative and quantitative insights, thus offering a more holistic understanding of the phenomena involved. Ultimately, the aim is to present a comprehensive model that considers a wide array of factors influencing groundwater behavior during tunnel construction. This model is expected to provide a more accurate and reliable tool for predicting and mitigating groundwater loss during tunnel construction, thereby offering a more reliable framework for environmental assessments and management practices, and significantly contributing to the mitigation of water loss and its ecological consequences, promoting sustainable tunnel excavation practices.

Literature Review

Impact of Tunnel Excavation on Groundwater Systems

The impact of tunnel excavation on groundwater systems, especially with regard to groundwater levels, aquifers, and nearby springs, has been the subject of extensive research. Tunneling activities, particularly in confined or fractured rock environments, can significantly alter groundwater flow, leading to water loss, reduced spring flow, and potential changes in water quality. For instance, Katibeh et al. [4] highlighted that tunneling could create substantial drawdown in surrounding aquifers, thereby affecting the availability of groundwater resources essential for local ecosystems and human consumption. Their study employed numerical modeling to demonstrate how tunnel excavation disrupts groundwater flow, especially in regions characterized by high permeability or fractured rock formations.

Building on this, Farhadian et al. [5] investigated the relationship between tunnel excavation and groundwater behavior, emphasizing that the extent of groundwater loss and aquifer depletion is heavily influenced by factors such as tunnel depth, surrounding geology, and excavation methods. Lee[6] and Wang[7] found that deeper tunnels, or those excavated in permeable strata, result in more pronounced hydrological changes. Similarly, Eftekhari et al. [8] focused on how tunnel excavation can reduce spring flow, underscoring the critical roles of tunnel design and construction techniques, particularly for tunnels traversing fractured rock.

An essential conceptual framework for understanding the risks associated with tunnel excavation is the Drawdown Hazard Impact (DHI), introduced by Dematteis et al. [9] DHI encapsulates the potential hazards arising from decreased groundwater levels due to tunnel construction, particularly affecting nearby aquifers, springs, and wells.

Dematteis et al. developed a framework to evaluate DHI by considering various influencing factors, including tunnel depth, surrounding geology, and the proximity to water-bearing layers. Their findings indicate that DHI is particularly pronounced in areas with highly permeable geological formations, where the tunneling process can lead to significant groundwater drawdown, impacting not only the immediate vicinity of the tunnel but also larger surrounding groundwater systems.

DHI is influenced by several parameters, such as excavation methods, tunnel depth, and the structural characteristics of the surrounding rock mass. Tunneling through fractured or karstic rock formations, for example, is particularly likely to cause substantial groundwater inflow into the tunnel, thereby decreasing the water available to neighboring springs. Dematteis's work emphasizes the need to consider DHI in the planning and design phases of tunnel projects, as its impacts could result in long-term alterations to groundwater flow patterns and the sustainability of local water resources.

Additionally, Aalianvari [10] made notable contributions to the understanding of the hydrogeological impacts of tunnel excavation.

Methods for Assessing Groundwater Inflows into Tunnels

Frenelus et al. [11] explored the impact of tunnel excavation on groundwater systems and reviewed various methods for evaluating groundwater inflows into tunnels. Their study emphasized the importance of accurately predicting groundwater inflows during tunnel construction, particularly in rocky environments, where complexities such as permeability variations and fracture networks can lead to unpredictable water inrushes.

The assessment or prediction of groundwater inflows into tunnels, especially in rocky environments, is one of the key challenges in tunnel design and construction. Accurate evaluation of these inflows is crucial for ensuring the stability of tunnels and mitigating potential environmental and structural impacts. Various methods have been developed for this purpose, each with its own strengths and limitations.

Analytical and Semi-Analytical Methods: Frenelus et al. [11] presented that these approaches are based on simplified assumptions, often modeling the rocky medium as homogeneous and isotropic. While they are computationally efficient, their accuracy is often limited due to the complex and heterogeneous nature of rocky environments.

Numerical Methods: These methods provide a more detailed and precise analysis of groundwater inflows, especially in heterogeneous or anisotropic media. Jahanmirir et al. [12] show that, these methods require extensive geological and hydrogeological data, making them resource-intensive in terms of both time and cost.

Empirical and Semi-Empirical Methods: Niu et al. [13] highlighted that these methods are often derived from field observations and adjusted for specific conditions. While more flexible in certain situations, their predictions are not always accurate across diverse geological contexts.

Machine Learning Methods: With recent advancements, Farhadian et al. [5] investigated machine learning techniques like neural networks, support vector machines, and hybrid models have been applied to predict groundwater inflows. These methods are highly effective when large and diverse datasets are available but require significant computational resources and expertise.

By combining these approaches and adapting them to the specific geological and hydrological conditions of tunnel projects, more accurate predictions can be achieved, leading to better design and safer construction practices.

Hydrogeological Consequences of Tunnel Excavation

The hydrogeological consequences of tunnel excavation, particularly in areas with confined aquifers, have been well.

documented in the literature. Niu et al. [13] used numerical simulations to analyze groundwater flow in response to tunneling activities. Their study highlighted the potential for significant changes in groundwater levels, which can lead to water shortages and changes in the quality of nearby springs. Liu et al. [14] also conducted field studies and experiments to assess the impact of tunnel excavation on surrounding groundwater systems. Their research found that in areas with fractured rock or karst formations, tunneling can result in considerable water inflow into the tunnel, affecting both the immediate groundwater system and the surrounding ecological environment.

Methodology

Parameter Selection and Weighting:

In this study, a questionnaire was prepared by examining all the parameters that can affect the water loss of springs and groundwater due to tunnel excavation. Using this questionnaire and presenting it to experts in this field to qualitatively score the impact of each of these parameters, initial data related to the level of impact and the ranking of the impact of these parameters were obtained. Using statistical methods and multi-criteria decision-making models such as AHP and artificial intelligence, the impact weights of various influential parameters can be determined according to the initial qualitative data and the different parameters can be ranked in different categories according to their importance (Fig.1). This ranking based on the obtained weights can be used to present a specific and efficient relationship that includes all the influential parameters in this process. After reaching a conclusion and classification, the desired relationship can be improved and a more efficient form can be presented for it using machine learning and artificial intelligence.

The weights for the 14 chosen parameters, calculated based on the average responses from 100 carefully structured questionnaires converted from qualitative to quantitative data, are presented in Figure 2. The online questionnaire was distributed to 100 professionals in the field. Among the respondents, 15% were university faculty, while the remainder consisted of practitioners in tunneling and geotechnical engineering. Notably, 35% of the participants held doctoral degrees, while the others had master's degrees. The collected responses were subjected to statistical analysis and reviewed individually.

$$n_{ij} = \frac{a_{ij}}{\sum_{k=1}^{n} a_{kj}} \quad (1)$$

Parameter Selection

In this study, the key parameters influencing the environmental risks of tunnel excavation were identified through a questionnaire distributed among experts and professionals in geotechnical engineering and water resource management. The questionnaire aimed to evaluate the relative importance of each parameter in affecting groundwater systems. After collecting responses, the data were analyzed using multi-criteria decision-making methods to determine the most significant parameters.

Analysis and Weighting:

1.Data Collection:

The questionnaire results were structured into a matrix that represented the relative importance of each parameter as assessed by the experts.

2.Importance Analysis Using AHP:

The Analytic Hierarchy Process (AHP) was employed to analyze the collected data. The steps included:

Constructing a Pairwise Comparison Matrix:

This matrix compared the relative importance of each parameter against others:

$$A = \{a_{ij}\},\ aij = \frac{\text{Importance of Parameter j}}{\text{Importance of Parameter i}}$$

Normalizing the Matrix:

Each element in a column was divided by the sum of its respective column:

Calculating Final Weights:

The final weight of each parameter was computed as the average of the normalized values in its row:

$$w_i = \frac{\sum_{j=1}^{n} n_{ij}}{n} \quad (2)$$

Where n is the number of iteration.

3.Consistency Check: To ensure the accuracy of the analysis, the **Consistency Index (CI)** and **Consistency Ratio (CR)** were calculated:

$$\mathrm{CI} = \frac{\lambda_{\max} - \mathrm{n}}{\mathrm{n}-1}, \ \mathrm{CR} = \frac{\mathrm{CI}}{\mathrm{RI}} \quad (3)$$

Where RI is the Random Index for the number of parameters (n). A CR<0.1indicates acceptable consistency. λ_{max} is the largest eigenvalue.

Selection of 14 High-Impact Parameters:

Based on the weight analysis, **14 parameters with the highest weights** were selected for further assessment. These parameters and their final weights are as follows:

Table 1. The Effective Parameters

	Karst Potential	
	Geomorphology	
Geological Parameters	Discontinuity	Joint set Frequency Aperture Roughness Direction Persistency Filling material
	Fault	Fault Type Displacement Crashed Zone Width Slip band Fracture intersected by fault Host rock permeability Gouge
	Formation	Rock Type Weathering Degree
Hydrologic Parameters	Rock Mass Permeability Basin Area Climate Annual Raining Groundwater Level	
Geometric Parameters	Tunnel Radius Tunnel Length Overburden Tunnel level relative to the spring Tunnel Direction Tunnel distance from the spring Tunnel position relative to the spring Spring Type	

After evaluating the introduced parameters and reviewing the opinions, the weight of each parameter was determined, which is shown in Figure 1.

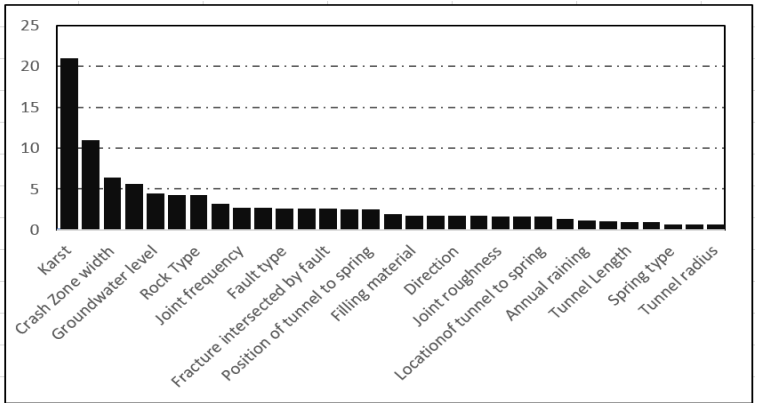


Figure 1. The Weight of Effective Parameters

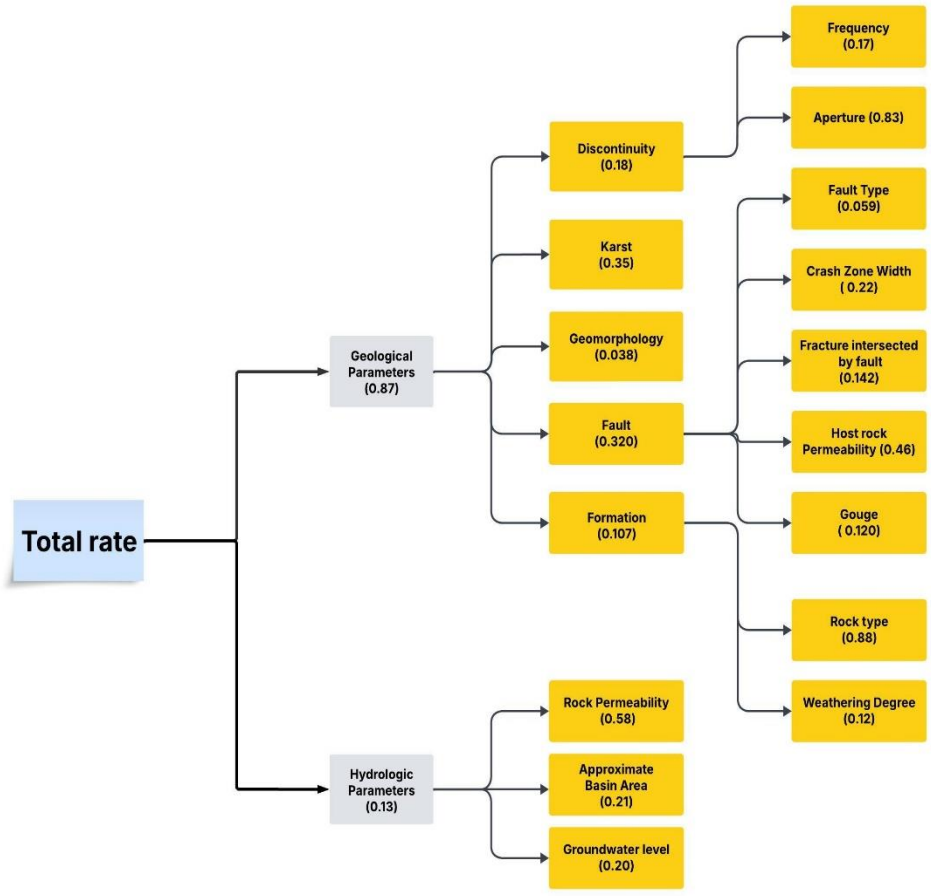


Figure 2. Total weight of all parameters

The selection of the 14 parameters with high weights in this study was based on a detailed and multi-step analytical process, as outlined below:

1.Identification of Key Criteria:

The criteria influencing groundwater behavior during tunnel excavation were identified through expert consultations in geotechnical engineering and water resource management. These criteria encompass

geological, hydrological, and tunnel design factors.

2.Application of Multi-Criteria Decision-Making (AHP):

The Analytic Hierarchy Process (AHP) was employed to evaluate and rank the relative importance of each parameter. This method allowed for pairwise comparisons of criteria, resulting in the calculation of each parameter's final weight based on its relative significance.

3.Normalization and Weight Calculation:

The weights derived for each parameter were normalized to represent their relative contribution within the final model. These weights quantify the influence of each parameter on groundwater systems.

4.Selection of Priority Parameters:

From the identified criteria, the 14 parameters with the highest weights were selected. This selection focused on those parameters most critical in influencing groundwater flow and the environmental impacts of tunnel excavation.

5.Integration of Qualitative and Quantitative Knowledge:

The selection process combined qualitative insights from experts with quantitative analysis, ensuring that the final model is both scientifically robust and practically applicable.

The primary goal of selecting these parameters is to develop a comprehensive and reliable model for predicting and mitigating the environmental and hydrological risks associated with tunnel excavation. This approach enables decision-makers and engineers to focus on key factors and adopt optimal strategies for managing tunnel construction projects effectively (Table.2).

Table 1. Final Weight of Selected Parameters

Parameter	Final Weight (%)
Karst	30
Host Rock Permeability	14
Aperture	12
Rock Type	8
Rock mass permeability (without fault)	8
Crashed Zone Width	6
Fracture intersected by fault	4
Joint Frequency	3
Fault Gouge	3
Geomorphology	3
Ground Water Level	3
Basin Area	3
Fault Type	2
Weathering Degree	1

This structure was selected as it has been found to be effective in groundwater inflow into tunnel. In addition, the rating value can also be easily understood by nongeotechnical specialists. From consideration of the field investigation of different tunnels in various geological conditions [Amirkabir Tunnel (23 km), Azad Dam Divergence Tunnel (3 km), Seymare Dam Divergence Tunnel (3 km), a tunnel in the west of Iran(10 km), and Sangtuda-2 Power Plant Tunnel (2 km) in Tajikistan],

literature review, numerical modeling, sensitivity analysis in each case, and finally, researcher experience in tunneling, it was noted that the parameters would have varying degrees of influence on the groundwater inflow into tunnels. To account for this, each of the parameters was attributed a maximum rating and an associated rating scale, reflecting its importance within the classification system (see Tables. 3).

Integration into the Final Risk Formula:

The selected parameters and their weights were incorporated into the final risk assessment formula:

$$R = \sum_{i=1}^{14} w_i, P_i$$

Where:

- w_i: Weight of parameter i.
- P_i: Score of parameter i based on its range and impact.

This methodology ensures that the most significant factors influencing groundwater risks during tunnel excavation are prioritized, providing a reliable framework for risk assessment.

Parameter Identification:

Fourteen critical parameters influencing groundwater systems were identified:

Table.3. Proposed rate foe relating parameters

Karst Development	Highly Developed 5	Developed 4	Moderate 3	Poorly Developed 2	Absent 1
Host Rock Permeability(m/s)	$>10^{-3}$ 5	10^{-4}–10^{-3} 4	10^{-5}–10^{-4} 3	10^{-6}–10^{-5} 2	$<10^{-6}$ 1
Aperture(mm)	More than 10 5	10-7 4	4-7 3	1-4 2	Less than 1 1
Rock Type	Carbonate 5	Sandstone 4	Combined layers 3	Shale & Slate 2	Igneous 1
Crashed Zone Width(m)	>10m 5	7-10m 4	4-7m 3	1-4m 2	<1m 1
Fracture Count	More than 5 5	30-50 4	10-30 3	5-10 2	Less than 5 1
Joint Frequency(l/m)	>10 5	7-10 4	4-7 3	1-4 2	<1 1
Gouge	Clean 5	Washable 4	Un washable 3	Close 2	
Ground Water Level(m)	>200 5	100-200 4	50-100 3	10-50 2	<10 1
Geomorphology	Steep 5	Moderately Steep 4	Rolling 3	Undulating 2	Flat 1
Fault Type	Normal slip 5	Strike slip 3	Reverse slip 1		
Weathering Degree	Very highly decomposed 5	Highly weathered 4	Moderately weathered 3	Slightly weathered 2	Fresh 1
Basin Area(Km2)	>500 5	500-300 4	300-100 3	100-50 2	<50 1

Steps for Using the Formula:

- **Determining Scores (P_i):** Extract the score for each parameter based on its actual value from relevant tables, such as permeability, distance from springs, or other related parameters
- **Weighting (w_i):** Determine the weights of parameters using evaluation methods like AHP or optimization algorithms (e.g., Genetic Algorithm or Particle Swarm Optimization).
- **Calculating the Final Index (R):** Substitute the scores and weights into the formula to calculate the final index.

Risk Assessment Framework:

Range of Final Index:

Based on the defined weights (w_i)and parameter scores (P_i), the calculated R value will always remain within the range of **120,480**. This is due to the following:

The total weights sum to **100%**, limiting the impact of scores.Even at the lowest (Pi=1) or highest (Pi=5) scores, R will remain within this controlled range. Scores are confined between **1 (minimum)** and **5 (maximum)**, ensuring Rmin=120 and Rmax=480 under practical conditions. Any R value outside this range would indicate errors in weight, scores, or calculation.This ensures a robust framework for risk assessment, aligning parameter impacts with realistic boundaries.

The table 4 categorizes the range of the final risk index into different levels of risk. This classification helps in identifying the necessary actions and level of monitoring required during the project.

Table 4. Risk Level Classification Based on Final Index (R)

Range of R	Risk Level	Description
120≤R<180	**Very Low**	Negligible impact; no specific actions are required.
180≤R<240	**Low**	Limited impact; regular monitoring is recommended.
240≤R<300	**Moderate**	Noticeable impact; optimization of methods or more detailed evaluation suggested.
300≤R<360	**High**	Significant impact; preventive actions or changes in project design are required.
360≤R<420	**Very High**	Major impact; immediate preventive measures are recommended.
420≤R≤480	**Critical**	Severe impact; project suspension or immediate protective measures are necessary.

Explanation of Risk Categories:

1. **Very Low (120 ≤ R < 180):**

Description: The impact is negligible, and the project poses minimal risks to groundwater or the surrounding environment.

Action Required: No specific actions are necessary, but basic monitoring can be maintained.

2. **Low (180 ≤ R < 240):**

Description: The impact is limited, with minor effects on groundwater systems.

Action Required: Regular monitoring is recommended to ensure the risks remain under control.

3. **Moderate (240 ≤ R < 300):**

Description: The impact is noticeable, and groundwater systems may experience measurable changes.

Action Required: Optimization of construction methods or a more detailed evaluation of risks is suggested.

4. **High (300 ≤ R < 360):**

Description: The impact is significant, potentially causing substantial effects on groundwater systems and the environment.

Action Required: Preventive actions or adjustments to the project design are required to mitigate risks.

5. **Very High (360 ≤ R < 420):**

Description: The impact is major, with a high likelihood of severe effects on groundwater systems.
Action Required: Immediate preventive measures should be implemented to reduce risks.

6. **Critical (420 ≤ R ≤ 480):**

Description: The impact is severe, posing critical risks to groundwater and requiring urgent attention.
Action Required: Project suspension or immediate protective measures are necessary to prevent irreversible damage.

Conclusion

This study presents a comprehensive and robust framework for assessing the impact of tunnel excavation on groundwater systems, integrating both qualitative expert insights and quantitative analytical methods. By employing the Analytic Hierarchy Process (AHP), the study identifies and prioritizes 14 key parameters that significantly influence groundwater behavior, with 'Karst' emerging as the most critical factor. The proposed risk assessment formula, which incorporates these parameters and their respective weights, provides a reliable tool for categorizing risk levels into six distinct categories—from Very Low to Critical. This framework not only enhances the ability to predict and mitigate environmental and hydrological risks associated with tunnel construction but also offers flexibility in adapting to specific project requirements. The integration of multi-criteria decision-making and advanced modeling techniques ensures that the model is both scientifically rigorous and practically applicable, making it a valuable resource for engineers, project managers, and environmental planners. Future research could focus on further refining the model by incorporating additional parameters or exploring its application in diverse geological and hydrological contexts. Additionally, the framework can be adapted to various types of projects and domains, making it a versatile tool for addressing the complex challenges of groundwater management in tunnel construction. Ultimately, this study contributes significantly to the advancement of knowledge in the field of groundwater hydrology and tunnel engineering, providing a reliable and practical framework for decision-makers and practitioners to navigate the complexities of tunnel excavation and groundwater management.

Statements and Declarations

The authors declare that they have no conflict of interest.

Competing Interests

This research work is not supported by any funding agency.

Financial Disclosure Statement

The author(s) received no specific funding for this work.

Funding

This research did not receive any specific grant from funding agencies in the public, commercial, or not-for-profit sectors.

Data Availability

The data presented in this study are available on request from the corresponding author

Consent for Publication

All the authors have read and agreed to the submitted version of the manuscript.

References

1. Yoo J. Ground settlement during tunneling in groundwater drawdown environment – influencing factors. *Tunn Undergr Space Technol.* 2016;20-29. doi:10.1016/j.undsp.2016.07.002.
2. Jiang D, Zhang H, Liu W. Tunnel-induced groundwater drawdown and its impact on nearby aquifers. *Tunn Undergr Space Technol.* 2018;73:183-94. doi:10.1016/j.tust.2012.01.002.
3. Zhang J, Liu S, Zhang P. The impact of tunnel excavation on spring flow: a case study. *Environ Geol.* 2019;56(3):467-77. doi:10.1007/s40808-025-02415-x.
4. Katibeh H, Aalianvari A. Common approximations to the water inflow into tunnels. *Drainage Systems.* 2012:75-88. doi:10.5772/36003.
5. Farhadian H, Aalianvari A, Katibeh H. Optimization of analytical equations of groundwater seepage into tunnels: a case study of Amirkabir tunnel. *J Geol Soc India.* 2012;80:96-100. doi:10.1007/s12594-012-0122-z.
6. Lee S, Kim H, Park J. Assessing the impact of railway tunnels on groundwater flow using numerical modeling. *Water.* 2023;15(13):2446. doi:10.12989/gae.2019.18.2.215.
7. Wang L, Chen K, Huang T. Application of Fuzzy Delphi and Fuzzy AHP methods in evaluating human errors in manual assembly processes. *Systems.* 2023;12(11):479.
8. Eftekhari A, Aalianvari A. An overview of several techniques employed to overcome squeezing in mechanized tunnels; a case study. *Geomech Eng.* 2019;18(2):215-24. doi:10.12989/gae.2019.18.2.215.
9. DeMatteis A, Fissore D. Drawdown Hazard Impact (DHI) assessment for tunnel excavation projects. *Tunn Undergr Space Technol.* 2001;16:217-27.
10. Anvari AA, Katibeh H, Sharifzadeh M. A new approach for computing permeability of fault zones case study: the upper reservoir of Azad pumped-storage power station in Iran. *Arch Min Sci.* 2010;55(3):605-21.
11. Frenelus W, Peng H, Zhang J. Evaluation methods for groundwater inflows into rock tunnels: a state-of-the-art review. *Int J Hydrol.* 2021;5(4):152-68.
12. Farhadian H. Optimizing minor drainage tunnel position to mitigate groundwater inflow in main tunnel projects. *J Hydraul Struct.* 2025 Mar 15:148-58.
13. Niu D, Zhao F, Wang L. Numerical simulation of groundwater flow due to tunneling activities. *Environ Earth Sci.* 2017;76(5).
14. Liu Z, Liu J, Yu X. Hydrogeological consequences of tunnel excavation: a combined field and experimental study. *Geosci J.* 2020;25(2):345-56.

© 2026 by the authors. Licensee SCU, Ahvaz, Iran. This article is an open access article distributed under the terms and conditions of the Creative Commons Attribution 4.0 International (CC BY 4.0 license) (http://creativecommons.org/licenses/by/4.0/).

River Behavior and Morphological Analysis of a Meandering Channel in the Ganga River System, India

Kuldeep Pareta [*,1], Upasana Pareta [2]

1. DHI (India) Water & Environment Pvt Ltd., New Delhi, India.
2. Omaksh Consulting Pvt Ltd, Greater Noida, UP. India.

***Corresponding Author:**
Kuldeep Pareta,

Email: kpareta13@gmail.com
Received: 2025.02.22
Accepted: 2025.05.18
J. Hydraul. Struct., 2026; 12(1):20-49
DOI: 10.22055/jhs.2025.49070.1340

ABSTRACT

The Rapti River and its tributaries exhibit a meandering morphology, characterized by a dynamic network of sinuous bends that undergo spatial and temporal variations in location and size annually. The most pronounced bankline modifications occur during the receding flow stages, as excess sediment accumulates in the form of point bars and side bars along the primary channel. This sediment deposition alters local flow dynamics and drives the migration of the thalweg. During flood events, river hydraulics undergo significant alterations, leading to variations in sediment transport dynamics and erosive forces, which in turn drive channel migration at multiple vulnerable reaches. A comprehensive understanding of river dynamics upstream and downstream of hydraulic structures is essential for their effective planning, design, and maintenance. Hydraulic analysis of river dynamics upstream and downstream of structures such as barrages and spurs are conducted to assess sediment deposition upstream and the effects of inadequate energy dissipation caused by skewed hydraulic jumps downstream. Morphological studies play a crucial role in sustainable river management, the design of restoration structures, and flood risk mitigation. To address these challenges, comprehensive analyses have been conducted, including assessments of river behavior and the impacts of barrages, embankments, and spurs on channel morphology. These areas are very much needed to pay attention. Effective stabilization of riverbanks in the study area requires the implementation of corrective measures, strategic planning, and governmental support to mitigate erosion and ensure long-term stability.

KEYWORDS
River behaviours, Rapti river, bank protection structures, remote sensing and GIS.

1. Introduction

Meandering rivers are among the most extensively analyzed fluvial systems globally [1]. Despite their ubiquity and significance, the intricate details of their dynamics remain partially understood [2, 3]. These systems are characterized by highly dynamic and fascinating processes, primarily driven by the interplay of bank erosion and sediment deposition [4]. Meandering rivers sculpt the floodplain through alternating patterns of erosion at the outer banks and deposition at the inner banks, creating their distinctive curvilinear structure as they flow downstream [5, 6]. Meander evolution is driven by the lateral migration of the river channel, which reshapes the floodplain and redistributes sediments through bank erosion and accretion processes [3, 7-9].

Meander classification provides critical insights into understanding these systems [3]. Meanders can be categorized based on planform geometry, flow characteristics, and sedimentary processes, reflecting the complex interaction between hydrodynamic forces and geological settings [10-12]. The formation of point bars—large sediment deposits at inner meander bends—further highlights the interplay between sediment transport and channel morphology [13-15]. Hydraulic structures, including barrages, embankments, and spur dikes, play a pivotal role in shaping the morphological evolution of natural river systems [16]. These structures influence the hydrodynamic and sedimentological processes that govern channel behavior, often resulting in both intended and unintended consequences [17]. The Rapti barrage, for instance, alters the natural flow regime by redistributing discharge patterns, which in turn affects sediment transport and deposition dynamics [18]. These changes can lead to notable modifications in channel morphology, including altered erosion and deposition zones, channel incision, or aggradation downstream of the barrage [19].

The phenomenon of why rivers meander in alluvial settings remains an intriguing and unresolved question in geomorphology [1]. A persistent challenge lies in understanding why confined riverine flows exhibit meandering behavior [20-22]. It is hypothesized that this behavior results from the system's response to self-induced transverse oscillations, influenced by various theoretical frameworks addressing the dynamics of water mass movement [23-25]. Numerous studies associate river meandering with sediment transport dynamics, stream load variations, and the systematic exchange of sediment between the riverbanks and the flowing water [26-28]. These processes are fundamental drivers of river meandering; however, none have entirely explained or accurately predicted meander scale. Meandering may develop as a response to deviations in river flow, leading to the formation of secondary flow patterns [29-33]. Numerous researchers interpret meandering as a stability-related phenomenon within river dynamics [20, 34-36]. Meandering is sometimes associated with the impact of the Coriolis force on river flow dynamic [37]. However, this may not be a crucial factor, as rivers in equatorial regions typically carry more water than those in higher latitudes. The hypothesis that meandering maximizes stream-energy losses has gained limited support [38-39], alternatively, the counter hypothesis suggests that meandering optimizes energy dissipation, making it the most probable river morphology, a perspective that remains compelling to some researchers [7, 40-42].

Human interventions do not directly alter the fundamental hydraulic and geomorphic processes, including sediment transport, erosion, and deposition. However, they influence the spatial distribution, intensity, and extent of these processes, resulting in substantial modifications to river morphology [43-44]. These changes can either accelerate or decelerate these processes, often with unintended consequences [45-46]. Human-induced modifications to river systems can be classified as direct or indirect. Direct interventions encompass water storage in reservoirs, flow diversion, channelization, the construction of levees and stop-banks, as well as bed and bank stabilization measures [47]. Poorly designed water development and river training structures, lacking comprehensive hydraulic assessments, can increase vulnerability by obstructing river flow and causing widespread inundation upstream and downstream [48]. Disruptions in water and sediment transfer have a direct impact on the structural and functional dynamics of the river, influencing both upstream and downstream regions of hydraulic infrastructure such as barrage [49-50].

Constructed by the Government of India between 1981 and 1985, the Rapti Barrage was designed to enhance irrigation in the adjacent agricultural regions. Functioning as

a point-source disturbance, the barrage exerts substantial off-site impacts, primarily by modifying the river's longitudinal connectivity and altering base-level conditions. The study area is subjected to multiple hydrological and geomorphological challenges, including recurrent flood inundation, bank erosion, elevated sediment loads, and dynamic river course shifts. A summary of extreme flood events occurring upstream and downstream of the Rapti Barrage is presented in Table 1.

Table 1. Chronological record of flood events occurring upstream and downstream of the Rapti Barrage from 1970 to 2024

Geographical extent of flood events	Flood event years*/#								
Nepal / Upper reach of the Rapti Barrage	-	-	1984	-	1989	1998	-	2007	2017
India / Lower reaches of the Rapti Barrage	1971	1974	-	1980	-	1998	2001	2007	2017

**Flood event years after 1970, # Source: National Institute of Disaster Management (NIDM)*

Embankments are commonly employed for flood management, riverbank stabilization, and enhancing navigational depth [51]. While these structures effectively mitigate risks associated with flooding and bank erosion, they also disrupt the natural flow processes of rivers [52]. By constraining lateral flow, embankments create localized hydraulic complexities, such as increased flow velocities near the structure and reduced velocities downstream [53]. These alterations can elevate flood levels and exacerbate sediment deposition within confined areas [54-55]. Furthermore, impermeable embankments, often designed to prevent water infiltration, can significantly disrupt sediment transport continuity [56-57]. This may result in sediment starvation downstream, causing riverbed degradation, or sediment accumulation upstream, which can reduce channel capacity and increase flood vulnerability [58]. By modifying flow and sediment dynamics, these hydraulic structures impact the natural equilibrium of rivers, highlighting the importance of their strategic design and placement to balance flood control, bank stabilization, and ecological integrity [59].

Spur dikes, widely employed for riverbank protection and channel alignment, exert a significant influence on river morphology by altering flow and sediment dynamics [60-61]. These hydraulic structures are strategically designed to redirect water flow away from erodible banks, reducing erosion risk and stabilizing the channel [62]. However, their presence introduces complex flow conditions, including turbulent eddies and localized flow acceleration, which often lead to the formation of scour holes immediately downstream of the structures [63-64]. This localized scouring is a direct consequence of the concentrated hydraulic forces generated by the deflection of flow, which increases shear stress on the riverbed in the vicinity of the spur dikes [65]. In addition to stabilizing banks, spur dikes can contribute to morphological changes along the river [66-67]. The spaces between adjacent spurs, referred to as embayments, often experience dynamic sedimentation processes [68-69]. These areas act as zones of reduced flow velocity, promoting sediment deposition and influencing the development of point bars or other depositional features [70]. Over time, this sediment accumulation can realign the main channel, affecting its curvature and overall planform geometry [71]. The interplay between sediment deposition in embayments and the scouring near spur tips creates a feedback mechanism that continuously modifies the riverbed and bank morphology [72].

These morphological changes are further amplified by the interactions between spur dikes and the river's hydraulic forces [73-75]. The resulting sediment dynamics can have both localized and system-wide impacts, altering flow paths, modifying floodplain connectivity, and influencing

habitat distribution [53]. A comprehensive understanding of these processes is critical for optimizing the design and placement of spur dikes to ensure effective riverbank protection while minimizing unintended consequences on river morphology and ecology [76]. Understanding the intricate relationships between meandering processes, hydraulic structures, and morphological changes is crucial for effective river management and conservation [5, 77-78]. This study utilizes remote sensing and GIS techniques to examine meander classification and assess the impacts of the Rapti barrage, embankments, and spur structures on channel morphology and sediment dynamics.

The primary objective of this study is threefold. Firstly, it aims to examine the behavior and classification of meanders within the Rapti River system, focusing on understanding its dynamic processes and geomorphological features. This includes categorizing the meanders based on their planform geometry, sediment transport mechanisms, and the interactions between flow dynamics and riverbank stability. These analyses have been carried out using remote sensing and GIS techniques, which facilitated the extraction and classification of meander patterns and morphological features from multi-temporal satellite imagery and spatial data. Secondly, the study investigates the impact of the Rapti barrage on the river system, particularly its influence on flow regulation, sediment deposition, erosion patterns, and overall channel morphology. The analysis conducted using temporal satellite data and geospatial overlays in GIS, assesses how the barrage alters the natural processes of sediment transport and its role in shaping the downstream river environment. Thirdly, the study evaluates the impact of various bank protection structures, such as embankments and spur dikes, on the morphological evolution of the channel. These structures, designed to mitigate erosion and stabilize riverbanks, are examined for their role in modifying flow patterns, sediment dynamics, and channel configuration. Remote sensing and GIS were employed to analyze spatial changes in channel geometry and to detect the influence zones of these hydraulic structures over time. The interactions between these hydraulic structures and the natural processes of alluvial rivers are studied to provide a comprehensive understanding of their effectiveness and potential unintended consequences. This paper consolidates the findings of the river morphology analysis, emphasizing their broader applicability to other alluvial river systems, such as the Ganga, Gandak, Sarda, Kamala, Bagmati, Ghaghara, Kosi, and Brahmaputra rivers. The insights gained from this study contribute to a deeper understanding of river dynamics and can inform the design and management of hydraulic structures and conservation strategies in similar fluvial environments worldwide.

2. About the study area

The Rapti River Basin of Ganga River System, located in the northern part of India, spans from 26°18'03" to 28°33'13" North and 81°33'13" to 83°45'03" East, encompassing a total drainage area of approximately 15,153 km². The Rapti River Basin elevation ranges from approximately 73 meters (minimum) to 1,877 meters (maximum) above mean sea level, with a mean elevation of around 325 meters. The river meanders, characterized by their unique geomorphological features and dynamic nature, have long been a subject of extensive study in the field of fluvial geomorphology [79-82]. This is due to their widespread occurrence, distinct morphological forms, and their significant role in shaping landscapes, as well as the practical implications of their movement for flood management, sediment transport, and channel stability [83].

In this study, several segments or reaches within the Rapti River system have been selected for detailed analysis, focusing on various aspects of river behavior, sediment dynamics, and morphological

changes. These segments were chosen based on their representative features, which provide insight into the river's hydrodynamics, erosion, deposition processes, and interactions with hydraulic structures. The specific study locations, including the respective reach characteristics, are summarized in Table 2. A location map illustrating the spatial extent of the study area and its key features is provided in Figure 1.

Table 2. Analyzed characteristics and specific locations within the Rapti River system in India

S. No.	Studied aspects	Locations within the Rapti river system
1.	Meander classification	Nine distinct meander patterns (A to G_2) have been identified in proximity to specific locations, including Bolua and others. A - Bolua; B_1 - Sukrooliya; B_2 - Kakra Kalan C - Andhra Purwa; D - Gosainpur; E - Shawagunj F - Sahiapur; G_1 - Gadrahia; G_2 - Bangarha Bugurg
2.	Impact of Rapti barrage on the river system	The Rapti Barrage (Laxmanpur Barrage) is located on the Rapti River at Laxmanpur Kothi in Shravasti District, Uttar Pradesh, at coordinates 27°51'53" N, 81°48'48" E.
3.	Impact of embankment structures on channel morphology	This study focuses on four morphologically active areas categorized based on the presence of bank protection structures: (A) absence of bank protection structures (near Karmohni), (B) partial bank protection structures (near Hanharpur), (C) single-sided bank protection structures (near Kakra Kalan), and (D) double-sided bank protection structures (near Bangarha Bugurg).
4.	Impact of spurs structures on channel morphology	A series of five repelling spurs is located in Duhiya (Harijan Basti) village, near the Maloni embankment, at coordinates 26°41'31" N,
5.	Development of embayment between spurs	83°23'26" E. This spur system is near Gorakhpur town, Uttar Pradesh.

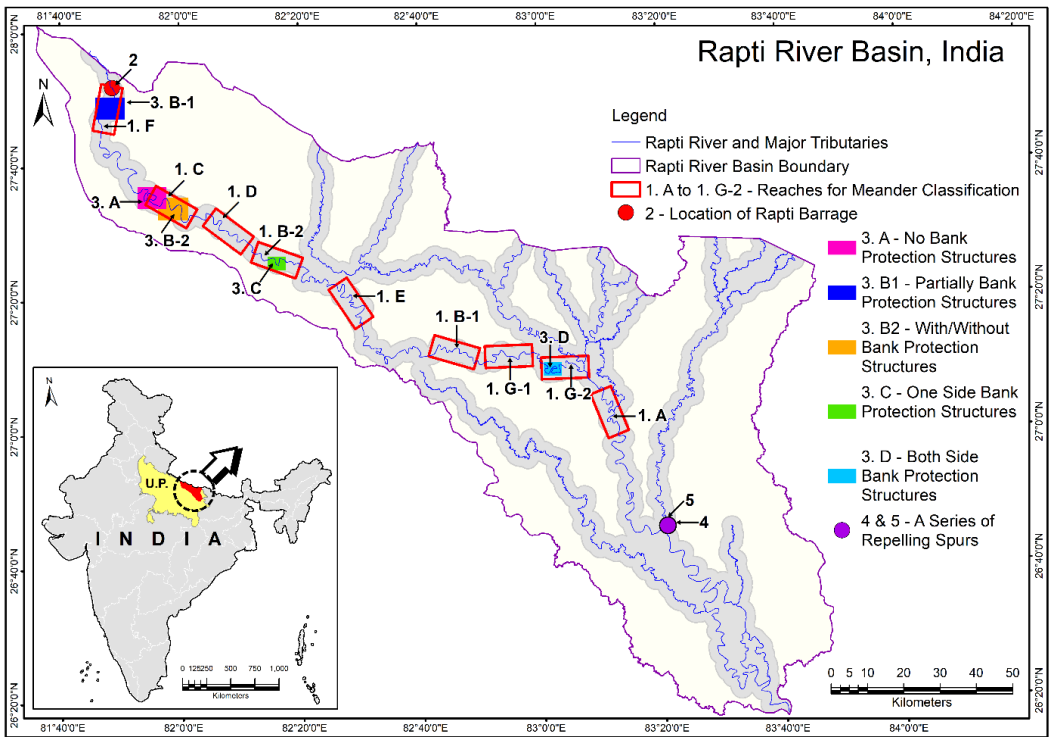


Figure 1. Location map of Rapti River Basin, India

3. Materials and Methods

3.1. Data used and sources

This study utilizes a range of spatial and temporal data sources to construct various thematic layers for the Rapti River system, which were integrated from satellite imagery, field surveys, and secondary data. The data sources and their descriptions are outlined below:

Satellite remote sensing data: multi-temporal, multi-spatial, and multi-spectral satellite remote sensing data spanning the entire Rapti River Basin from 1975 to 2024 were acquired from the U.S. Geological Survey (USGS) Earth Explorer platform. These data include Landsat imagery with a spatial resolution ranging from 30m to 60m, which were used to analyze land use changes, river morphology, and vegetation dynamics. The satellite images were carefully selected based on their temporal coverage and spatial alignment with the study area.

- Landsat-2 MSS: 1975
- Landsat-3 MSS: 1980
- Landsat-5 TM: 1988, 1990, 1998, 2004, 2006-2010
- Landsat-7 ETM+: 2001, 2011-2012
- Landsat-8 OLI: 2013-2024
- Source: U.S. Geological Survey Earth Explorer, http://earthexplorer.usgs.gov

Elevation data: Digital Elevation Model (DEM) data from the Advanced Land Observing Satellite (ALOS) Phased Array type L-band Synthetic Aperture Radar (PALSAR) was used to generate elevation and terrain information for the Rapti River basin. The DEM data, with a spatial resolution of 12.5 meters, were used to assess the topography of the river basin, identify slope variations, and derive hydrological and hydraulic models. This data provides critical information for understanding floodplain dynamics and the influence of elevation changes on river morphology.

- Source: ALOS PALSAR DEM Data, https://vertex.daac.asf.alaska.edu/
- Acquisition Date: 02 December 2007

River infrastructure data: Data on riverine infrastructure, including the locations and physical characteristics of bridges, embankments, spurs, and studs, were digitized using high-resolution satellite imagery from Google Earth©. These infrastructure elements are essential for understanding the impact of human interventions on the river system's hydrodynamics and sediment transport. The data was updated based on the most recent imagery available and provides detailed spatial coordinates of various river structures.

- Source: Google Earth© Satellite Imagery
- Acquisition Date: 26 September 2024

Barrage details: Information regarding the Rapti and Banganga barrages, including their locations and technical specifications, was obtained from the India-WRIS (Water Resources Information System) website. The data provided insights into the operational characteristics of the barrages, their role in flow regulation, sediment transport, and their influence on river morphology.

- Source: India-WRIS Website, http://indiawris.gov.in/wris/#/

Each of these data layers was processed and analyzed to provide a comprehensive understanding of the geomorphological processes within the Rapti River system, as well as the influence of infrastructure and hydrological modifications on its natural behavior.

3.2. Methodology

The methodology encompasses a comprehensive analysis of river morphology, focusing on the classification of meander bends, and assessing the impacts of hydraulic interventions such as barrages, embankments, and spur structures. Additionally, the development and morphological implications of embayments

between spur structures are systematically examined.

Classification of meander bends: Temporal changes in bankfull width and sinuosity were analyzed for nine meandering reaches of the Rapti River from 1992 to 2024 using Landsat satellite imagery and geospatial techniques. Meander patterns were classified based on modified Brice [84] criteria, with width measured at 1 km intervals and sinuosity calculated as the ratio of channel to valley length.

Several researchers have categorized river meanders according to their morphological processes and sinuosity characteristics [84-88]. The Rapti River system exemplifies a meandering river, and a modified version of the meander classification proposed by Brice [84] has been applied. The classification is largely derived from observational criteria and effectively distinguishes three levels of confinement commonly observed in meandering rivers. Nine types of meander patterns, as suggested by Brice, have been identified in the Rapti River system, as illustrated in Figure 2. Furthermore, the bankfull widths and sinuosity ratios of the selected nine river reaches were systematically analyzed.

.

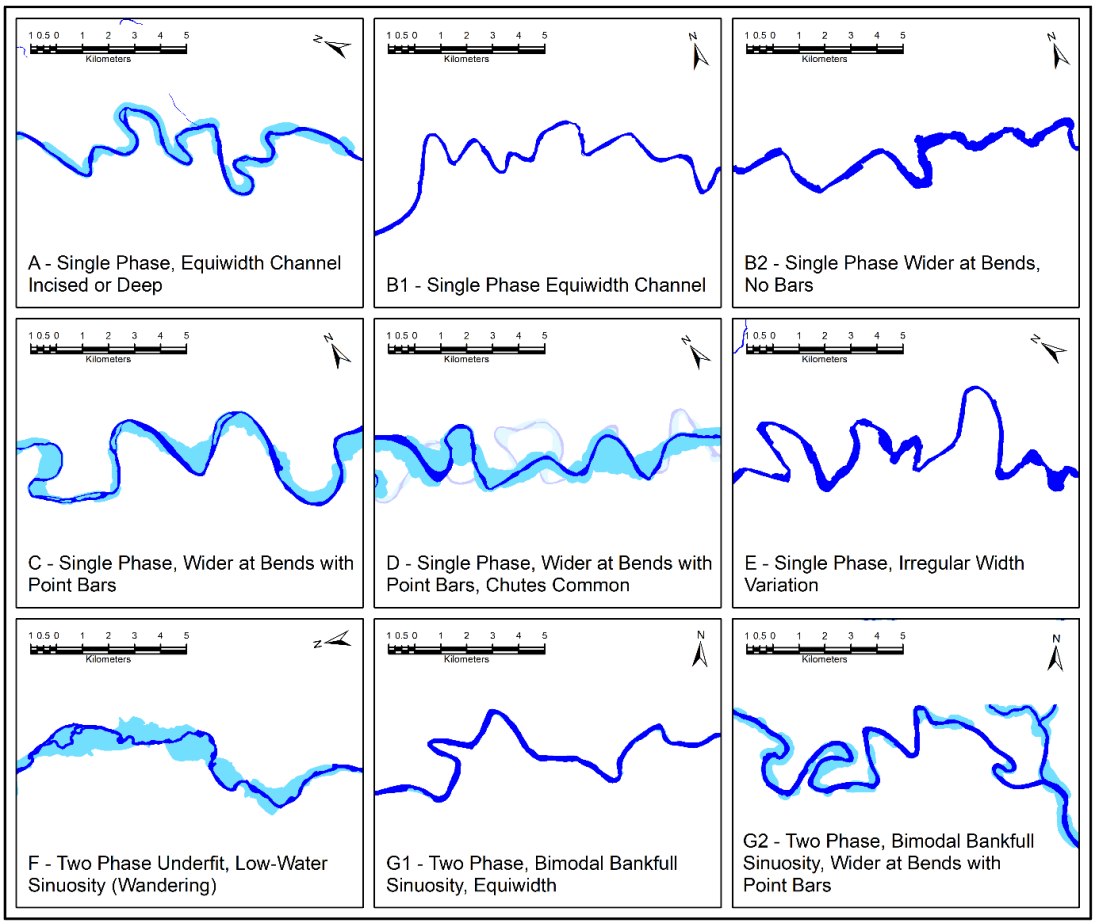


Figure 2. Modified Brice classification of Rapti river system

Sinuosity is a key index used to quantify river meandering and serves as a distinctive feature of river patterns [89-91]. It is intrinsically linked to the morphological, sedimentological, and hydraulic properties of alluvial channels [92]. Sinuosity has been widely employed in functional, comparative, and historical studies.

Sinuosity, defined as the ratio of channel length to valley length, quantifies the degree of curvature in a river's course when observed in plain view. According to Leopold [93], Schumm [85], and Chorley [94], a meandering reach is characterized by a sinuosity greater than 1.5. A ratio of 1 corresponds to a straight river course, while a sinuosity ratio between 1 and 1.5 indicates a sinuous course, and values ranging from 1.5 to 4 suggest a meandering course.

Impact of barrage on river morphology: The influence of the Rapti barrage on river morphology was analyzed using Landsat satellite imagery and geospatial techniques spanning 1975-2024. Remote sensing data were processed and interpreted within a GIS environment to assess temporal variations in channel planform and sediment dynamics. Pre- and post-installation periods revealed significant changes in meandering patterns, river width, and sediment deposition has been analysed.

Impact of embankment on river morphology: Morphological changes in the Rapti River system were analyzed using Landsat imagery (1975-2024), data, and geospatial techniques to evaluate the impacts of embankments. Remote sensing data were processed and interpreted within a GIS environment to extract planform changes, monitor sediment dynamics, and assess bankline shifts over time.

Channel stabilization and bank protection works, including embankments, groynes, spurs, and other structures, are used to control erosion and ensure flood safety [95-97]. While these measures address river instability, they also impact hydro-geomorphic processes [98-99]. They alter channel width, roughness, and bed slope, leading to changes in sediment transport, potential floodplain aggradation, riverbed erosion, and decreased water conveyance capacity [100-101]. Embankments and levees can exacerbate peak flows, causing downstream impacts [102].

Multi-temporal satellite imagery, including Landsat-2 MSS (1975), Landsat-3 MSS (1980), Landsat-5 TM (1990, 2000, 2003, 2006, and 2009), Landsat-7 ETM+ (2012), and Landsat-8 OLI (2015, 2018, 2021, and 2024) for pre-monsoon periods, were analyzed. Four distinct morphological active areas were identified: (i) Regions with partially implemented bank protection structures, (ii) Regions lacking bank protection measures, (iii) Regions with bank protection installed along one bank, and (iv) Regions with bank protection implemented on both banks. Erosion and deposition patterns, along with sinuosity indices, were assessed for these areas. The Rapti River, being morphologically dynamic, poses a flooding risk to surrounding areas in the absence of embankments, which limit bankline movement. This pattern was observed in several vulnerable regions.

Impact of spurs on river morphology: The impacts of spur structures on the Rapti River's channel morphology were assessed using GoogleEarth satellite imagery (2005-2024), field data, and geospatial analysis techniques. Remote sensing imagery was interpreted within a GIS environment to identify, map, and evaluate changes in bankline position, channel configuration, and sediment deposition patterns associated with spur construction. Of 187 identified spurs, 163 were under 90 m, limiting detailed visibility in satellite data.

Embayment development between spurs: The development of embayments between spur structures along the Rapti River was analyzed at Duhiya village near Gorakhpur using GoogleEarth satellite imagery (2005-2024), integrated with remote sensing and GIS techniques. Erosion, deposition, river segment lengths between spurs, and bankline migration rates were studied before and after the installation of five repelling spurs (2008-2009).

4. Result and discussion

4.1. Meander classification

Remote sensing data were processed and analyzed using ArcGIS 10.7 for automated planform extraction and spatial measurements. An inverse correlation

between bankfull width and sinuosity was observed in certain reaches, where wider channels displayed lower sinuosity. The application of remote sensing and GIS tools provided critical insights into the morphological dynamics influencing the Rapti River's meandering patterns over time.

The temporal variations in bankfull width and sinuosity ratio for nine selected meandering patterns of the Rapti River were analyzed using multi-temporal satellite remote sensing data. The study utilizes Landsat archive data spanning approximately thirty-three years (1992–2024) at a spatial resolution of 30 meters to assess temporal changes in the river's morphological characteristics. River width was measured at 1 km intervals along each of the nine defined river reaches, and the average widths are presented in Figure 3(a). In addition, channel and valley lengths were derived from satellite remote sensing data using ArcGIS 10.7, enabling the calculation of sinuosity ratios to evaluate meandering dynamics. The computed sinuosity ratios for each reach over the study period are summarized in Figure 3(b).

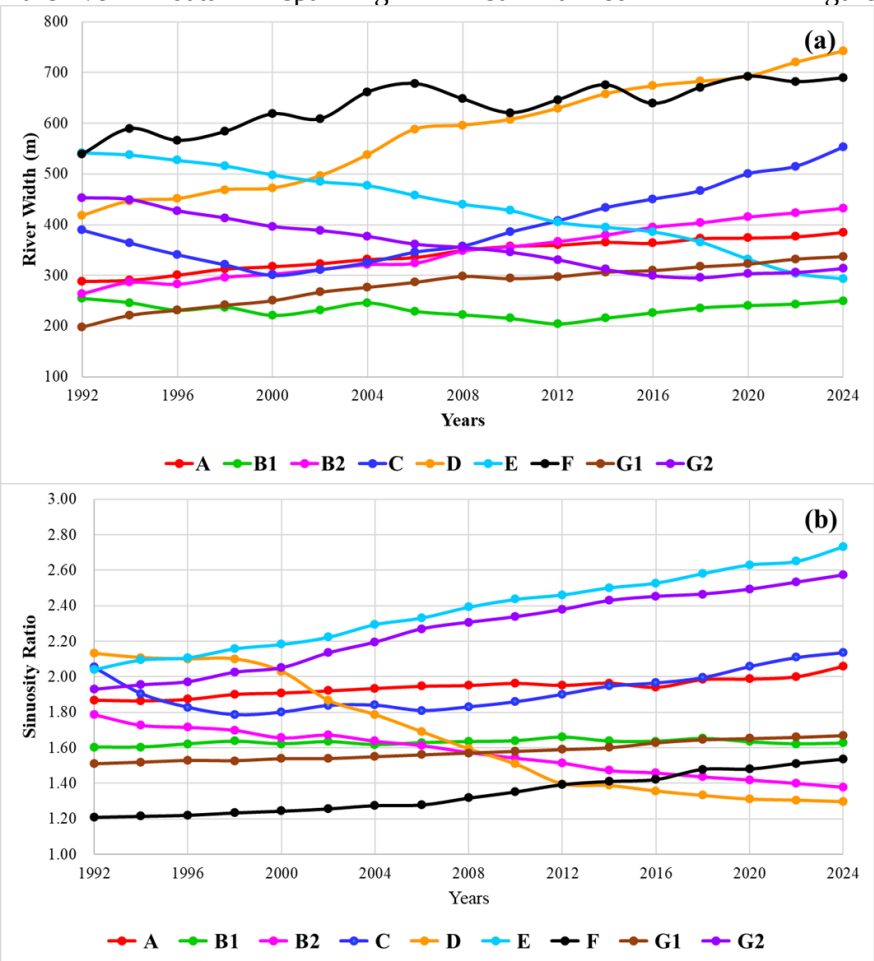


Figure 3. (a) Temporal changes in average river width (RW) and, (b) temporal progression of river sinuosity (SI) over the years

The evolution of bankfull river width in a meandering river is illustrated in Figure 3 (a), while the increasing sinuosity of the river over time is shown in Figure 3 (b), except for reach-E and reach-G2. Initially, the Rapti River exhibited low sinuosity (Si = 1.21 in 1992, reach-F). As the planform developed, the river valley length increased while the channel length remained relatively stable, resulting in a progressive increase in sinuosity, reaching a maximum value of

2.73 in reach-E by 2024. The analysis of bankfull river width and sinuosity ratio for each reach reveals a strong correlation between these two parameters.

According to Brice [103], stable meanders can be identified based on their width characteristics, particularly in equiwidth channels, as observed in reaches B1 and G1. Actively migrating channels generally display spatial variability in bankfull width, with the widest sections often occurring at bend apices, where curvature is most pronounced, and migration rates tend to be highest. Brice [103] and Lagasse [104] identified a distinct category of rivers where variations in bankfull width are independent of curvature, leading to reduced migration rates. Based on observations from nine reaches of the Rapti River, the following classifications for meandering river evolution are proposed: (i) rivers with minimal systematic width variation, (ii) rivers with apexes narrower than crossings, and (iii) rivers with apexes wider than crossings, with case (iii) being the most common in rivers exhibiting significant migration rates [104]. Observations indicate that the maximum bankfull width typically occurs downstream of the bend apex, while in some instances, the minimum width is found upstream. However, this pattern is not consistent across all cases, as illustrated in Figure 3 (a). A direct relationship between river width and sinuosity ratio was identified, wherein an increase in river width is associated with a decrease in sinuosity, and conversely, a decrease in width corresponds to higher sinuosity (see reach-B2, D, E, and G2, Table 3). Sinuosity tends to increase when the outer bank of a bend erodes faster than the inner bank, a process explained by alluvial meander theory in terms of hydraulic dynamics. Although channel narrowing was evident, particularly in Reach-D, the channel continued to increase in sinuosity until the initial formation of a neck cutoff.

Table 3. Correlation between bankfull river width and sinuosity ratio

S. No.	Adapted Brice classification of the Rapti River meandering patterns.	Bankfull river width		Sinuosity ratio	
		Width#	In/St/De*	Sinuosity#	In/St/De*
A	Single-phase, uniform-width channel characterized by incision or significant depth.	M	In	M	St
B_1	Single-phase channel with uniform width.	L	St	M	St
B_2	Single-phase channel with increased width at bends and absence of bars.	L	In	H	De
C	Single-phase channel characterized by increased width at bends and the presence of point bars.	M	In	H	In
D	Single-phase channel exhibiting greater width at bends, characterized by the presence of point bars and frequent chutes.	M->H	In	H->L	De
E	Single-phase channel with irregular variations in width.	H->L	De	H	In
F	Two-phase underfit channel with low-water sinuosity, exhibiting a wandering pattern.	H	In	L	In
G_1	Two-phase channel with bimodal bankfull sinuosity and uniform width.	L->M	St	L	St
G_2	Two-phase channel with bimodal bankfull sinuosity, exhibiting greater width at bends and the presence of point bars.	M->L	De	H	In

*Increasing (In) / Stable (St) / Decreasing (De) order. # H = High, M = Medium, L = Low

4.2. Impact of Rapti barrage on the river morphology

Upstream, the river transitioned from a meandering to a more straightened flow, gradually reverting to a meandering state, while downstream shifts in meandering direction were constrained by riparian vegetation. Disturbances in sediment transport and deposition were prominent between 1981 and 2005, stabilizing post-2006. The analysis highlights potential long-term impacts of the barrage, including sediment accumulation upstream, reduced water velocities, and enhanced downstream erosion caused by the release of sediment-depleted water. The application of remote sensing and GIS provided a robust framework to detect and quantify these

morphological transformations over time.

River width upstream and downstream of the Rapti barrage was analyzed before and after its construction. Prior to the barrage installation, the river width was relatively consistent. Disturbances began in 1981 with the start of barrage construction, and it took approximately 25 years (until 2006) for the river to readjust. After 2006, the river width upstream and downstream became more balanced (Figure 4 a). Geomorphic response times to river engineering works vary, typically requiring 20 to 100 years for the river to reach a new equilibrium, depending on the extent of flow alterations, sediment supply, and vegetation cover. Sediment deposit upstream and downstream of the Rapti barrage was analyzed. From 1981 to 2005, sediment deposition was disrupted, with increased deposition upstream and reduced deposition downstream. However, between 1975-1980 (pre-barrage) and 2006-2024 (post-barrage), sediment deposition patterns were more-or-less balanced upstream and downstream (Figure 4 b), supporting the previous observations.

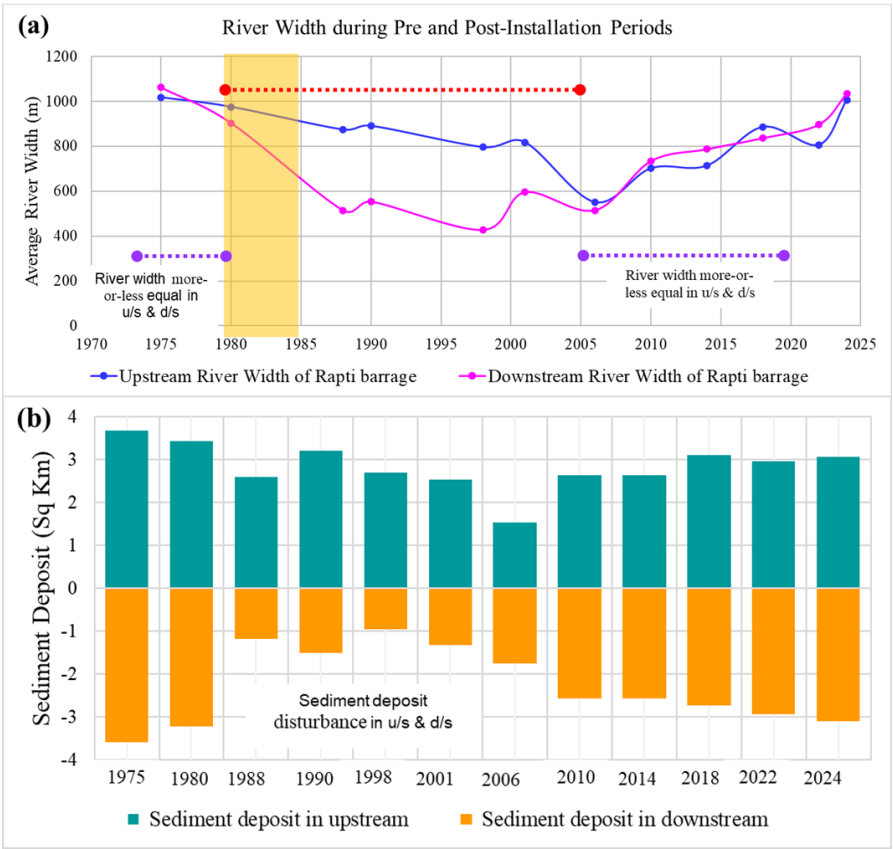


Figure 4. (a) Variation in river width before and after the installation of the Rapti Barrage, and (b) Sediment deposition patterns upstream and downstream of the Rapti Barrage

Prior to the construction of the barrage, the Rapti River exhibited a uniform channel width of approximately 1000 meters both upstream (U/S) and downstream (D/S). However, following the commencement of barrage construction, a divergence in channel width between the upstream and downstream sections became evident. The downstream width progressively decreased relative to the upstream width, reaching a maximum disparity of approximately 400 meters in 1998. By 2006, this difference further widened, with the upstream width exceeding the downstream width by nearly 800 meters. Projections indicate that by 2024, the downstream width is expected to

revert to its pre-construction condition, aligning with the width observed in 1975.

4.3. Impact of bank protection structure - embankment on channel morphology

Erosion, deposition, and sinuosity dynamics were examined across four zones: unprotected areas, partially protected sections, one-sided protection, and fully embanked stretches. A detailed 25 km river segment was divided into five sections for comparative analysis of pre- and post-embankment conditions. Results showed reduced meandering and localized erosion near embankments, while downstream areas experienced intensified erosion and altered sediment deposition due to modified flow dynamics. The integration of remote sensing and GIS enabled a systematic evaluation of spatial-temporal morphological responses to embankment interventions. The different types of morphological active areas are illustrated in Figure 5.

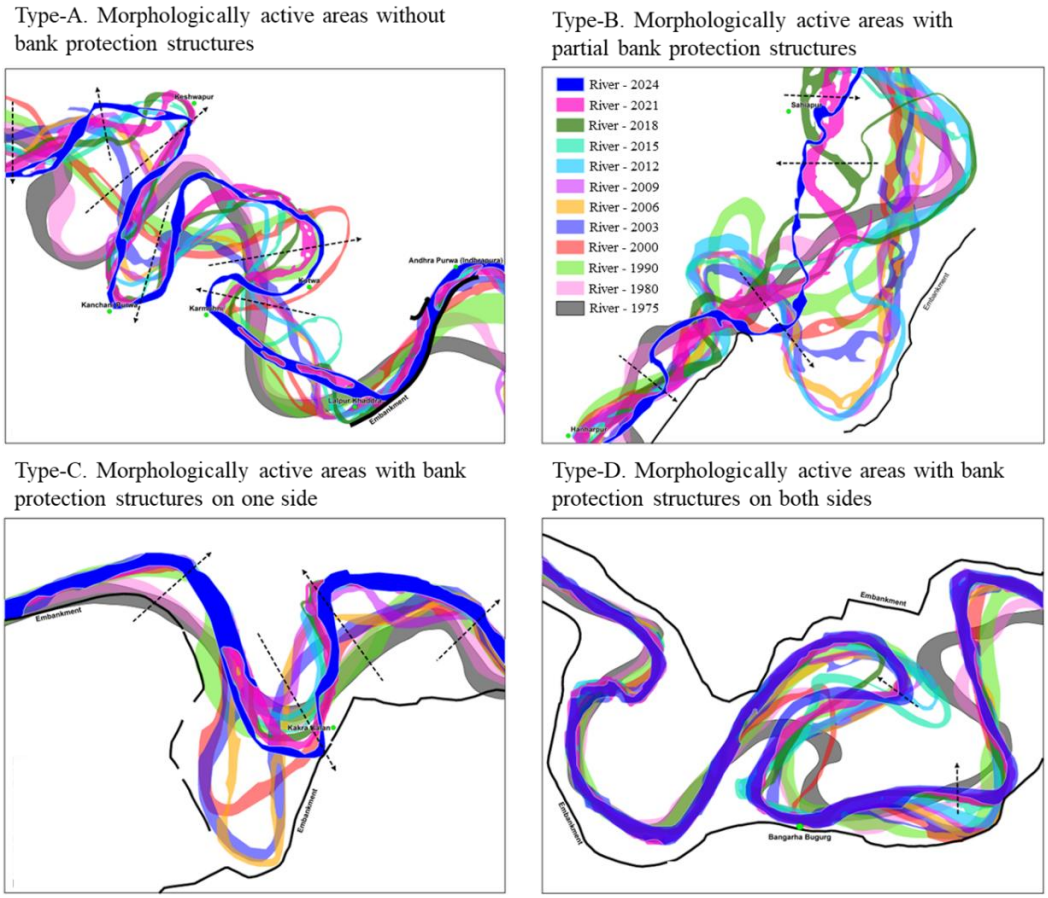


Figure 5. Four distinct morphological activity zones within the Rapti River system

It was observed that embankments restrict the Rapti River from meandering to the left or right. In areas without embankments, the river exhibits a greater tendency to meander freely. In multiple flood-prone areas, embankments restrict the natural meandering dynamics of the river, thereby safeguarding settlements and agricultural land from erosion and inundation. In certain areas, where embankments are present on both sides, the river's meandering occurs within the confines of the embankments. These embankments prevent the river from altering its course beyond their boundaries, thus safeguarding the land outside from

flooding and submergence. Consequently, embankments on both sides of the river effectively limit its meandering to within the embankment limits. Statistical analysis and graphical representations of erosion/deposition patterns and sinuosity indices for four types of morphological active areas. Figure 6 illustrates the classification of morphological activity zones within the Rapti River system, categorized as follows: (i) partially protected regions, (ii) unprotected regions, (iii) areas with bank protection on one side, and (iv) areas with bank protection on both sides.

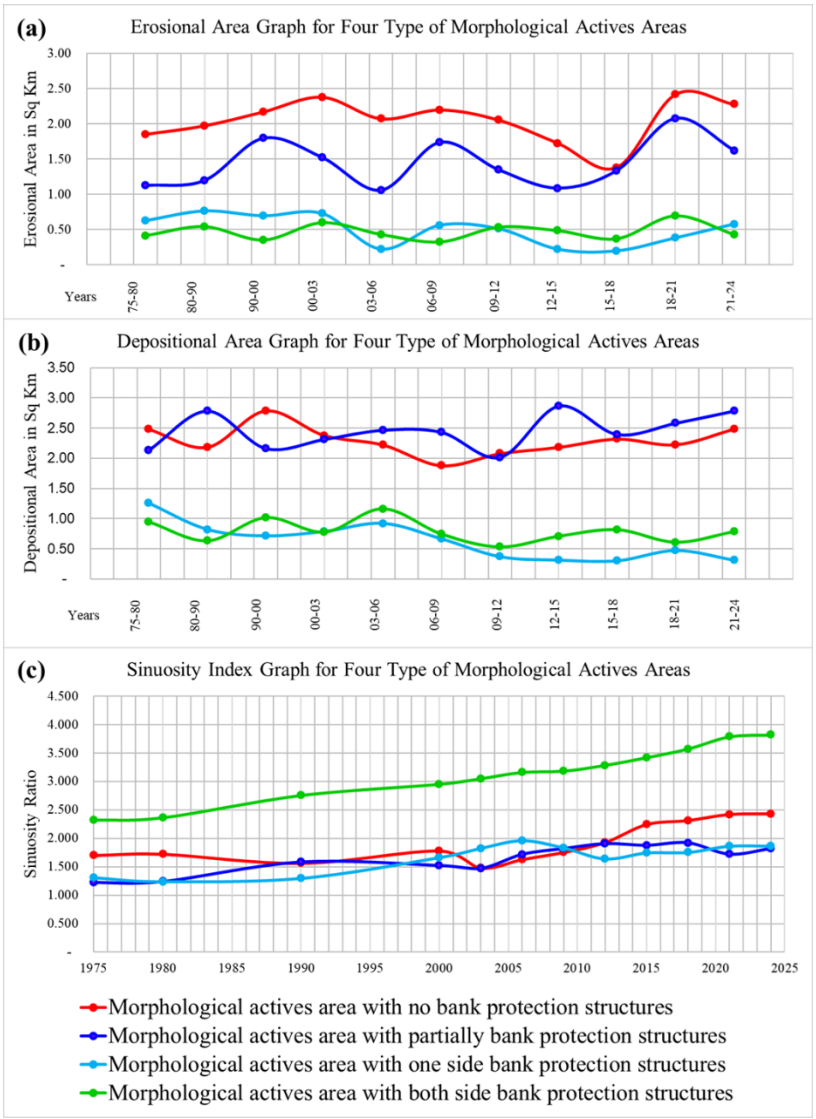


Figure 6. Analysis of (a) erosion patterns, (b) sediment deposition, and (c) sinuosity index across four distinct morphological activity zones within the Rapti River system.

The evaluation of the presented figures demonstrates notable correlations among the four distinct morphological activity zones, as summarized in Table 4.

Table 4. Key relationships among the four types of morphological active areas

S. No.	Categories of morphological active areas and their parameters	Erosion	Deposition	Sinuosity index
1	Morphologically active areas without bank protection structures	High	High	Low
2	Morphologically active areas with partial bank protection structures	Moderate	High	Low
3	Morphologically active areas with bank protection structures on one side	Low	Low	Moderate
4	Morphologically active areas with bank protection structures on both sides	Low	Low	High

Morphologically active areas lacking bank protection structures - such as embankments, spurs, or studs - exhibit significant fluvial dynamics characterized by intense lateral erosion and sediment deposition. The absence of confinement allows for unrestricted channel migration, promoting the formation of broad meander loops between natural or anthropogenic stabilization points, and yielding a lower sinuosity index (Table 4). In areas with partially bank protection, structures interventions constrain the river's lateral mobility only at select locations. This localized confinement results in upstream and downstream morphological instability, marked by moderate bank erosion and substantial sediment deposition. Consequently, the channel develops moderate to large meander loops, maintaining a low sinuosity index.

Where bank protection is present unilaterally, channel migration is impeded on the protected bank while remaining unrestricted on the opposite side. This asymmetrical constraint induces differential morphological evolution, limiting erosional and depositional processes along the protected margin. The resulting adjustment in flow direction and sediment transport dynamics typically produces a moderate sinuosity index.

In fully confined reaches, where embankments are present on both banks, lateral channel migration is substantially restricted. This confinement minimizes fluvial erosion and deposition beyond the embankments. However, despite these structural controls, the highly dynamic nature of the Rapti River permits limited in-channel adjustments. Analysis of temporal changes from 1975 to 2024 reveals an increasing trend in channel sinuosity, attributed to elevated discharge events and continued meander development within the confined corridor. Therefore, the sinuosity index in these reaches is projected to remain high due to persistent intra-embankment morphological activity.

From 1975 to 2024, the sinuosity index exhibited an increasing trend across all four morphological activity types. Among these, reaches with partially bank-protected structures recorded the lowest average sinuosity index (1.665), indicating relatively less channel meandering. In contrast, reaches confined by bank protection structures on both sides exhibited the highest average sinuosity index (3.139), reflecting a pronounced increase in meandering despite structural constraints.

A 25 km river segment, comprising 12 km upstream and 12 km downstream of the Right-Balrampur embankment, was selected to assess the embankment's influence on river morphology. Constructed between 2004 and 2007, this embankment is situated upstream of the Aghenpurwa Bridge in Sidharth Nagar district. Composed of earthen materials with boulder pitching, the embankment divides the study reach into five equal 5 km sections: Sections A and B are upstream, Section C aligns with the embankment location, and Sections D and E are downstream. Statistical analyses, along with graphical representations of erosion-deposition trends and sinuosity index, were conducted for both the pre-installation (1975–2004) and post-installation (2007–2024) periods, as illustrated in Figure 7.

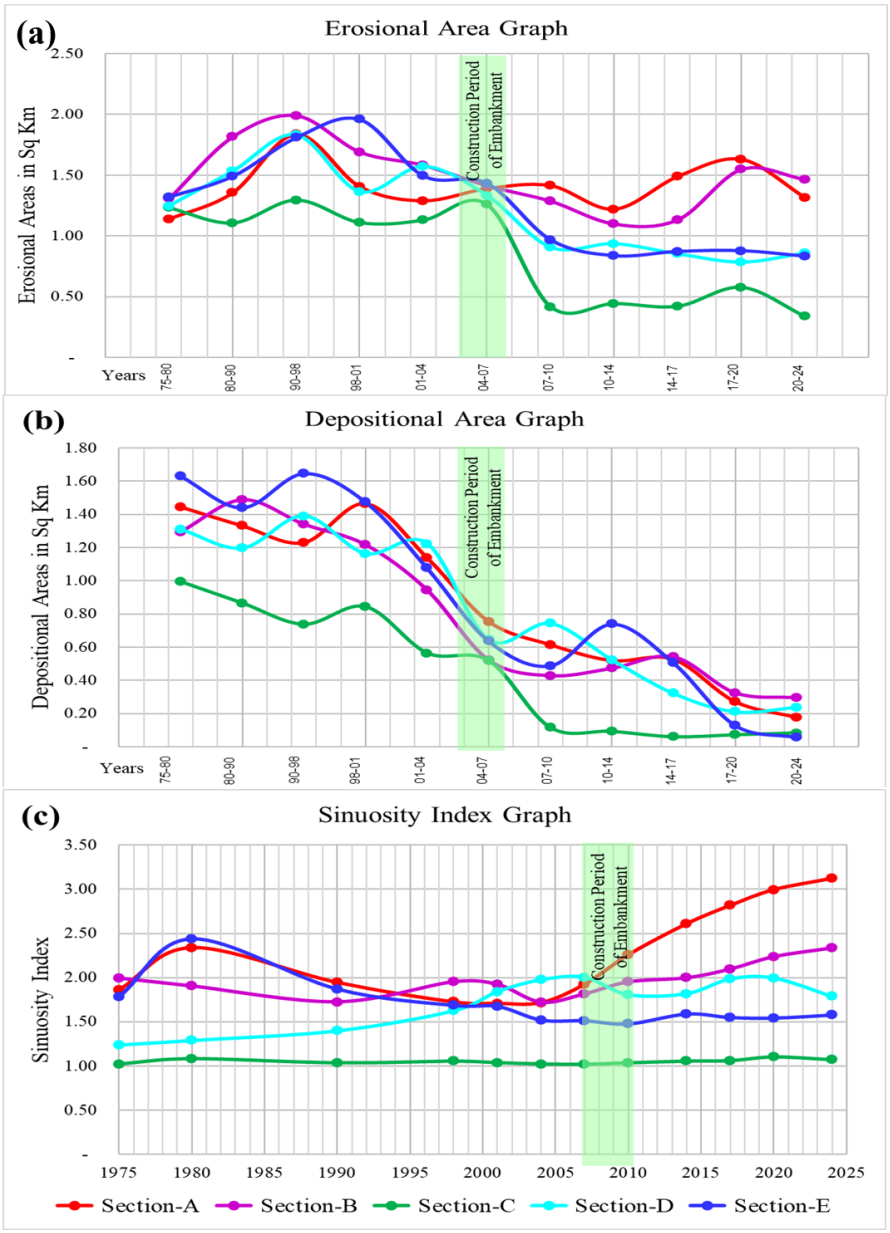


Figure 7. (a) Erosion, (b) sediment deposition, and (c) sinuosity index analysis for evaluating the impact of embankment construction on river morphology

Prior to the construction of the embankment, the erosion pattern within the studied river segment exhibited irregular behavior, enabling the Rapti River to erode different land areas. After the embankment was installed (2004–2007), erosion upstream (Sections A and B) decreased but mostly remained unaffected. In Section C, where the embankment is located, the erosion process significantly reduced, as the embankment restricted the river's meandering. In the downstream sections (D and E), comparable patterns were observed, with the river experiencing greater impacts than the upstream sections due to modifications in flow dynamics and direction. These changes compelled the river to develop moderate to large meandering loops. In terms of deposition, a noticeable reduction was observed downstream, particularly in Section C, where deposition decreased substantially.

The embankment influenced deposition downstream, with no significant change observed upstream, indicating that embankments promote erosion downstream. Changes in the sinuosity index were significant post-installation. In Sections A, B, and D, the sinuosity index increased, reflecting changes in water flow and direction caused by the embankment, leading to the formation of moderate-to-large meandering loops. In Section C, where the river became relatively straight, the sinuosity index remained near 1.0, indicating limited meandering.

Prior to the construction of embankments, the Rapti River exhibited a relatively low average sinuosity index of 1.64. Following the implementation of embankment structures, the average sinuosity index increased to 1.83, indicating enhanced meandering within confined boundaries. Spatially, the sinuosity index is higher in sections A, B, and C (1.93) compared to sections D and E (1.72), suggesting varying degrees of channel adjustment along different reaches.

Furthermore, the embankment construction has significantly mitigated fluvial dynamics, leading to a marked reduction in both erosion and deposition rates. The average annual erosion decreased from 1.05 km²/year to 0.38 km²/year, while deposition declined from 1.22 km²/year to 0.37 km²/year post-embankment construction, highlighting the stabilizing influence of these structural interventions on river morphology.

4.4. Impact of bank protection structure - Spurs on channel morphology

A critical site at Duhiya, near Gorakhpur, was analyzed, focusing on a 2.1 km segment divided into seven sections. Spurs constructed between 2008 and 2009 reduced erosion along the left bankline downstream, promoted upstream deposition, and redirected flow, intensifying erosion on the right bankline downstream. Deposition was most pronounced where spurs were arranged in ascending order. The integration of remote sensing and GIS allowed for a spatially explicit assessment of morphological responses to spur interventions.

Spurs are structures constructed perpendicular or at an angle to the dominant flow direction along the riverbank, designed to achieve several objectives [105-107]. They guide the river along a specified course, reducing the concentration of flow at vulnerable points and directing the flow's axis [108-109]. Spurs also create areas of slack flow, promoting sediment deposition near the riverbank and assisting in bank stabilization [110-111]. Additionally, they protect eroding banks by diverting flow away from them, facilitate sediment deposition where necessary, and trap bed load to encourage the formation of new riverbanks [112].

Data on spurs, including their locations and lengths, was obtained from the Irrigation and Water Resources Department of Uttar Pradesh for the Rapti River system. The records show a total of 187 spurs, with 163 of these having a length of less than 90 meters (approximately three pixels in Landsat-8 imagery), which makes identification on satellite images difficult. When these structures were overlaid on Google Earth, 32 spurs were not visible above the water surface, possibly having been washed away by the flow. Due to this, Google Earth satellite imagery was used for the analysis; however, continuous imagery from 2006 to 2024 was not available for the study area. Consequently, Duhiya (Harijan Basti) near Gorakhpur was identified as a critical site for analysis due to the availability of extensive satellite imagery from Google Earth. Between April 2008 and March 2009, a series of five repelling spurs were constructed along a 300-meter stretch adjacent to the Maloni embankment. These structures were designed to alter flow direction, induce sediment deposition, and reduce flow velocities along the riverbank. For the analysis, a 2.1 km river segment was selected, extending 900 meters upstream and 900 meters downstream from

the spur series. The segment was divided into seven equal sections to assess erosion and deposition patterns. Statistical analyses and graphical representations of erosion and deposition patterns along the right and left banklines across all seven sections were conducted, as illustrated in Figure 8.

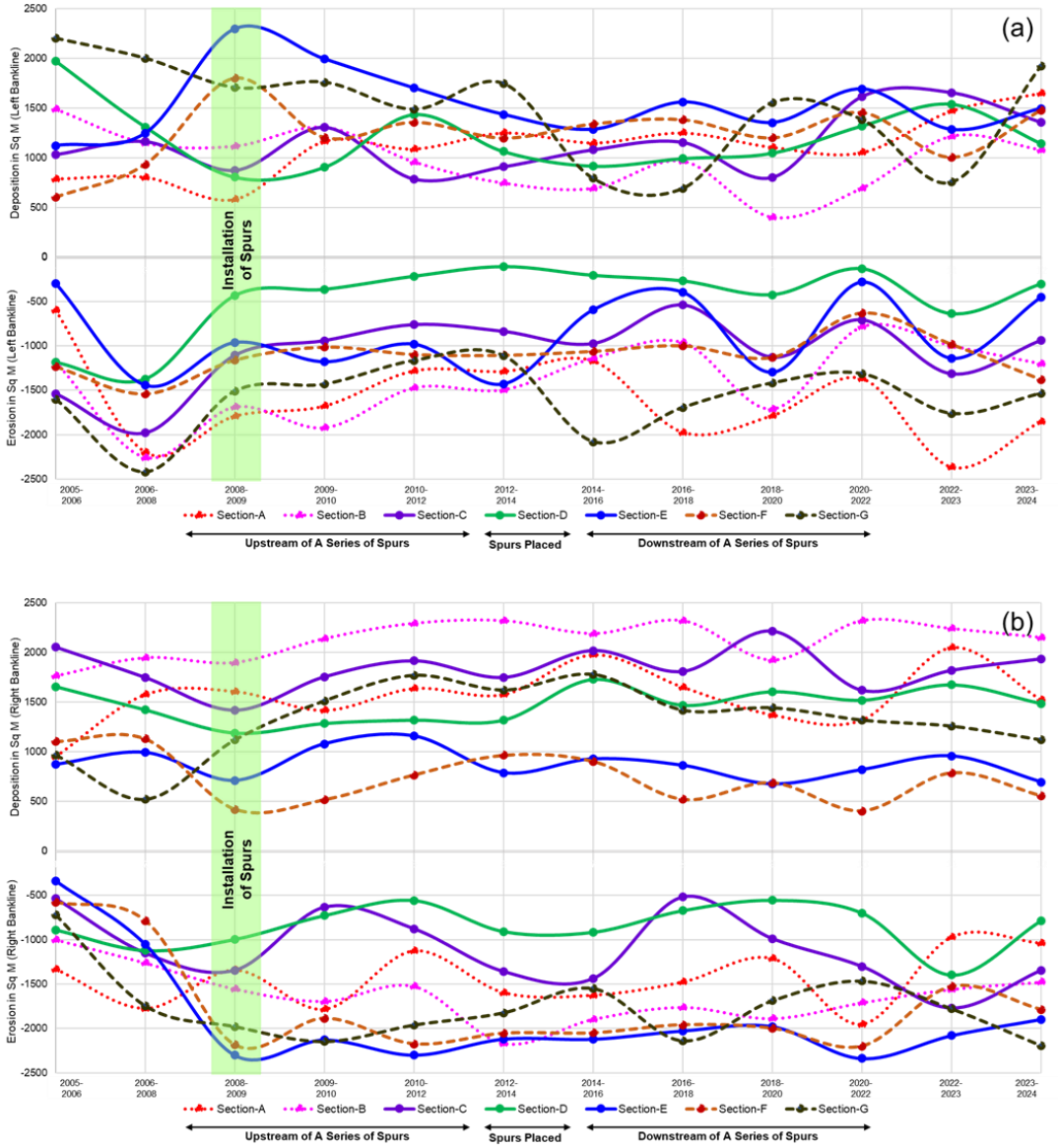


Figure 8. Erosion and deposition patterns along (a) the left bankline and (b) the right bankline

A detailed analysis of erosion and deposition patterns from 2005 to 2024 across the seven sections revealed that deposition predominates in Section-A and Section-B on the right bank (upstream of the spurs), and in Section-F and Section-G on the left bank (downstream of the spurs). Erosion is more prominent in Section-E and Section-F on the right bank (downstream of the spurs). Prior to the installation of the repelling spurs in 2008, erosion and deposition patterns exhibited a zigzag trend without a clear direction. After the installation, erosion significantly reduced in Section-D, particularly on the left bankline (where the spurs were located), as the spurs altered flow dynamics, moving erosive forces away from the bank. The sequential installation of spurs in ascending order led to

increased sediment deposition compared to the reverse arrangement. Along the right bankline, moderate erosion was observed in Section D, while more pronounced erosion occurred in Sections E, F, and G. This pattern is due to the redirected water flow from the left bank, which increased erosion on the right bank, especially in the narrow sections (40-50m wide) of Section-D.

4.5. Formation of embayments between spurs

The analysis, covering three years prior and fourteen years post-installation, divided the river into six sections, with Section-A identified as critical due to its proximity to the first spur. Results highlighted significant alterations in bankline migration and sediment dynamics across the sections.

Spurs are typically constructed in a sequential arrangement to optimize their effectiveness, with each structure facilitating the development of embayments between adjacent spurs [113-114]. These embayments significantly influence flow dynamics and sediment transport, both within the embayment and along the main river [115-116]. Generally, spur dikes reduce flow velocity, leading to sediment deposition between them [117]. As an indirect bank protection method, spur dikes deflect currents away from the bank or reduce flow velocity, thus offering protection against erosion [118]. The key parameters used to describe embayment development are illustrated in Figure 9.



Figure 9. Embayment formation between spurs

GoogleEarth satellite imagery from 2005 to 2024 was utilized to analyze a series of five repelling spurs located at Duhiya (Harijan Basti) near Gorakhpur town, installed between 2008 and 2009. Time-series data spanning three years before and nine years after the spur installation were used to assess erosion/deposition patterns, river segment length between spurs, and bankline migration rates. The spur series was categorized into six sections (A, B, C, D, E, F), with Section A positioned at the critical location where the initial spur is constructed, directly impacting flow

dynamics. The statistical analysis and graphical representation of erosion and deposition patterns for these sections are illustrated in Figure 10.

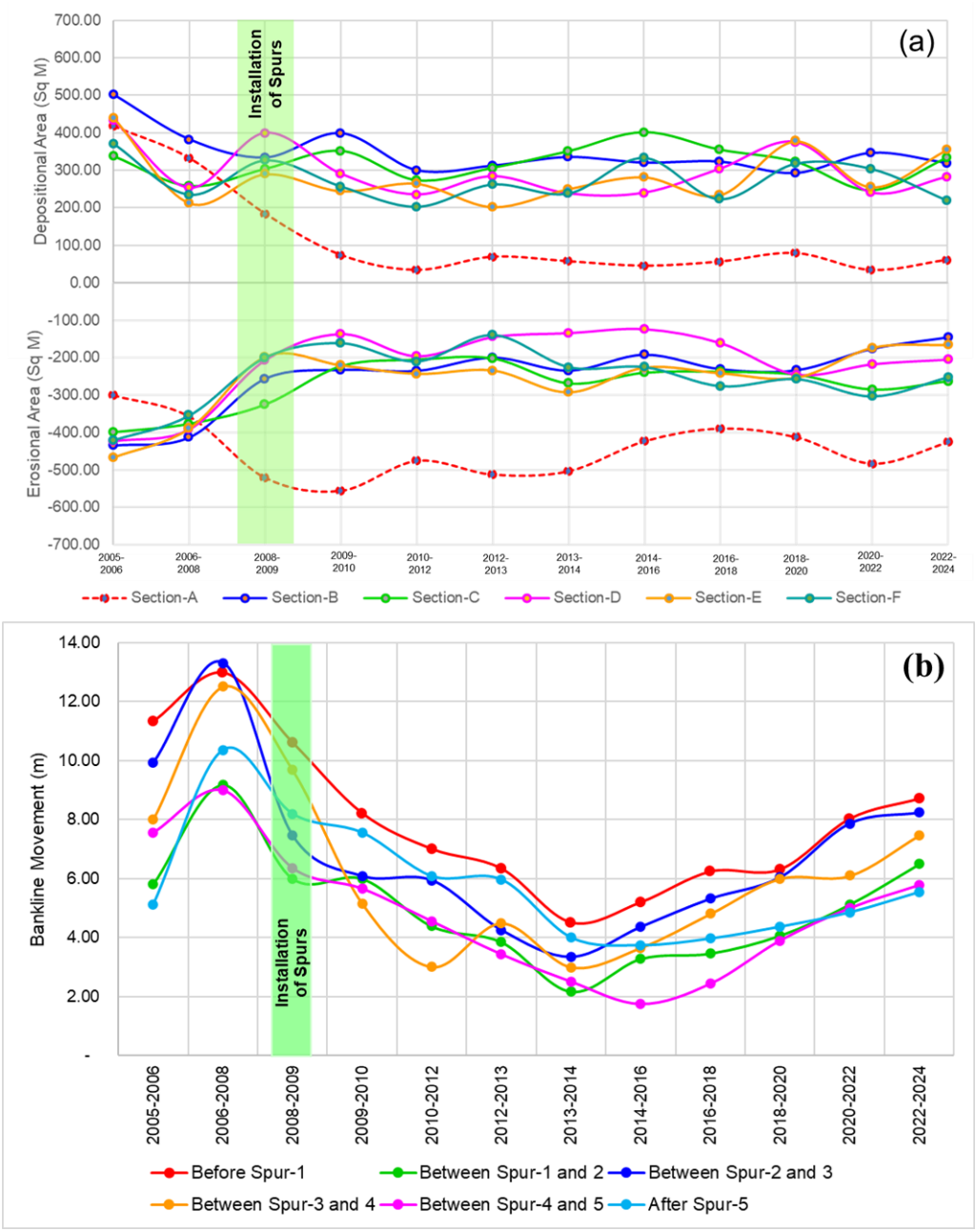


Figure 10. (a) Patterns of erosion and deposition, and (b) Bankline migration in the vicinity of the spur series

Figure 10 (a) shows that before the spur construction (2008-2009), Section-A experienced significant erosion and minimal deposition. After the installation of the spurs, erosion decreased, and deposition increased. Bankline migration analysis reveals that prior to spur construction, the bankline eroded at 13.73 m/year. Following spur installation, erosion slowed to 4.71 m/year, as observed from GoogleEarth images (2005-2024). However, recent images (2015-2024) indicate that erosion has intensified near spur-1, particularly towards the embankment. The analysis of

all five spurs indicates a progressive lateral shift of the river towards the embankment, with an estimated bankline erosion rate of approximately 5.13 m/year (Figure 10 (b)).

Following the construction of spurs 1 to 5, embayments progressively formed between these structures, becoming more distinct in the years 2010 and 2012. Sedimentation between the spurs increased, and over time, the river's course sometimes shifted abruptly due to high sediment flux. Analysis of historical Google Earth imagery reveals a shift in erosion dynamics and bankline migration following the implementation of bank protection structures. Before the installation of spurs (2005–2009), the average rate of bankline migration was 13.51 m/year. However, after the installation of spurs (2010–2024), this rate significantly declined to 4.22 m/year.

5. Discussion

Multiple studies [119-122] and institutional reports [123-126] have indicated that the construction of the Rapti Barrage (Laxmanpur Barrage) is inconsistent with established international regulations. Nepalese communities argue that the barrage was built only 4.5 km from the Nepalese border, whereas international standards require it to be at least 16.5 km away. These studies attribute the escalation of flood events, intensified bank erosion, elevated sediment loads, and alterations in river course dynamics in Nepal to the construction and operation of the Rapti Barrage. Furthermore, it is argued that the construction of the Rapti Barrage, along with the Kalkaluwa afflux bund, has intensified these challenges by impeding the natural drainage of the West Rapti River [127]. However, it is essential to recognize that the Rapti River basin, extending across both India and Nepal, is inherently susceptible to flooding.

The following factors substantiate this assertion: (i) the Rapti Barrage (Laxmanpur Barrage) is situated 4.5 km downstream of the India-Nepal border, with the submergence zone confined to Indian territory; (ii) the barrage functions as a diversion structure for non-monsoon flows rather than a storage reservoir, facilitating unimpeded water passage during flood events without elevating water levels or exacerbating inundation; (iii) the full reservoir level (pond level) of the Rapti Barrage is 127.60 m above mean sea level (amsl), whereas the general ground elevation on the Nepalese side is 131.00 m amsl, which exceeds the pond level; and (iv) the barrage remains non-operational, as the gates have not been lowered.

Prior to the construction of the Rapti Barrage, the river exhibited a meandering pattern, with a noticeable rightward shift in its upstream course, as observed in satellite imagery from 1975 and 1980. Following the barrage installation, the upstream river channel underwent straightening, as evident in the 1988 and 1990 images. However, in the subsequent years, the river gradually reverted to a meandering morphology. Additionally, before the barrage was constructed, the river made a pronounced 90° rightward bend approximately 5 km downstream. After the barrage installation, the river shifted left but was restricted by riparian vegetation and afforestation (evident in the 1988 imagery). Beyond this vegetative zone, the river adopted a zigzag meandering pattern. Over time, the river gradually moved away from the vegetation, but by 2017, downstream meandering decreased.

The operation of the Rapti barrage will lead to significant changes in river morphology both upstream and downstream. Upstream, reduced water velocities will cause increased sediment accumulation, lowering the riverbed and promoting channel widening or braiding [128-130]. Downstream, the release of sediment-free water will carry more energy, leading to erosion of the channel bed and banks. This "hungry water" will erode the river system, resulting in bed incision and widening, with the river gradually re-adjusting to a new characteristic state over a period of 20 to 100 years.

Sarif et al. [131] conducted a comprehensive morphological assessment of the Ganga River in the vicinity of the Farakka Barrage, the construction of which began in 1961 and was completed in 1975. Their analysis focused on planform dynamics, particularly the sinuosity index, which was observed to range between 1.19 and 1.24 during the period 1965–2017. These values indicate that the Ganga River maintained a sinuous channel pattern in the Farakka region. The study also revealed spatial variations in erosion and deposition patterns before and after barrage construction. Specifically, prior to construction, upstream reaches exhibited relatively low erosion, whereas following the commissioning of the barrage, erosion significantly decreased in the downstream reaches. Conversely, sediment deposition in the upstream decreased after construction, while erosion intensified downstream. These findings closely align with observations from the Rapti River study, where post-construction alterations in flow regime and sediment dynamics led to comparable changes in channel morphology.

6. Conclusion

This study employs remote sensing and Geographic Information System (GIS) techniques extensively for analyzing the Rapti River system. Free Landsat series satellite imagery from 1972 to 2024, provided by the United States Geological Survey (USGS), has been utilized, which is widely accessible and has become a standard tool for monitoring global environmental changes. These satellite images facilitate the generation and analysis of long-term time series data, extending over the past five decades. Various segments of the Rapti River were selected for detailed analysis, focusing on different aspects of river morphology and dynamics. The study encompasses meander classification, an assessment of the Rapti Barrage's influence on the river system, an evaluation of the effects of bank protection measures—including embankments, spurs, and studs—on channel morphology, and an investigation into the formation of embayments between successive spur structures. The time span of the analysis covers the period from 1975 to 2024, using Landsat satellite imagery to monitor and quantify these changes over time.

The Rapti River has been classified into nine distinct meander patterns based on morphological processes and sinuosity characteristics. A detailed assessment of bankfull river width and sinuosity ratio has been performed for all nine meander types, resulting in the identification of significant correlations between these morphological parameters. The study also examined the river width and sediment deposition both upstream and downstream of the Rapti Barrage before and after its construction. Prior to the barrage installation, the river width upstream and downstream was nearly equal. However, disturbances began when the construction of the barrage commenced in 1981. It took approximately 25 years (until around 2006) for the river to readjust to its new morphological state. Post-2006, the equilibrium between upstream and downstream river width was largely reestablished, suggesting that the geomorphic response time to river engineering interventions is influenced by the type of modifications and their effects on flow dynamics, stream power, sediment transport, and vegetation cover. Achieving a new characteristic state may take anywhere from 20 to 100 years, depending on the extent of the engineering works.

The impact of bank protection structures on channel morphology was investigated by studying four types of morphological active areas: those without bank protection, partially protected areas, areas with one-sided protection, and areas with protection on both sides. Significant relationships were established between these four types of areas. The findings provide valuable insights into regions requiring immediate flood protection intervention, facilitating the efficient allocation of resources for river training and flood protection measures. This

study offers essential data for effective budget planning and prioritization of flood protection infrastructure.

Acknowledgment

Authors are grateful to Managing Director, DHI (India) Water & Environment Pvt Ltd, New Delhi. India for providing the necessary facilities to carry out this work.

Declations

Funding Statement: This research was conducted without any external funding.

Conflict of Interest: The authors declare that they have no conflict of interest.

AI Statement: The authors did not use any AI tools or services in the preparation of this work.

Author Contributions: All authors contributed to the study's conception and design. Material preparation, data collection, and analysis were conducted by Kuldeep Pareta (KUPA) and Upasana Pareta (UPPA). KUPA drafted the initial manuscript, and all authors reviewed and provided feedback on previous versions. All authors have read and approved the final manuscript.

References

1. Kleinhans MG, McMahon WJ, Davies NS. What even is a meandering river? A philosophy-enhanced synthesis of multilevel causes and systemic interactions contributing to river meandering. Geol Soc Lond Spec Publ. 2024;540:43–74. https://doi.org/10.1144/sp540-2022-138
2. Best J. The fluid dynamics of river dunes: A review and some future research directions. Earth Surf Process Landforms. 2005;110(F4). https://doi.org/10.1029/2004JF000218
3. Hooke J. River meander behaviour and instability: a framework for analysis. Geomorphology. 2003;28(2):238–53. https://doi.org/10.1111/1475-5661.00089
4. Koutalakis P, Gkiatas G, Xinogalos M, Iakovoglou V, Kasapidis I, Pagonis G, et al. Estimating stream bank and bed erosion and deposition with innovative and traditional methods. Land. 2024;13(2):232. https://doi.org/10.3390/land13020232
5. Güneralp İ, Marston RA. Process–form linkages in meander morphodynamics: Bridging theoretical modeling and real-world complexity. Prog Phys Geogr Earth Environ. 2012;36(6):718–46. https://doi.org/10.1177/0309133312451199
6. Vázquez-Tarrío D, Ruiz-Villanueva V, Garrote L, Benito G, Calle M, Lucía A, et al. Effects of sediment transport on flood hazards: Lessons learned and remaining challenges. Geomorphology. 2024;446:108976. https://doi.org/10.1016/j.geomorph.2023.108976.
7. Leopold LB, Wolman MG. River meanders. Bull Geol Soc Am. 1960;71(6):769–94.
8. Edwards BF, Smith DH. River meandering dynamics. Phys Rev E. 2002;65:1–12.
9. Hooke JM, Yorke L. Rates, distributions and mechanisms of change in meander morphology over decadal timescales, River Dane, UK. Earth Surf Process Landforms. 2011;35:1601–14.
10. Stolum HH. Planform geometry and dynamics of meandering rivers. Geol Soc Am Bull. 1998;110(10):1485–98. https://doi.org/10.1130/0016-7606(1998)110
11. Sahoo S, Sharma A. Turbulent flow mechanisms in meandering channels with sediment transport. Water Pract Technol. 2023;18(3):484–500. https://doi.org/10.2166/wpt.2023.035

12. Yılmazer C, Arı Güner HA. Physical and numerical modeling of flow in a meandering channel. Water. 2024;16(11):1547. https://doi.org/10.3390/w16111547
13. Nanson GC, Hickin EJ. Channel migration and incision on the Beatton River. J Hydraul Eng. 1983;109:327–37.
14. Legleiter CJ, Harrison LR, Dunne T. Effect of point bar development on the local force balance governing flow in a simple, meandering gravel bed river. J Geophys Res. 2011;116:18–38.
15. Kasvi E, Alho P, Vaaja M. Spatial and temporal distribution of fluvio-morphological processes on a meander point bar during a flood event. Hydrol Res. 2013;44(6):1022–39.
16. Maurya OP, Nandi KK, Modalavalasa S, Dutta S. Flow hydrodynamics influences due to flood plain sand mining in a meandering channel. In: Deka D, Majumder SK, Purkait MK, editors. Sustainable Environment. NERC 2022. Singapore: Springer; 2023. https://doi.org/10.1007/978-981-19-8464-8_16
17. Liu Y, Chai Y, Yu M, Zhou Y. Influences of channel bed morphology on flow structures in continuous curved channels. Front Environ Sci. 2024;12. https://doi.org/10.3389/fenvs.2024.1431021
18. Pareta K, Pareta U. Meander classification and trend analysis using multi-temporal Landsat series satellite imagery. Indian J Eng. 2021;18(49):88–101. https://www.discoveryjournals.org/engineering/current_issue/2021/v18/n49/A9.pdf
19. Nadudvari Á, Czajka A, Wyżga B, Zygmunt M, Wdowikowski M. Patterns of recent changes in channel morphology and flows in the Upper and Middle Odra River. Water. 2023;15(2):370. https://doi.org/10.3390/w15020370
20. Parker G. On the cause and characteristic scales of meandering and braiding in rivers. J Fluid Mech. 1976;76(3):457–79. https://doi.org/10.1017/S0022112076000748
21. Finotello A, D'Alpaos A, Bogoni M, Ghinassi M, Lanzoni S. Remotely sensed planform morphologies reveal fluvial and tidal nature of meandering channels. Sci Rep. 2020;10:54. https://doi.org/10.1038/s41598-019-56992-w
22. Ielpi A, Lapôtre MGA. The impact of vegetation on meandering rivers. Nat Rev Earth Environ. 2022;3:165–78. https://doi.org/10.1038/s43017-021-00249-6
23. Exner FM. Dunne and meander waves form the solid surface of the earth, its growth and movement. Geogr Ann. 1921;3:327–35.
24. Fujiyoshi Y. Theoretical treatise on the meandering of rivers. Jpn Sci Rev. 1950;1:29–34.
25. Anderson JD. A comparison of the life histories of coastal and montane populations of Ambystoma macrodactylum in California. Am Midl Nat. 1967;77(2):323–55.
26. Matthes GH. Basic aspects of stream-meanders. Trans Am Geophys Union. 1941;22:632–6.
27. Ackers P, Charlton FG. The geometry of small meandering streams. Proc Inst Civ Eng. 1970;Paper 7328:289–317.
28. Hooke R, Le B. Distribution of sediment transport and shear stress in a meander bend. J Geol. 1975;83:543–66.
29. Thomson J. On the origin of windings of rivers in alluvial plains, with remarks on the flow of water round bends in pipes. Proc R Soc Lond. 1876;25:5–8.
30. Leliavsky S. An introduction to fluvial hydraulics. London: Constable & Co.; 1955. p. 257.
31. Tanner WF. Florida coastal classification. Trans Gulf Coast Assoc Geol Soc. 1960;10:259–66.

32. Shen F, Royden LH, Burchfiel BC. Large-scale crustal deformation of the Tibetan Plateau. J Geophys Res. 2001;106(B4):6793–816.
33. Komura S, Simons DB. Riverbed degradation below dams. J Hydraul Div Proc Am Soc Civ Eng. 1967;93:1–14.
34. Reynolds AJ. Waves on the erodible bed of an open channel. J Fluid Mech. 1965;22:113–33.
35. Callander RA. Instability in river channels. J Fluid Mech. 1969;36:465–80.
36. Engelund F. The solitary sand waves. In: Progress Report. Copenhagen: Institute of Hydrodynamics and Hydraulic Engineering, Technical University of Denmark; 1971. Vol. 24, p. 51–4.
37. Eakin HM. Placer mining in the Ruby district, Alaska. US Geol Surv Bull. 1914;592:363–9.
38. Jefferson M. Limiting width of meander belts. Natl Geogr Soc. 1902.
39. Inglis CC. The behaviour and control of rivers and canals. Poona: Research Publication of Central Waterpower, Irrigation and Navigation Research Station; 1949.
40. Chatley H. The hydrology of the Yangtse River. J Inst Civ Eng. 1940;14:227–34.
41. Langbein WB, Leopold LB. River meanders - theory of minimum variance. US Geol Surv Prof Pap. 1966;422-H:1–15.
42. Chang HH. Geometry of rivers in regime. J Hydraul Div ASCE. 1979;105:691–706.
43. Fryirs KA, Brierley GJ. Human impacts on river systems. In: Geomorphic Analysis of River Systems: An Approach to Reading the Landscape. Wiley Online Library. https://doi.org/10.1002/9781118305454.ch13
44. Ortega JA, Razola L, Garzón G. Recent human impacts and change in dynamics and morphology of ephemeral rivers. Nat Hazards Earth Syst Sci. 2014;14:713–30. https://nhess.copernicus.org/articles/14/713/2014/nhess-14-713-2014.pdf
45. Van der Wiel MJ, Coulthard TJ, Macklin MG, Lewin J. Modelling the response of river systems to environmental change: Progress, problems and prospects for palaeo-environmental reconstructions. Earth Sci Rev. 2011;104(1–3):167–85. https://doi.org/10.1016/j.earscirev.2010.10.004
46. Ali ANA, Ariffin J, Razi MAM, Jazuri A. Environmental degradation: A review on the potential impact of river morphology. MATEC Web Conf. 2017;103:04001. https://www.matec-conferences.org/articles/matecconf/pdf/2017/17/matecconf_iscee2017_04001.pdf
47. Zeiringer B, Seliger C, Greimel F, Schmutz S. River hydrology, flow alteration, and environmental flow. In: Schmutz S, Sendzimir J, editors. Riverine Ecosystem Management. Aquatic Ecology Series, vol. 8. Cham: Springer; 2018. https://doi.org/10.1007/978-3-319-73250-3_4
48. Iqbal U, Riaz MZB. Blockage at cross-drainage hydraulic structures – Advances, challenges and opportunities. Heliyon. 2024;10(16):e35786. https://doi.org/10.1016/j.heliyon.2024.e35786
49. Wohl E, Bledsoe BP, Jacobson RB, Poff NL, Rathburn SL, Walters DM, et al. The natural sediment regime in rivers: Broadening the foundation for ecosystem management. BioScience. 2015;65(4):358–71. https://doi.org/10.1093/biosci/biv002
50. Hauer C, Leitner P, Unfer G, Pulg U, Habersack H, Graf W. The role of sediment and sediment dynamics in the aquatic environment. In: Schmutz S, Sendzimir J, editors. Riverine Ecosystem Management. Aquatic Ecology Series, vol. 8. Cham: Springer; 2018.

https://doi.org/10.1007/978-3-319-73250-3_8
51. Bettess R, Reeve CE. Performance of river flood embankment. HR Wallingford; 1995. https://eprints.hrwallingford.com/361/1/SR384.pdf
52. Saikumar G, Pandey M, Dikshit PKS. Natural River Hazards: Their Impacts and Mitigation Techniques. In: Pandey M, Azamathulla H, Pu JH, editors. River Dynamics and Flood Hazards. Disaster Resilience and Green Growth. Singapore: Springer; 2023. https://doi.org/10.1007/978-981-19-7100-6_1
53. Teraguchi H, Nakagawa H, Kawaike K, Baba Y, Zhang H. Effects of hydraulic structures on river morphological processes. Int J Sediment Res. 2011;26(3):283–303. https://doi.org/10.1016/S1001-6279(11)60094-2
54. Hupp CR, Pierce AR, Noe GB. Floodplain geomorphic processes and environmental impacts of human alteration along Coastal Plain rivers, USA. Wetlands. 2009;29:413–29. https://doi.org/10.1672/08-169.1
55. Normand JCL, Heggy E. Assessing flash flood erosion following storm Daniel in Libya. Nat Commun. 2024;15:6493. https://doi.org/10.1038/s41467-024-49699-8
56. Nile Basin Initiative (NBI). Flood embankment design, operation and maintenance manual, Sudan. Hydraulics Research Station (HRS), Ministry of Irrigation and Water Resources, Sudan; 2010. https://nilebasin.org/sites/default/files/2023-09/31%2520SDN_FIN_Flood_Embankment_Design.pdf
57. Johnston I, Murphy W, Holden J. A review of floodwater impacts on the stability of transportation embankments. Earth Sci Rev. 2021;215:103553. https://doi.org/10.1016/j.earscirev.2021.103553
58. Kondolf GM, Gao Y, Annandale GW, Morris GL, Jiang E, Zhang J, et al. Sustainable sediment management in reservoirs and regulated rivers: Experiences from five continents. Earth's Future. 2014;2:250–80. https://doi.org/10.1002/2013EF000184
59. Brown RA, Pasternack GB. Hydrologic and topographic variability modulate channel change in mountain rivers. J Hydrol. 2014;510:551–64. https://doi.org/10.1016/j.jhydrol.2013.12.048
60. Patel HK, Kumar B. Hydro-morphological behavior around T-shaped spur dikes with downward seepage. Sci Rep. 2023;13:10454. https://doi.org/10.1038/s41598-023-37694-w
61. Chakravarty S, Patel HK, Mohanty B, Kumar B. Review on different shapes of spurs and their effects on channel morphology. Water Pract Technol. 2024;19(1):241–62. https://doi.org/10.2166/wpt.2023.221
62. Klingeman PC, Kehe SM, Owusu YA. Streambank erosion protection and channel scour manipulation using rockfill dikes and gabions. Water Resources Research Institute, Oregon State University, Oregon. Report No. WRRI-98; 1984. https://www.usbr.gov/tsc/techreferences/hydraulics_lab/pubs/PAP/PAP-0734.pdf
63. Kim HS, Nabi M, Kimura I, Shimizu Y. Numerical investigation of local scour at two adjacent cylinders. Adv Water Resour. 2014;70:131–47. https://doi.org/10.1016/j.advwatres.2014.04.018
64. Yang Y, Qi M, Li J, Ma X. Evolution of hydrodynamic characteristics with scour hole developing around a pile group. Water. 2018;10(11):1632. https://doi.org/10.3390/w10111632
65. Li YT, Zhan JM, Wai WHO. A study of the effect of local scour on the flow field near the spur dike. Theor Appl

Mech Lett. 2024;14(2). https://doi.org/10.1016/j.taml.2024.100510
66. Rao AR, Sitaram N. Stability and mobility of sand-bed channels affected by seepage. J Irrig Drain Eng. 1999;125(6):370–9. https://doi.org/10.1061/(ASCE)0733-9437(1999)125:6(370)
67. Pandey M, Valyrakis M, Qi M, Sharma A, Lodhi AS. Experimental assessment and prediction of temporal scour depth around a spur dike. Int J Sediment Res. 2021;36(1):17–28. https://doi.org/10.1016/j.ijsrc.2020.03.015
68. Gill MA. Erosion of sand beds around spur dikes. J Hydraul Div. 1972;98(9). https://doi.org/10.1061/JYCEAJ.0003406
69. Ettema R, Kirkil G, Muste M. Similitude of large-scale turbulence in experiments on local scour at cylinders. J Hydraul Eng. 2006;132(1):33–40. https://doi.org/10.1061/(ASCE)0733-9429(2006)132:1(33)
70. Moody JA. Dynamic relations for the deposition of sediment on floodplains and point bars of a freely meandering river. Geomorphology. 2019;327:585–97. https://doi.org/10.1016/j.geomorph.2018.11.032
71. Nicoll TJ, Hickin EJ. Planform geometry and channel migration of confined meandering rivers on the Canadian prairies. Geomorphology. 2010;116(1–2):37–47. https://doi.org/10.1016/j.geomorph.2009.10.005
72. Sukhodolov A, Uijttewaal WSJ, Engelhardt C. On the correspondence between morphological and hydrodynamical patterns of groyne fields. Earth Surf Process Landf. 2002;27(3):289–305. https://doi.org/10.1002/esp.319
73. Athar M, Mansoor T, Nishank A. Effects of spur dyke's orientation on bed variation in channel bend. Hydro Sci Mar Eng. 2021;3(2):1–9. https://doi.org/10.30564/hsme.v3i2.3834
74. Wang M, Tian Y, Li X. Experimental study on pressure distribution of spur dike under the combined action of landslide surge and water flow. AIP Adv. 2022;12(7):075305. https://doi.org/10.1063/5.0099656
75. Xu H, Li Y, Zhao Z, Wang X, Zhang F. Experimental study on the local scour of submerged spur dike heads under the protection of soft mattress in plain sand-bed rivers. Water. 2023;15(3):413. https://doi.org/10.3390/w15030413
76. Ten Brinke WBM, Kruyt NM, Kroon A, Van den Berg JH. Erosion of sediments between groynes in the River Waal because of navigation traffic. In: Fluvial Sedimentology VI. Wiley; 1999. p. 147–60. https://doi.org/10.1002/9781444304213.ch11
77. Hooke J. Morphodynamics of active meandering rivers reviewed in a hierarchy of spatial and temporal scales. Geomorphology. 2023;439:108825. https://doi.org/10.1016/j.geomorph.2023.108825
78. Qin Y, Jin X, Du K, Jin Y. Changes in river morphology and influencing factors in the upper Yellow River over the past 25 years. Geomorphology. 2024;465:109397. https://doi.org/10.1016/j.geomorph.2024.109397
79. Hooke JM. River meandering. In: Shroder J, editor-in-chief; Wohl E, editor. Treatise on Geomorphology. Vol. 9, Fluvial Geomorphology. San Diego, CA: Academic Press; 2013. p. 260–88. https://doi.org/10.1016/B978-0-12-374739-6.00241-4
80. Kasvi E, Hooke J, Kurkela M, Vaaja MT, Virtanen J-P, Hyyppä H, Alho P. Modern empirical and modelling study approaches in fluvial geomorphology to elucidate sub-bend-scale meander dynamics. Prog Phys Geogr.

2017;41(5):533–69. https://doi.org/10.1177/0309133317715870
81. Pareta K. River Morphology of Meandering River, Analysis and Modelling through Remote Sensing and GIS Techniques. Saarbrücken: LAP Lambert Academic Publishing; 2021. https://my.lap-publishing.com/catalog/details/store/gb/book/978-620-3-85470-1/river-morphology-of-meandering-river
82. Hooke J. Morphodynamics of active meandering rivers reviewed in a hierarchy of spatial and temporal scales. Geomorphology. 2023;439:108825. https://doi.org/10.1016/j.geomorph.2023.108825
83. Pareta K, Pareta U. Form and process based geomorphic classification and mapping of a meandering river using satellite remote sensing data. Arab J Geosci. 2021;14:2064. https://doi.org/10.1007/s12517-021-08412-5
84. Brice JC. Airphoto interpretation of the form and behavior of alluvial rivers. Final report to the U.S. Army Research Office, Durham, NC. St. Louis, MO: Washington University; 1975. p. 10.
85. Schumm SA. The fluvial system. New York: Wiley Inter-Science; 1977. p. 338.
86. Schumm SA. Evolution and response of the fluvial system, sedimentologic implications. Spec Publ Soc Econ Paleontol Mineral. 1981;31:19–29.
87. Montgomery DR, Buffington JM. Channel-reach morphology in mountain drainage basins. Geol Soc Am Bull. 1997;109(5):596–611.
88. Rosgen DL. A classification of natural rivers. Catena. 1994;22:169–99.
89. Ran Y, Liu Y, Wu S, Li W, Zhu K, Ji Y, et al. A higher river sinuosity increased riparian soil structural stability on the downstream of a dammed river. Sci Total Environ. 2021;802:149886. https://doi.org/10.1016/j.scitotenv.2021.149886
90. Stanislawski LV, Kronenfeld BJ, Buttenfield BP, Shavers EJ. At what scales does a river meander? Scale-specific sinuosity (S3) metric for quantifying stream meander size distribution. Geomorphology. 2023;436:108734. https://doi.org/10.1016/j.geomorph.2023.108734
91. Yu Z, Fu Y, Zhang Y, Liu Z, Liu Y. Quantifying the impact of changes in sinuosity on river ecosystems. Water. 2023;15(15):2751. https://doi.org/10.3390/w15152751
92. Montgomery K. Sinuosity and fractal dimension of meandering rivers. Trans Inst Br Geogr. 1996;28(4):491–500. https://www.jstor.org/stable/20003734
93. Leopold LB, Wolman MG. River channel patterns: meandering, braiding, and straight. Geol Surv Prof Pap. 1957;282-B. Washington, DC: US Government Printing Office.
94. Chorley RJ, Schumm SA, Sugden DE. Geomorphology. London: Methuen; 1984.
95. Sarker MH, Thorne CR, Aktar MN, Ferdous MR. Morpho-dynamics of the Brahmaputra–Jamuna River, Bangladesh. Geomorphology. 2014;215:45–59. https://dx.doi.org/10.1007/978-3-319-00972-819
96. Ham GA, de Groot MB, Mastbergen DRA. A semi-empirical method to assess flow-slide probability. In: Krastel S, et al., editors. Submarine Mass Movements and Their Consequences. Gewerbestrasse, Switzerland: Springer International Publishing; 2016. https://dx.doi.org/10.1007/978-3-319-00972-819
97. Van der Wal M. Bank protection structures along the Brahmaputra-Jamuna River, a study of flow slides. Water. 2020;12(9):2588. https://doi.org/10.3390/w12092588

98. Brierley G, Hooke J. Emerging geomorphic approaches to guide river management practices. Geomorphology. 2015;251:1–5. https://doi.org/10.1016/j.geomorph.2015.08.019
99. Dawson C, Ashmore P, Corry R. Evaluating river morphology change with a geomorphic form variation approach. Earth Surf Process Landf. 2023;49(2):855–74. https://doi.org/10.1002/esp.5744
100. Reinfelds I, Cohen T, Batten T, Brierley G. Assessment of downstream trends in channel gradient, total and specific stream power: a GIS approach. Geomorphology. 2004;60:403–16. https://doi.org/10.1016/j.geomorph.2003.10.003
101. Frings RM, Kleinhans MG. Complex variations in sediment transport at three large river bifurcations during discharge waves in the river Rhine. Sedimentology. 2008;55:1145–71. https://doi.org/10.1111/j.1365-3091.2007.00940.x
102. Heine RA, Pinter N. Levee effects upon flood levels: an empirical assessment. Hydrol Process. 2011;26(21):3225–40. https://doi.org/10.1002/hyp.8261
103. Brice JC. Stream channel stability assessment. Washington, DC: US Department of Transportation, Federal Highway Administration; 1982. Report FHWA/RD-82/021. p. 42.
104. Lagasse P, Spitz W, Zevenbergen L, Zachmann D. Handbook for predicting stream meander migration. Washington, DC: National Cooperative Highway Research Program (NCHRP); 2004. Report No. 533. p. 107.
105. Bormann NE, Julien PY. Scour downstream of grade-control structures. J Hydraul Eng. 1991;117:579–94.
106. Dingorkar NA, Kulkarni D, Hirave P. Study of river training work on permeable groynes. Int J Civ EngTechnol.2017;8(6):262–70. http://www.iaeme.com/IJCIET/issues.asp?JType=IJCIET&VType=8&IType=6
107. Patel HK, Qi M, Kumar B. Downward seepage effects on flow near an L-shape spur dike and bed morphology. Int J Sediment Res. 2024;39(2):194–208. https://doi.org/10.1016/j.ijsrc.2023.11.005
108. Mojtaba RNS, Mahmood SB. Effects of upward seepage on depth of scour hole downstream of free-falling jets under constant tail water depth. J Water Sci. 2013;5:31–9.
109. Talling PJ, Baker ML, Pope EL, et al. Longest sediment flows yet measured show how major rivers connect efficiently to deep sea. Nat Commun. 2022;13:4193. https://doi.org/10.1038/s41467-022-31689-3
110. Sattar AMA, Plesiński K, Radecki-Pawlik A, Gharabaghi B. Scour depth model for grade-control structures. J Hydroinform. 2017;20:117–33.
111. Bajelvand S, Gohari S, Heydari M. Experimental study of the effect of hockey spur dikes angle on scouring and comparison with L-shape spur dike. Water Irrig Manag. 2022;12(3):455–66. https://jwim.ut.ac.ir/article_88210.html
112. Julien PY. River Mechanics. Chapter 9 - Riverbank Protection. Cambridge: Cambridge University Press; 2018. p. 230–59. https://doi.org/10.1017/9781316107072.010
113. Ikeda S, Yoshiike T, Sugimoto T. Experimental study on the structure of open channel flow with impermeable spur dikes. Proc Hydraul Eng. 1999;43:281–6. https://doi.org/10.2208/prohe.43.281
114. Vaghefi M, Radan P, Akbari A. Flow pattern around attractive, vertical, and repelling T-shaped spur dikes in a mild bend using CFD modeling. Int J Civ Eng. 2019;17:607–17. https://doi.org/10.1007/s40999-018-0340-x

115. Ke X, Evans G, Collins MB. Hydrodynamics and sediment dynamics of The Wash embayment, eastern England. Sedimentology. 1996;43(1):157–74. https://doi.org/10.1111/j.1365-3091.1996.tb01465.x
116. Juez C, Thalmann M, Schleiss AJ, Franca MJ. Influence of lateral embayments on suspended sediment transport under unsteady flow conditions. River Flow 2018 - Ninth International Conference on Fluvial Hydraulics. E3S Web Conf. 2018;40:03017. https://doi.org/10.1051/e3sconf/20184003017
117. Giglou AN, McCorquodale JA, Solari L. Numerical study on the effect of the spur dikes on sedimentation pattern. Ain Shams Eng J. 2018;9(4):2057–66. https://doi.org/10.1016/j.asej.2017.02.007
118. Talaat A, Attia K, Elsaeed G, Ibraheem M. Implementation of spur dikes to reduce bank erosion of temporary diversion channels during barrages construction. Aust J Basic Appl Sci. 2009;3(4):3190–205. https://www.ajbasweb.com/old/ajbas/2009/3190-3205.pdf
119. Bhusal JK. Consequences of river training structures: A case of Laxmanpur barrage and afflux bunds near the Indo-Nepal border. J Hydrol Meteorol. 2004;1(1):1–5.
120. Adhikari BR. Flooding and inundation in Nepal Terai: Issues and concerns. Hydro Nepal. 2013;12:59–65.
121. Gautam DK, Phaiju AG. Community-based approach to flood early warning in west Rapti river basin of Nepal. J Integr Disaster Risk Manag. 2013;3(1):155–69.
122. Shrestha HM. Naumore storage project should be the last resort of development on the main course of Rapti (West), Nepal. Hydro Nepal. 2016;18:1–5.
123. Osti R. A feasibility study on integrated community-based flood disaster management in Banke district, Nepal, Phase-1 baseline study. Int Cent Water Hazard Risk Manag (ICHARM), Public Works Res Inst (PWRI). 2008;4122(11):1–111.
124. Nepal Development Research Institute (NDRI). Assessment of flood inundation in lower west Rapti basin under the effect of climate change. Kathmandu, Nepal; 2012. p. 1–113.
125. Sanstha JV. Climate vulnerability and gap assessment report on flood and drought (lower Rapti river Basin case study). Global Water Partnership (GWP), Nepal and Jalsrot Vikas Sanstha (JVS); 2014. p. 1–45.
126. Devkota RP. Flood adaptation strategies under climate change in Nepal - A socio-hydrological analysis [PhD thesis]. University of Southern Queensland; 2014.
127. United Nations Development Programme (UNDP). ISDR global assessment report on poverty and disaster risk. Kathmandu, Nepal; 2009.
128. U.S. Environmental Protection Agency (EPA). National Management Measures to Control Nonpoint Source Pollution from Hydromodification, Chapter 2: Background. 2007. https://www.epa.gov/sites/default/files/2015-09/documents/chapter_2_background_web_0.pdf
129. Hohensinner S, Hauer C, Muhar S. River Morphology, Channelization, and Habitat Restoration. In: Schmutz S, Sendzimir J, editors. Riverine Ecosystem Management. Aquatic Ecology Series, vol 8. Cham: Springer; 2018. https://doi.org/10.1007/978-3-319-73250-3_3
130. Rhoads BL. Chapter 15 - Human Impacts on River Dynamics. In: River Dynamics Geomorphology to Support Management. Cambridge University Press; 2020. p. 343–68. https://doi.org/10.1017/9781108164108.015

131. Sarif MN, Siddiqui L, Islam MS, Praveen N, Saha M. Evolution of river course and morphometric features of the River Ganga: A case study of up and downstream of Farakka Barrage. Int Soil Water Conserv Res. 2021;9(4):578–90. https://doi.org/10.1016/j.iswcr.2021.01.006



© 2026 by the authors. Licensee SCU, Ahvaz, Iran. This article is an open access article distributed under the terms and conditions of the Creative Commons Attribution 4.0 International (CC BY 4.0 license) (http://creativecommons.org/licenses/by/4.0/).

Effect of bed roughness shape on mitigating scour the downstream of parallel sluice gates

Iman Akbari [1], Mohammad Hemmati [*,1] , Sung-Uk Choi [2], Yousef Ramezani [3], Babak Mahmoudi [1]

1. Department of Water Engineering, Urmia University, Urmia, Iran.
2. Department of Civil & Environmental Engineering, Yonsei University, Korea.
3. Department of Water Engineering, University of Birjand, Birjand, Iran.

***Corresponding Author:**
Mohammad Hemmati,

Email: m.hemmati@urmia.ac.ir
Received: 2025.02.12
Accepted: 2025.05.21
J. Hydraul. Struct., 12(1):50-68
DOI: 10.22055/jhs.2025.48994.1337

ABSTRACT

Parallel sluice gates are crucial components in hydraulic structures, offering cost-effective and operationally flexible solutions for flow control in wide channels. This laboratory investigation examines the effectiveness of different bed roughness configurations—specifically trapezoidal and cubic geometries—in mitigating local scour downstream of parallel sluice gates, a persistent challenge that threatens structural integrity. The study systematically evaluated scour parameters under varying flow conditions and gate configurations, employing both quantitative measurements and qualitative flow visualization techniques. Results demonstrate that trapezoidal roughness elements significantly outperform their cubic counterparts across all measured parameters. Specifically, trapezoidal configurations achieved reductions of 25.3% in Average scour depth, 22% in scour length, 30.5% in cross-sectional area, and 50% in scour volume, compared to modest reductions of 20%, 14.35%, 21.57%, and 34.7% respectively for cubic roughness elements. The flow expansion ratio (e) emerged as a critical parameter, with optimal performance observed at e = 0.56 (two gates open). However, effectiveness significantly decreased at lower expansion ratios (e = 0.283, single gate open) due to asymmetric hydraulic jumps and reverse flow patterns. Analysis of Froude number (Fr) effects revealed that trapezoidal roughness maintains superior performance even under high Froude numbers (Fr > 5) during asymmetric flow conditions, while cubic roughness shows diminished effectiveness. These findings provide valuable insights for optimizing hydraulic structure design, emphasizing the superiority of trapezoidal bed roughness configurations for enhanced scour protection and system stability in irrigation and drainage applications.

KEYWORDS

Bed roughness, Parallel sluice gates, Local scour mitigation, Scour reduction.

1. Introduction

Sluice gates are pivotal hydraulic structures widely utilized to control water levels, discharge sediments in diversion dams, maintain desired water levels, and measure flow in open channels [1]. However, using a single wide gate for Wide channels is often neither cost-effective nor operationally practical due to maintenance and control challenges. Consequently, engineers prefer deploying multiple parallel gates to achieve similar results [2].

The hydraulic conditions downstream of these parallel gates can become complex due to variations in gate openings. Adjusting all open gates to a certain value may result in more favorable flow conditions, which can be impractical under real-world constraints [2]. When multiple gates are operated in parallel, challenges may arise during low-flow periods, potentially reducing downstream water delivery. A common practice is to open all gates slightly to share the flow evenly. However, this strategy is susceptible to blockages caused by floating debris or sediments and operational issues due to lifting forces, which may lead to gate malfunctions. Alternatively, opening fewer gates with larger openings has been suggested by [1]. This approach, while beneficial in certain scenarios, can disrupt flow dynamics, influence velocity profiles and flow patterns, and potentially increase scour risk [3]. Additionally, improper gate operation can lead to severe localized scour downstream of the stilling basin [4].

Understanding the scour phenomenon is crucial when scour depth is significant enough to affect the foundations of river structures, potentially threatening their stability or causing substantial damage. Traditional methods for evaluating scour depth primarily rely on empirical formulas or physical modeling [5]. Despite extensive research in this field, a comprehensive and general formula for predicting local scour depth around river structures remains elusive. This gap has led researchers to focus on specific cases and conduct laboratory experiments to address this knowledge gap [6]. One effective method to reduce scour hole dimensions is through bed roughening. Rajaratnam [7] was the first to investigate hydraulic jumps over rough beds and demonstrated that hydraulic jump lengths are shorter on rough surfaces than on classical smooth beds. Since then, various configurations of bed roughness have been examined to determine their effects on hydraulic jump length [8–11]. Numerous studies have also evaluated these configurations, assessing their impact downstream of sluice gates.

The following sections review research on the influence of bed roughness and flow expansion on the characteristics of hydraulic jumps [12–19]. Moreover, several studies have investigated the effects of bed roughness and adverse slopes on hydraulic jumps [20–22]. Finally, extensive research on the impact of bed roughness on downstream scour of sluice gates is discussed in the subsequent sections [22–29].

Karimi et al [12] investigated the influence of bed roughness on pressure fluctuations within a stilling basin featuring sudden divergence. Their findings demonstrated that roughness elements substantially dampened turbulent hydraulic jump fluctuations. Their observations revealed that the maximum pressure fluctuation intensity coefficient for a rough divergent jump was 0.023, representing a reduction of approximately 53% compared to a smooth divergent jump and 70% compared to a classical hydraulic jump. Furthermore, Abbaspour and Abdian Rukni [13] conducted a comprehensive study examining the combined effects of bed roughness and stilling basin divergence on hydraulic jump characteristics. Their results demonstrated that increasing the basin's divergence angle reduced the conjugate depth by up to 25.5% and the jump length by as much as 66.2% when rough beds were incorporated into the design. The implementation of cubic roughness elements alone was found to reduce jump length by an average of 60.3%. Their study also examined the effects of basin divergence without bed roughness, revealing that under these conditions, the hydraulic jump length decreased by 37% to 47%, with more substantial reductions observed at higher divergence angles. These findings emphasize the significance of both wall divergence and bed roughness in reducing hydraulic jump length and conjugate depth, which can significantly enhance the cost-effectiveness of basin

designs and improve control over hydraulic jumps. These insights provide valuable contributions to engineering applications in water management systems.

Daneshfaraz et al. [14] examined the impact of channel bed roughness on secondary jump depth and length reduction. Their research indicated that diverging stilling basins with rough beds reduced conjugate jump depth by an average of 12% to 16% compared to smooth-bed diverging basins, regardless of opening ratios. The average reduction in jump length across all opening ratios for diverging basins with rough beds was approximately 20%. Moreover, Hasani et al. [16] investigated hydraulic jump pressure fluctuations within a stilling basin featuring a rough bed. Their findings demonstrated that the introduction of bed roughness significantly reduced the intensity of pressure fluctuations in stilling basins with sudden expansions. In these expanded sections, energy loss increased while pressure fluctuation intensity decreased, a phenomenon attributed to lateral vortex formation. Mahtabi et al. [17] analyzed 581 data points, including 280 natural bed data and 301 artificial bed data, using artificial neural networks to classify hydraulic jumps in uneven beds. Their findings revealed that shear stress in rough beds was significantly higher than in smooth beds and increased sharply with rising Froude numbers. Fallahi and Heidarpour [18] introduced an innovative approach to analyzing hydraulic jump characteristics under varying conditions, including expansion ratios (1, 1.33, 1.6, and 2), bed roughness (0, 1.33, and 2 cm), and Froude numbers (4.9–9.5). Their research demonstrated that abrupt expansions combined with bed roughness reduced sequent depth and jump length by 49.5% and 22.34%, respectively. Energy dissipation was enhanced by 31.1% compared to classical hydraulic jumps.

Akib et al. [19] conducted a study to explore the effects of various roughness shapes on hydraulic jumps. The findings revealed that at lower Froude numbers, the influence of rough bed elements was minimal. However, as the Froude number increased, the roughness shapes played a significant role in reducing the hydraulic jump length. Gandhi's research [20] focused on hydraulic jumps in a rectangular canal with sudden expansions. His findings highlighted the significant benefits of incorporating baffle blocks and sills. These structural elements enhanced energy dissipation, leading to more controlled and efficient flow behavior. Tahmasbipour et al. [21] investigated T-jumps in channels with abrupt expansions and sinusoidal bed roughness. Their results demonstrated that the introduction of this roughness resulted in a decrease in energy dissipation. Sajadi et al. [22] examined S-jumps in expanded canals, employing cross-beam roughness elements arranged in various configurations. Their innovative approach successfully stabilized the flow, eliminated asymmetry, and reduced the length of the hydraulic jump.

Parsamehr et al. [23] investigated hydraulic jump behavior on rough beds with reverse slopes, demonstrating that increasing roughness element height and spacing, in combination with steeper reverse slopes and higher Froude numbers, contributed to a reduction in secondary jump depth, while simultaneously increasing energy loss and shear stress. Gupta and Dwivedi [24] studied the effect of gravel size on hydraulic jumps in stilling basins. Their results showed that larger gravel reduced relative jump height and increased energy dissipation. These findings highlight the role of optimized bed roughness in improving energy dissipation and hydraulic performance.

Hamidifar and Nasrabadi [25] conducted 33 experiments investigating the erosion behavior of noncohesive sediments downstream of smooth and rough aprons under five roughness conditions (k = 0, 1, 1.85, 3.35, and 5 mm). Their results demonstrated that rough aprons significantly reduced scour characteristics, achieving a minimum 60% reduction in maximum scour depth compared to smooth beds. Increased submergence factors further

reduced scour depth while altering scour hole geometry, resulting in flatter dune formations. Additionally, hydraulic jump length exhibited a positive correlation with submergence levels. In a related study, Ali et al. [26] investigated the impact of triangular serrated bed designs within stilling basins, demonstrating significant improvements in scour mitigation. The serrated bed configuration notably reduced both scour depth and length compared to traditional designs. Specifically, the serrated bed achieved a 63.4% reduction in scour depth for fine sands and a 44.2% reduction for coarse sands. Furthermore, scour length decreased by 30.2% for fine sands and 20.6% for coarse sands, highlighting the effectiveness of incorporating rough bed designs in optimizing stilling basin performance. Aamir and Ahmad [27] further examined the effectiveness of roughened stilling basins in mitigating maximum scour depth. Their research documented substantial reductions in scour depth, ranging from 69.8% to 82.8%, demonstrating the potential of roughened surfaces to significantly enhance hydraulic performance.

Urbański et al. [28] investigated the effects of various energy dissipator designs on local scour downstream of sluice gates, comparing three configurations: flat slabs, slabs with baffle blocks, and riprap layers. Their findings indicated that flat slabs resulted in the greatest scour depth and erosion rate, posing significant risks to structural integrity. In contrast, baffle blocks and riprap layers effectively reduced scour depth and delayed erosion. Among these configurations, double-row baffle blocks proved most efficient, providing superior scour mitigation and structural stability. An experimental study by Aamir et al. [29] investigated scour behavior under wall jet influence, focusing on differences between rough and smooth stiff aprons. Their research demonstrated that maximum scour depth decreased with larger sediment sizes, wider sluice openings, and longer apron lengths. Specifically, rough aprons significantly reduced maximum scour depth compared to smooth counterparts. Finally, Maleki and Fiorotto [30] examined the influence of bed roughness on hydraulic jump and scour dynamics. Their findings revealed that increased roughness reduced subcritical depth and jump length, leading to a 30–35% reduction in stilling basin dimensions. Rough beds also mitigated scour intensity by decreasing near-bottom velocities and altering shear stress distributions. An experimental study conducted by Mahmoudi et al. [1] investigated the phenomenon of local scour occurring downstream of parallel sluice gates. The research highlighted that as the gate opening ratio decreased, the scour dimensions increased significantly, compared to scenarios where the gates were fully open. Additionally, Mahmoudi et al. [31] proposed a predictive equation specifically designed to estimate the scour depth downstream of parallel sluice gates.

While considerable research has been dedicated to understanding the effects of bed roughness on hydraulic jumps and its role in mitigating scour, there remains a notable gap in studies focusing on the specific impact of rough bed structures on scour downstream of parallel sluice gates. To address this research deficiency, the present study undertakes experimental investigations aimed at evaluating the influence of cubic and trapezoidal roughness elements on the dimensions of scour holes downstream of parallel sluice gates. By examining these effects, this study seeks to contribute valuable insights into improving scour mitigation strategies and advancing hydraulic engineering practices.

2. Materials and Methods

2.1. Laboratory equipment

The present study was conducted in a laboratory flume located in Farhoudi's applied Hydraulic Laboratory at Urmia University. The flume, featuring a rectangular cross-section, measured 8 meters in length, 60 cm in width, and 75 cm in height. A sediment recess, integrated into the flume setup, was 20 cm deep and 1.8

meters long. The flume walls were constructed from transparent plexiglass, enabling clear observation of sediment transport and flow dynamics within the channel and sediment recess. The experimental setup included a pump capable of delivering a nominal flow rate of 60 Lit/sec. Flow rates were precisely measured using an ultrasonic flow meter (model UFM610P) manufactured by Krohne, with an accuracy of ±2%. Water depth measurements were conducted using a point gauge with an accuracy of 1 mm, while the final bed profiles were determined using a laser meter with the same level of accuracy. To examine the effects of parallel sluice gates on hydraulic behavior, three steel sluice gates, each with a width of 17 cm (3.4 b/a), were installed. The minimum gate opening was set to 5 cm to avoid scale effects, as recommended by Roth and Hager [32]. Based on the gate opening and the design criteria of the USBR Type I stilling basin, the stilling basin length was established at 164 cm. An end gate was employed to stabilize the hydraulic jump inside the flume and to form a free jump. The hydraulic jump was adjusted by manipulating the end gate according to the sliding gate openings and the inflow entering the channel. For each experimental scenario, the gate opening was maintained constant while the upstream water level was modified to achieve the desired Froude number range of 3.5 to 6.5 (Based on laboratory limitations) .

The positioning of roughness elements within the flume was guided by established recommendations. Abdellateef [33] suggested that the distance between the first roughness element and the gate should be twice the maximum gate opening, while Aboulatta [34] recommended this distance to be 4.5 times the initial depth of the hydraulic jump. Considering these guidelines and accounting for the flow contraction coefficient, the first row of roughness elements was placed 13.75 cm downstream from the gates. Regarding roughness element dimensions, Abdelsalam [35] recommended that for Froude numbers between 4 and 8, the height of roughness elements should not exceed half of the initial hydraulic jump depth. In this study, with a gate opening of 5 cm and a flow contraction coefficient of 0.61, the initial depth of the hydraulic jump was calculated to be 3.05 cm. Consequently, the height of the roughness elements was determined to be 1.5 cm.

2.2. Experimental procedure

To mitigate the occurrence of initial unwanted scour in the sediment recess, a controlled experimental procedure was implemented. The channel was pre-filled with water before the gradual opening of the main gate valve. This method allowed for the establishment of the required upstream water level in a controlled manner. The progression of scour profiles was systematically monitored under various test scenarios using a digital camera, which was positioned at a fixed distance from the sedimentation recess to ensure consistency in data collection. The frequency of measurements was adjusted over time to capture the evolution of scour profiles effectively. During the first hour, measurements were taken every 5 minutes. This interval was extended to every 15 minutes during the second hour and subsequently to every 30 minutes for the remainder of the experiment. The digital images of the scour profiles were processed using specialized software, Get Data, to extract quantitative information. Long-term experimental tests, conducted over a 12-hour period, revealed that more than 90% of the maximum scour depth was achieved within the first 8 hours of testing. These findings align with previous research conducted by Mahmoudi et al. [1], further validating the methodology and results. A schematic representation of the experimental flume setup, including the layout of parallel gates, is illustrated in Figure 1. Additionally, Figure 2 provides a detailed depiction of the roughness elements utilized in this research.

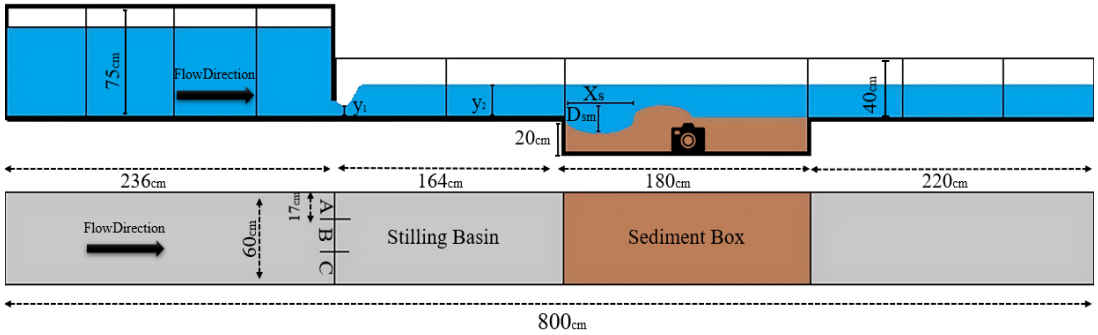


Figure 1. Schematic View of a Laboratory Flume

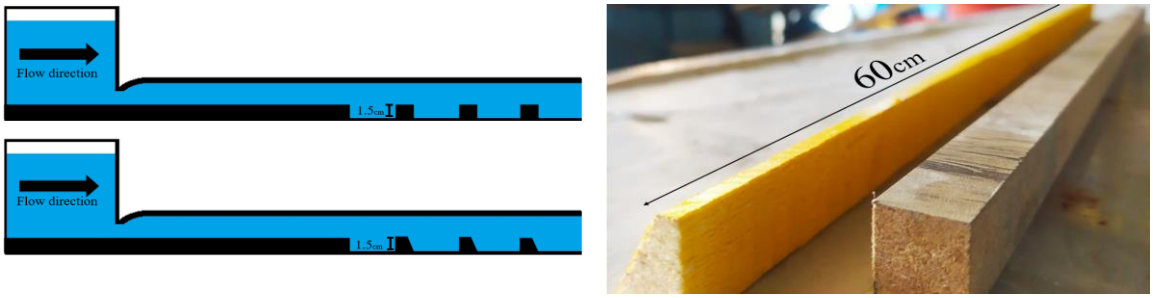


Figure 2. Schematic Diagram of Roughness Elements

2.3. Dimensional analysis

Local scour downstream of parallel sluice gates under different operating conditions is a complex phenomenon. Based on the investigations conducted, the parameters influencing the scour indices examined in this study (scour depth D_{sm}, scour volume $\forall$, scour hole length x_s, and scour cross-sectional area A) are as follows:

$$f(D_{sm}, x_m, A, \forall) = f\begin{pmatrix} h, y_1, y_2, y_t, v_1, g, b, B, a, \\ L, L_r, L_w, L_o, d_r, D_{50}, \rho_s, \varphi, \\ \sigma_g, F.S, \rho, \mu, t \end{pmatrix} \quad (1)$$

where y_1 and y_2 represent the conjugate depths located upstream and downstream of the hydraulic jump, y_t is the tailwater depth, V_1 is the velocity at the constriction section, g is the acceleration due to gravity, b is the width of the gates, B is the channel width, a is the opening of the gate or gates, L is the length of the stilling basin, L_r is the height of the roughness elements, L_W is the length of the divided wall, b_w is the width of the divided wall, L_o is the distance between roughnesses, D_{50} is the mean diameter of sediment particles, ρ_s is the specific weight of sediment particles, σ_g is the geometric standard deviation of particles, C_u is the uniformity coefficient of particles, F_S is the shape factor of sediment particles, ρ is the specific weight of water, μ is the dynamic viscosity of water, and t is time. Buckingham π theorem, the dimensionless parameters are defined as equation (2).

$$f\begin{pmatrix} \varphi, \sigma_g, C_u, F.s, \frac{a}{h}, \frac{y_2}{a}, \frac{y_t}{a}, \frac{b}{a}, \frac{B_c}{a}, \\ \frac{y_1}{a}, \frac{L_w}{L}, \frac{L_r}{a}, \frac{d_r}{a}, \frac{D_{50}}{a}, \frac{\rho_s}{\rho}, \mathrm{Re}, Fr \end{pmatrix} = 0 \quad (2)$$

Table 1 presents the distribution of sediment particle sizes used in this research. According to Raudkivi [36], when the geometric standard deviation of the particles (σ_g) is less than 1.3, the effect of particle non-uniformity on erosion is minimal. Furthermore, Das [37] suggests that if the uniformity coefficient of the particles (C_u) is less than 4, the sediment can be considered uniform.

Table 1. Characteristics of Sediment Particles (Unit: mm)

D_{10}	$D_{15.9}$	D_{30}	D_{50}	D_{60}	D_{84}	σ_g	Cu
1	1.1	1.24	1.37	1.45	4.7	1.24	1.45

$$Cu = \frac{D_{60}}{D_{10}} \quad (3)$$

$$\sigma_g = \sqrt{\frac{D_{84.1}}{D_{15.9}}} \quad (4)$$

In the realm of sediment transport research, simplifying complex systems into manageable models is crucial for advancing our understanding. According to the findings presented in Table 1, several parameters in sediment flow experiments can be justifiably disregarded due to their uniformity and constancy. This section explores these parameters and the rationale behind their exclusion from analytical considerations. Firstly, the consistency in sediment particle distribution allows us to overlook certain intrinsic properties such as the angle of repose, average particle diameter, and particle volume mass. Additionally, the dimensions of the divided walls, which are consistent across experimental setups, are also deemed negligible in influencing the outcomes. These decisions are grounded in the assumption that such uniformities do not significantly alter the dynamics under investigation. The experimental conditions further justify the exclusion of specific parameters. The experiments were conducted under free flow conditions at the outlet, indicating that the depth of flow exiting the gate or gates did not impose any constraints on the system. Consequently, the outlet depth parameter was omitted from the analyses.

$$\frac{D_{sm}}{a}, \frac{x_m}{a}, \frac{A}{a^2}, \frac{\forall}{Ba^2} = f\left(Fr, \frac{b}{B}\right) \quad (5)$$

In the following discussion, for the sake of brevity, the dimensionless parameter $\frac{\forall}{BL_w{}^2}$ representing scour volume will be referred to as V_s. Additionally, the expansion ratio will be denoted by the letter e

2.4. Experimental Matrix

The experiments were categorized into different scenarios based on gate configurations (single or dual gate openings), Froude numbers, expansion ratios, and bed roughness shapes (smooth, trapezoidal, cubic). The experimental matrix is detailed in Table 2.

Table 2. Experimental Matrix

No.	*Test Identifier*	*Open Gates*	F_r	*e*	*roughness shape*
1	T_1	*A*	6.5	0.283	*smooth*
2	T_2	*A*	6.5	0.283	*trapezoidal*
3	T_3	*A*	6.5	0.283	*cubic*
4	T_4	*B*	6.5	0.283	*smooth*
5	T_5	*B*	6.5	0.283	*trapezoidal*
6	T_6	*B*	6.5	0.283	*cubic*
7	T_7	*A&B*	6.5	0.56	*smooth*
8	T_8	*A&B*	6.5	0.56	*trapezoidal*
9	T_9	*A&B*	6.5	0.56	*cubic*
10	T_{10}	*A*	5	0.283	*smooth*
11	T_{11}	*A*	5	0.283	*trapezoidal*
12	T_{12}	*A*	5	0.283	*cubic*
13	T_{13}	*B*	5	0.283	*smooth*
14	T_{14}	*B*	5	0.283	*trapezoidal*
15	T_{15}	*B*	5	0.283	*cubic*
16	T_{16}	*A&B*	5	0.56	*smooth*
17	T_{17}	*A&B*	5	0.56	*trapezoidal*
18	T_{18}	*A&B*	5	0.56	*cubic*
19	T_{19}	*A*	3.5	0.283	*smooth*
20	T_{20}	*A*	3.5	0.283	*trapezoidal*
21	T_{21}	*A*	3.5	0.283	*cubic*
22	T_{22}	*B*	3.5	0.283	*smooth*
23	T_{23}	*B*	3.5	0.283	*trapezoidal*
24	T_{24}	*B*	3.5	0.283	*cubic*
25	T_{25}	*A&B*	3.5	0.56	*smooth*
26	T_{26}	*A&B*	3.5	0.56	*trapezoidal*
27	T_{27}	*A&B*	3.5	0.56	*cubic*

3. Results and Discussion

3.1. Maximum scour depth

Scour depth is a critical factor in the design and evaluation of hydraulic structures, as it can lead to unpredictable alterations of the riverbed, potentially resulting in structural damage and jeopardizing safety and functionality Melville [5] and Chow [38]. Consequently, accurately understanding and predicting scour depth is paramount for ensuring the stability of these structures. This research underscores the significant influence of bed roughness on mitigating scour depth downstream of parallel sluice gates.

All results and scour depth reductions in this study are presented in dimensionless form to enhance the generalizability of the findings and ensure their independence from specific units of measurement. The analysis demonstrates that bed roughness, particularly cubic and trapezoidal configurations, effectively reduces scour depth, achieving an average reduction of 22% with a maximum reduction of 56%. Notably, trapezoidal roughness exhibits a more pronounced impact, achieving average reductions of 25.3% compared to 20% for cubic roughness (Table 3). These results align with prior investigations focused on scour reduction downstream of single sluice gates. Studies by Ali et al. [26], Amir and Ahmad [39], and Amir et al. [29] have documented significant scour reductions ranging from 30% to 63%, 31% to 82%, and 70% to 83%, respectively. A crucial factor governing scour downstream of parallel sluice gates is the flow expansion ratio (e), a dimensionless parameter representing the ratio of effective gate

opening to the channel width. This study explored various scenarios and identified that roughness elements performed optimally with an expansion ratio of 0.56 (two gates open), while the least effective results were observed with an expansion ratio of 0.283 (one gate open). Trapezoidal roughness elements yielded average reductions of 30.3% and 20.85% in scour depth for expansion ratios of 0.56 and 0.283, respectively. Similarly, cubic roughness configurations resulted in average reductions of 33% and 14.05% for the same respective expansion ratios. These findings align with prior research by Mahmoudi et al. [1] and Khalili Shayan et al. [40], which highlights the complexities arising from central sluice gate operation in abruptly expanding stilling basins. Specifically, the formation of an asymmetric S-jump, characterized by concentrated high-velocity jets along one sidewall and reverse flow along the opposite wall, leads to uneven energy dissipation. This uneven distribution intensifies the potential for localized scour near the sidewalls, posing a significant threat to the structural integrity and long-term durability of stilling basin infrastructure [41].

As Figure 3 shows, for side gate operation, both cubic and trapezoidal roughness configurations modestly attenuate the scour development rate, reducing the slope from 0.18 (smooth bed) to 0.15. Middle gate operation demonstrates more nuanced behavior. The significant impact of roughness on scour downstream of the middle gate, particularly at low Froude numbers (Fr), results in a steeper slope for both roughness types. Slopes increase to 0.47 for cubic and 0.80 for trapezoidal roughness (Note the difference in the starting point of the scour on the D_{sm}-Fr line.), compared to 0.27 for a smooth bed. However, at Fr exceeding 5, all configurations converge to a similar slope of 0.25, indicating diminished sensitivity to roughness effects at higher flow velocities. With both side gates open, both roughness types effectively mitigate scour development at Fr below 5, with slopes decreasing to 0.27 for cubic and 0.20 for trapezoidal roughness compared to 0.40 for a smooth bed. Conversely, at Fr exceeding 5, scour development intensifies, with slopes increasing to 0.53 for cubic and 0.27 for trapezoidal roughness, highlighting the superior performance of trapezoidal roughness in high-velocity flow conditions.

Table 3. Percentage Reduction of Observed Scour Hole Depth in Different Experiments

Test Identifier	*Percentage reduction in scour depth*	*Test Identifier*	*Percentage reduction in scour depth*	*Test Identifier*	*Percentage reduction in scour depth*
T_2	%18	T_5	%9	T_8	%29
T_3	%13	T_6	%4	T_9	%17
T_{11}	%27	T_{14}	%7.6	T_{17}	%34
T_{12}	%20	T_{15}	%7.6	T_{18}	%34
T_{20}	%19	T_{23}	%56	T_{26}	%28
T_{21}	%14	T_{24}	%26	T_{27}	%45

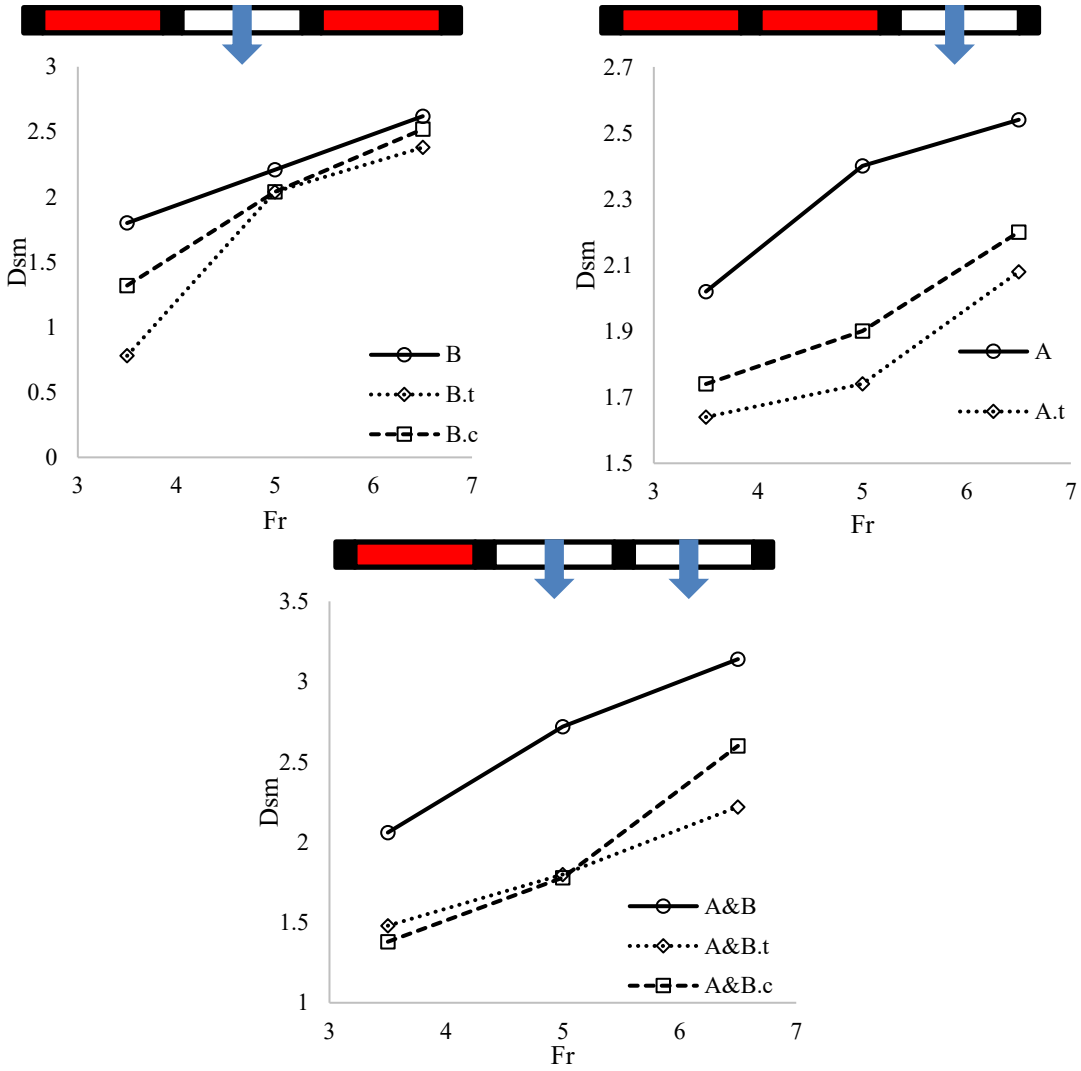


Figure 3. Effect of Roughness Shape on Scour Hole Depth under Different Gate Opening Conditions (Refer to the Symbols Section)

3.2. Length of scour

The formation and length of scour holes downstream of hydraulic structures are critical considerations in hydraulic engineering, as excessive scour can compromise the structural integrity of downstream installations. Current research highlights the effectiveness of incorporating bed roughness elements, specifically trapezoidal and cubic designs, in mitigating the extent of local scour downstream of parallel sluice gates. This study demonstrates that these roughness elements can significantly reduce scour hole length, with trapezoidal roughness emerging as the more effective option. The implementation of trapezoidal and cubic bed roughness elements has been shown to achieve an average reduction in scour hole length of 18.5%. Among these, trapezoidal roughness elements outperform cubic designs, achieving an average reduction of 22.6%, compared to 14.3% for cubic roughness elements. This distinction underscores the potential of trapezoidal roughness as a superior method for controlling local scour in hydraulic systems. Previous Studies on maximum scour length reduction have shown varying results across different research efforts. Amir and Ahmad [39] documented a maximum reduction of 64%, while Ali et al. [29] observed a slightly

higher reduction of 68%. Notably, the findings of the present study align with the latter, also reporting a maximum reduction of 68% (Table 4).

The present study also examines the impact of sluice gate configurations on flow dynamics and the efficacy of bed roughness elements in reducing scour length. When one or more gates are closed, the flow divides into primary and return flows (Sauida [42], Sauida [43] and Elsayed et al. [4]). This bifurcation becomes more pronounced when both side gates are open, as the reduced cross-sectional area for return flow diminishes the influence of bed roughness on scour mitigation. In scenarios where both side gates are open, the average reduction in scour hole length is 15.7% for trapezoidal roughness and 6.1% for cubic roughness. The diminished effectiveness in this configuration can be attributed to the limited interaction between the return flow and the bed roughness elements. When a single side gate is open, the effectiveness of both types of bed roughness elements improves. In this configuration, trapezoidal roughness achieves an average reduction in scour length of 19%, while cubic roughness achieves an average reduction of 15.6%. This increase highlights the importance of flow dynamics in optimizing the performance of bed roughness elements. The most significant reductions in scour length are observed when the middle gate is open. Under this configuration, trapezoidal roughness elements achieve a remarkable average reduction of 33.3%, while cubic roughness elements achieve an average reduction of 21.3%. These results indicate that central flow alignment enhances the interaction between flow and bed roughness, maximizing scour mitigation effectiveness (Table 4).

As Figure 4 shows, analysis of the Xs-Fr relationship reveals distinct behavioral patterns across different gate configurations. For side gate openings, the Xs-Fr line slope for trapezoidal and cubic roughness elements is 12.7 and 14, respectively, at Froude numbers below 5, decreasing to 2 and 0.33 at higher Froude numbers. A similar trend is observed with simultaneous side gate openings, where the slope values are 9.4 and 3.06 for Froude numbers below 5, reducing to 0.93 and 0.66 for higher Froude numbers. This significant variation in slope characteristics is attributed to the combined influence of Froude number and intensified backflows at elevated velocities.

Under symmetric gate opening conditions, particularly during middle gate operation, the Xs-Fr relationship exhibits notably different characteristics. The rate of change of scour pit length for Froude numbers lower than 5 is 10.8 and 7.7 times, and for numbers greater than 5 is 4.4 and 3.7 times for trapezoidal and cubic roughness, respectively. This stability is primarily attributed to symmetric flow patterns and reduced backflow effects. Across all gate configurations, trapezoidal roughness demonstrates superior consistency in performance across varying Froude numbers, underscoring its reliability and effectiveness in scour Length reduction.

Table 4. Percentage Reduction in Scour Hole Length in Different Experiments

Test Identifier	*Percentage reduction in scour hole*	*Test Identifier*	*Percentage reduction in scour hole*	*Test Identifier*	*Percentage reduction in scour hole*
T_2	%0	T_5	%18	T_8	%0
T_3	%0	T_6	%17	T_9	%0
T_{11}	%8	T_{14}	%12	T_{17}	%4
T_{12}	%1	T_{15}	%7	T_{18}	%3
T_{20}	%48	T_{23}	%68	T_{26}	%43
T_{21}	%46	T_{24}	%39	T_{27}	%15

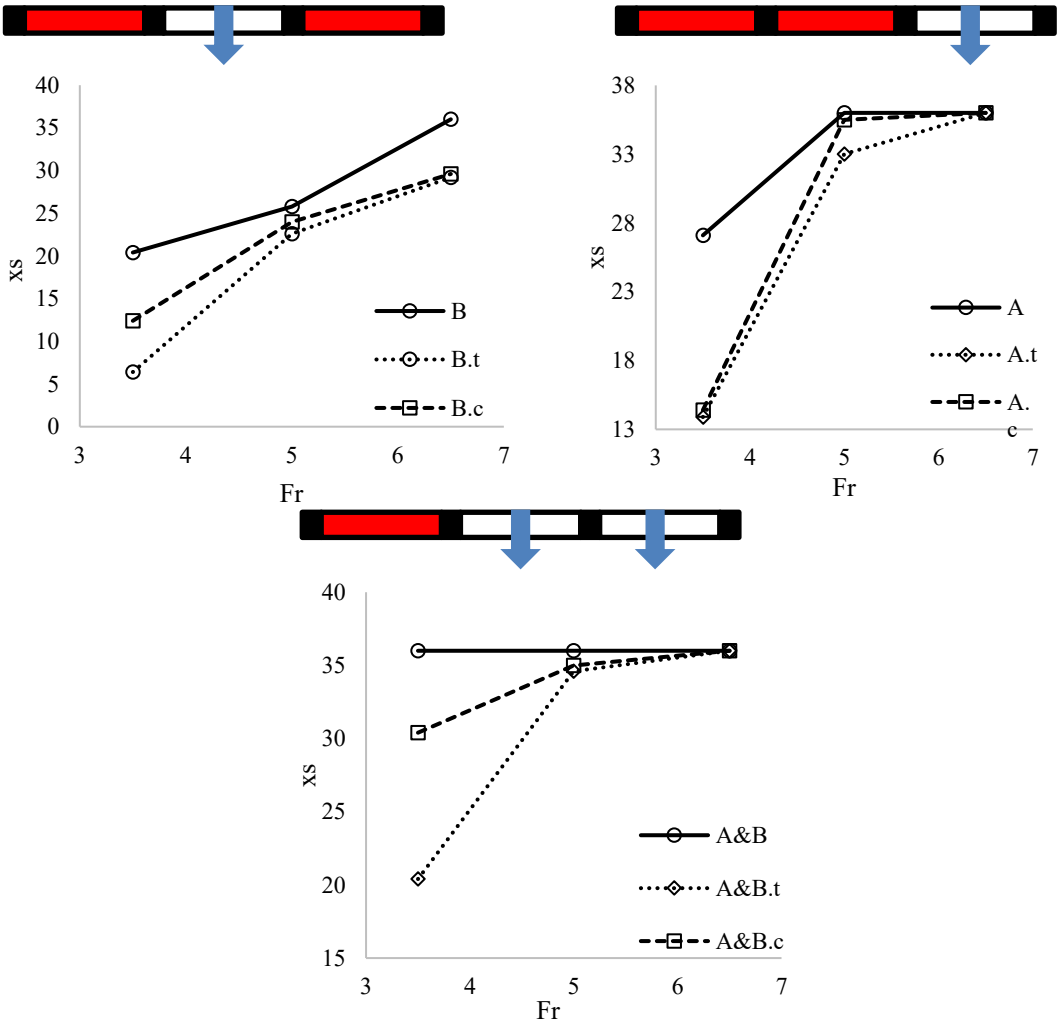


Figure 4. Effect of Roughness Shape on Scour Hole Length under Different Gate Opening Conditions

3.3. The Cross-sectional area of scour

This investigation elucidates the paramount significance of bed roughness in attenuating the scour cross-sectional area downstream of parallel sluice gates. The empirical findings demonstrate that the strategic implementation of roughness elements on the bed surface manifests a substantial mitigation in scour propagation, yielding an average reduction of 26.04%. Among the investigated roughness configurations, trapezoidal geometry performed better than cubic roughness in scour mitigation. Specifically, trapezoidal roughness achieved a 30.52% mean reduction in scour cross-sectional area, significantly exceeding the 21.57% reduction observed with cubic elements (Table 5). As evidenced in Figure 5, the most pronounced variations in the A-Fr gradient occurred during the simultaneous activation of two side gates, particularly in the presence of roughness elements. For trapezoidal and rectangular roughness configurations at low Froude numbers ($Fr < 5$), the recorded values were 69 and 78 respectively, while at higher Froude numbers ($Fr > 5$), values of 34 and 16 were observed, demonstrating disparities of 34.2 and 62.3 units. Similarly, side gate operation resulted in distinct rate differentials across various Froude regimes. For $Fr < 5$ flows, trapezoidal and rectangular roughnesses exhibited values of 77 and 95 respectively, while $Fr > 5$

conditions these values changed to 88 and 55, indicating variations of 10 and 39 units.

This behavioral pattern underwent substantial modification during the middle gate operation. At low Froude numbers (Fr < 5), the A-Fr gradient manifested values of 59 and 63 for trapezoidal and cubic roughnesses respectively, while higher Froude numbers (Fr > 5) conditions produced values of 51 and 34, revealing disparities of 7.7 units for trapezoidal and 29 units for cubic configurations. These trends underscore the significant influence of gate operational modes and bed roughness characteristics.

The distinctive performance differential is attributed to the respective roughness configurations' inherent geometrical and hydraulic properties. Through its sophisticated design, the trapezoidal roughness geometry demonstrates enhanced capability in turbulence generation and flow separation mechanisms compared to its cubic counterpart. These characteristics effectively disrupt high-velocity flow regimes and facilitate superior energy dissipation, consequently attenuating the erosive forces acting upon the bed surface.

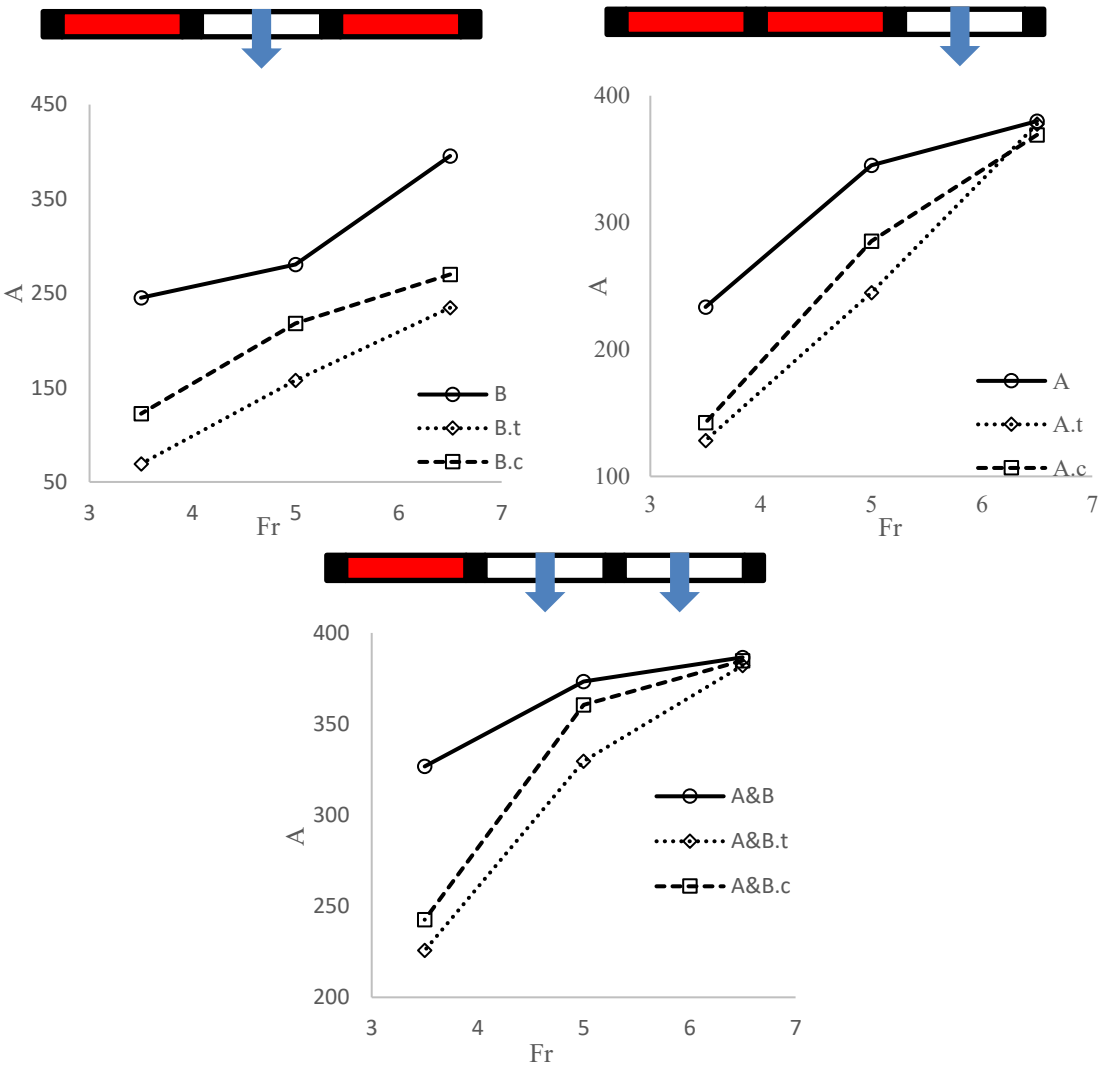


Figure 5. Effect of Roughness Shape on the Cross-Sectional Area of Scour Under Different Gate Opening Conditions

Table 5. Percentage Reduction of the Cross-Sectional Area of Scour Hole in Different Experiments

Test Identifier	*Percentage reduction in cross-section*	*Test Identifier*	*Percentage reduction in cross-section*	*Test Identifier*	*Percentage reduction in cross-section*
T_2	%1	T_5	%40	T_8	%1
T_3	%3	T_6	%31	T_9	%2
T_{11}	%29	T_{14}	%43	T_{17}	%11
T_{12}	%17	T_{15}	%22	T_{18}	%3.5
T_{20}	%45	T_{23}	%71	T_{26}	%30
T_{21}	%39	T_{24}	%50	T_{27}	%25

3.4. Scour volume

The present study underscores the significant potential of strategically implemented bed roughness elements in mitigating erosive process and reducing scour volume. Our findings demonstrate that the introduction of these elements can achieve an average scour volume reduction of 44.2%, highlighting their effectiveness as a scour countermeasure. The efficacy of bed roughness elements, however, is demonstrably influenced by their geometric properties. Among the configurations evaluated, trapezoidal roughness elements exhibited superior performance, achieving a 50% reduction in scour volume. Cubic elements, while still effective, provided a more moderate reduction of 34.7%. These results emphasize the importance of careful consideration and selection of roughness element geometry to optimize the hydraulic performance of the system. Previous investigations, such as that conducted by Ibrahim et al. [42], have explored various protective measures and reported scour volume reductions ranging from 33% to 89%. In comparison, the present study observed a reduction range from 18% to 63% (Table 6) when employing bed roughness elements.

According to Figure 6, the differences between the development rates of scour volume for different roughness shapes at various Froude numbers are closer to each other compared to other investigated parameters. However, the asymmetrical operation of the gates still has significant effects on the slope of the Vs-Fr line. When both side gates are open, the slope of the line for trapezoidal and cubic roughness shapes at Froude numbers below 5 is 9.4 and 11.3, respectively, while for Froude numbers above 5, it is 7.6 and 4.6, showing a difference of 1.8 and 6.7 units, respectively.

This trend is also evident when a single side gate is open, where the slopes for trapezoidal and cubic roughness shapes at Froude numbers below 5 are 5.8 and 8.8, respectively, and for Froude numbers above 5 are 7.4 and 5.8, resulting in differences of -1.6 and 3 units, respectively. However, this trend is completely corrected when the middle gate is open. The performance of bed roughness for Froude numbers below 5 is 4.46 and 5.46, and for Froude numbers above 5, it is 4.78 and 5.56, indicating differences of only 0.3 and 0.1 units for trapezoidal and cubic roughness shapes, respectively.

Scouring poses a significant threat to the stability of downstream structures, often leading to costly repairs and structural failures. This study demonstrates that both gate operation methods and optimal bed roughness design significantly influence scour pit parameters and associated risks. The findings emphasize that incorporating well-designed roughness elements into hydraulic systems can substantially enhance their durability and stability. Careful consideration of roughness geometry during the design phase is crucial for optimizing scour mitigation and developing more resilient and sustainable hydraulic infrastructure.

Table 6. Percentage Reduction in Scour Volume in Different Experiments

Test Identifier	*Percentage reduction in scour volume*	*Test Identifier*	*Percentage reduction in scour volume*	*Test Identifier*	*Percentage reduction in scour volume*
T_2	%36	T_5	%61	T_8	%42
T_3	%27	T_6	%49	T_9	%39
T_{11}	%49	T_{14}	%43	T_{17}	%40
T_{12}	%29	T_{15}	%18	T_{18}	%25
T_{20}	%60	T_{23}	%53	T_{26}	%63
T_{21}	%52	T_{24}	%18	T_{27}	%51

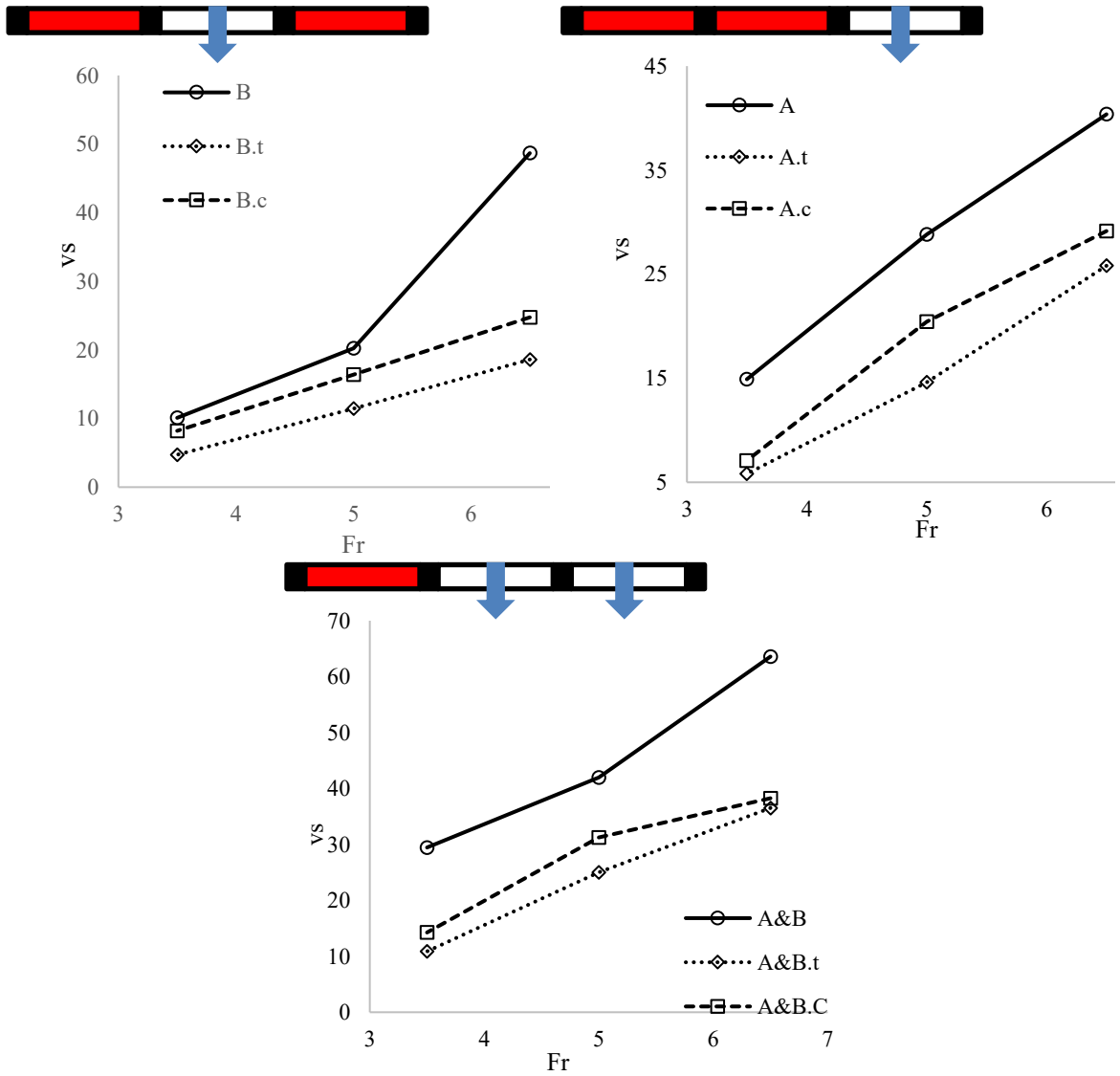


Figure 6. Effect of Roughness Shape on Scour Volume Under Different Gate Opening Conditions

4. Conclusion

This study comprehensively investigates the significant influence of bed roughness configurations on mitigating local scour downstream of parallel sluice gates under a variety of hydraulic conditions. Through an exhaustive analysis of multiple scour parameters, this research unequivocally establishes that trapezoidal roughness elements consistently outperform cubic configurations across all measured indices. Experimental results demonstrate substantial reductions in key scour parameters: maximum scour depth (25.3% for trapezoidal vs. 20% for cubic), scour length (22.6% vs. 14.35%), cross-sectional area (30.52% vs. 21.57%), and scour volume (50% vs. 34.7%). This consistent pattern of superior performance by trapezoidal roughness elements highlights their effectiveness in controlling erosion and dissipating energy.

The flow expansion ratio (e) is identified as a critical parameter affecting the efficacy of bed roughness elements. Optimal performance is observed at an expansion ratio of 0.56 (corresponding to two gates open), where cubic and trapezoidal roughness achieved scour depth reductions of 33% and 30.3%, respectively. In contrast, at lower expansion ratios (e = 0.283, one gate open), the effectiveness diminished significantly, yielding reductions of 14.05% and 20.85% for cubic and trapezoidal configurations, respectively. This variation can be attributed to the formation of asymmetric S-shaped hydraulic jumps and the resulting flow patterns.

The influence of the Froude number (Fr) on scour line slope development rate exhibits distinct patterns across different gate configurations, revealing the complex interplay between flow conditions and roughness effectiveness. Under symmetric flow conditions during middle gate operation, both roughness types demonstrate remarkable consistency across the Froude number range, with trapezoidal and cubic roughness maintaining stable scour volume expansion rates. This stability can be attributed to the symmetric flow patterns and minimized backflow effects typical of middle gate operation. However, during simultaneous side gate operation, performance diverged significantly at higher Froude numbers. While both roughness types effectively controlled scour development at Fr < 5, trapezoidal roughness maintained its effectiveness at Fr > 5, while cubic roughness showed diminished performance. This superior stability of trapezoidal roughness under high-velocity conditions, coupled with its consistent performance across various gate configurations, establishes it as a more reliable solution for scour mitigation in hydraulic systems.

The findings of this study have significant implications for hydraulic engineering practice, particularly in the design and optimization of stilling basins and parallel sluice gate systems. The superior performance of trapezoidal roughness elements in reducing scour parameters suggests that their implementation could significantly enhance the longevity and stability of hydraulic structures. The consistent effectiveness across various flow conditions and gate configurations further indicates that trapezoidal roughness elements offer a robust solution for scour mitigation in hydraulic systems.

Future research should focus on the further optimization of roughness geometries, especially exploring hybrid configurations that combine the beneficial characteristics of different shapes. Additionally, investigating the performance of roughness elements under extreme flow conditions and prolonged exposure to varying hydraulic loads could provide valuable insights for practical applications. The integration of computational fluid dynamics (CFD) modeling with experimental results could further enhance our understanding of complex flow patterns and energy dissipation mechanisms

associated with different roughness configurations.

Symbols:

A	: A gate opens
B	: B gate opens
A & B	: A & B gates open
A.t	: A gate opens with trapezoidal roughness
B.t	: B gate opens with trapezoidal roughness
A & B.t	: A & B gates open with trapezoidal roughness
A. c	: A gate opens with rectangular roughness
B. c	: B gate opens with rectangular roughness
A & B. c	: A & B gates open with rectangular roughness
e	: Expansion ratio

Statements and Declarations

Competing Interests

The authors declare that they have no competing interests.

Financial Disclosure

The authors confirm that no financial support was received for the conduct, analysis, or publication of this research.

Authors' Contributions

The first author was responsible for conducting the laboratory experiments, collecting data, developing the research methodology, and drafting the initial version of the manuscript. The second author contributed to data analysis and critically revised the manuscript for scientific accuracy and clarity. The third author performed scientific editing. The fourth and fifth authors contributed to the critical revision and editorial refinement of the manuscript. All authors made substantial contributions to the conception and design of the study, as well as to data acquisition, analysis, and interpretation. All authors have read and approved the final version of the manuscript and consent to its publication.

Data Availability

The data supporting the findings of this study are available from the corresponding author upon reasonable request.

AI Statement

No artificial intelligence (AI) tools or technologies were employed in the preparation of this manuscript.

Consent for Publication

All authors have read and approved the final manuscript and consent to its submission for publication.

References

1. Mahmoudi B, Hemmati M, Yasi M, Hamidi SA. Investigation of local scour downstream of parallel sluice gates. Iranian Journal of Irrigation & Drainage. 2022;16(5):937–49. 20.1001.1.20087942.1401.16.5.5.0
2. Clemmens AJ. Avoiding submergence transition zone for radial gates in parallel. In: Critical transitions in water and environmental resources management. 2004: Utah. 10.1061/40737(2004)276
3. Jahanshahlou M, Bijan Khan M, Kouchakzadeh S, Khaki I. Immersion threshold curve of multiple parallel sliding gates. In: 15th National Hydraulic Conference of Iran.2016: Imam Khomeini International University, Qazvin, Iran. https://civilica.com/doc/562925
4. Elsayed H, Helal E, El-Enany M, Sobeih M. Impacts of multi-gate regulator operation schemes on local scour downstream. ISH Journal of Hydraulic Engineering. 2021;27(1):51–64. 10.1080/09715010.2018.1511386
5. Melville BW, Coleman SE. Bridge scour. Water Resources Publication; 2000.
6. Richardson E V, Davis SR. Evaluating scour at bridges. United States. Federal Highway Administration. Office of Bridge Technology; 2001.

7. Rajaratnam N. Hydraulic jumps on rough beds. Trans Eng Inst Canada. 1968;11(A-2):1–8. 10.1061/(ASCE)0733-9429(2002)128:7(656)
8. Bejestan MS, Neisi K. A new roughened bed hydraulic jump stilling basin. 2009. 10.3923/ajaps.2009.436.445
9. Ead SA. Effect of bed corrugated on the characteristics of a hydraulic jump. King Soud University. Final research report; 2007.
10. Ead SA, Rajaratnam N. Hydraulic jumps on corrugated beds. Journal of Hydraulic Engineering.2002;128(7):656–63.10.1061/(ASCE)0733-9429(2002)128:7(656)
11. Izadjoo F, Shafai-Bajestan M. Effects of trapezoidal shape corrugated bed on the characteristics of hydraulic jump. In: 17th Canadian hydrotechnical conference, Alberta, Canada. 2005. p. 17–9.
12. Karimi M, MUSAVI JSH, SHAFAI BM. The effect of roughness in pressure fluctuations in the stilling basin with sudden expansion. 2014.10.22060/ceej.2016.678
13. Abbaspour A, Abdian Rokni MR. Study of hydraulic jump characteristics in diverging stilling basins with square bars roughness. Iranian Journal of Irrigation & Drainage. 2016;10(5):636–48.
14. Daneshfaraz R, Majedi Asl M, Mirzaeereza R. Experimental study of expanding effect and sand-roughened bed on hydraulic jump characteristics. Iranian Journal of Soil and Water Research. 2019;50(4):885–96. 20.1001.1.2008479.1398.50.4.10.8
15. Parsamehr P, Farsadi Zadeh D, Hosein Zadeh Dalir A, Nasr Esfahani MJ, Abbaspour A. Investigation of Pressure Fluctuations of Hydraulic Jump on Rough Bed. Irrigation Sciences and Engineering. 2018;41(2):197–210.
16. Hasani MN, Nekoufar K, Biklarian M, Jamshidi M, Pham QB, Anh DT. Investigating the pressure fluctuations of hydraulic jump in an abrupt expanding stilling basin with roughened bed. Water (Basel). 2022;15(1):80. 10.3390/w15010080
17. Mahtabi G, Chaplot B, Azamathulla HM, Pal M. Classification of hydraulic jump in rough beds. Water (Basel). 2020;12(8):2249.10.3390/w12082249
18. Fallahi B, Heidarpour M. Experimental Study of the Hydraulic S-Jump with Bed Roughness. 2023. 10.21203/rs.3.rs-3373043/v1
19. Akib S, Ahmed AA, Imran HM, Mahidin MF, Ahmed HS, Rahman S. Properties of hydraulic jump over apparent corrugated beds. Dam Engineering. 2015;25(2):65–77.
20. Gandhi S. Empirical Modeling of Flow Characteristics in Suddenly Expanding Channels. Journal of Applied Fluid Mechanics. 2024;17(4):857–69. 10.47176/jafm.17.4.2213
21. Tahmasbipour M, Azizi Nadian H, Ahadiyan J, Oliveto G, Sajjadi SM, Kiyani AM. Experimental Investigation of T-Jump Stabilization Using Water Jets and Sinusoidal Corrugated Beds. Water (Basel). 2024;16(23):3513. 10.3390/w16233513
22. Sajadi SM, Feridani FE, Ahadiyan J. Numerical study of energy loss and S-type hydraulic jump length using cross beams as roughness in sudden expansion. Advanced Technologies in Water Efficiency. 2025; 5 (1): 78-97. 10.22126/atwe.2025.11522.1148
23. Parsamehr P, Hosseinzadeh DA, Farsadizadeh D, Abbaspour A. Hydraulic Jump on a Bed with Half Cylindrical Shape Bars. Journal of Water and Soil Science. 2012; 26(3):775-785
24. Gupta SK, Dwivedi VK. Evaluation of hydraulic jump characteristics in rough sloping surfaces for sustainable environment: A laboratory investigation. Sigma Journal of Engineering and Natural Sciences. 2025;43(1):148–59. 10.14744/sigma.2025.00012
25. Hamidifar H, Omid MH, Nasrabadi M. Scour downstream of a rough rigid apron. World Appl Sci J. 2011;14(8):1169–78.
26. Ali HM, El Gendy MM, Mirdan AMH, Ali AAM, Abdelhaleem FSF. Minimizing downstream scour due to submerged hydraulic jump using corrugated aprons. Ain

Shams Engineering Journal. 2014;5(4):1059–69.
27. Aamir M, Ahmad Z. Effect of apron roughness on flow characteristics and scour depth under submerged wall jets. Acta Geophysica. 2021;1–17. 10.1007/s11600-021-00672-9
28. Urbański J, Kiraga M, Bajkowski S. The impact of energy dissipation devices on the size of local scour beds on the sluice gate model. Archives of Civil Engineering. 2020;66(4):507–24. DOI: 10.24425/ace.2020.135234
29. Aamir M, Ahmad Z, Pandey M, Khan MA, Aldrees A, Mohamed A. The effect of rough rigid apron on scour downstream of sluice gates. Water (Basel). 2022;14(14):2223. 10.3390/w14142223
30. Maleki S, Fiorotto V. Hydraulic jump stilling basin design over rough beds. Journal of Hydraulic Engineering. 2021;147(1).
31. Mahmoudi B, Hemmati M, Yasi M, Ahmad Hamidi S. Experimental Study of the Time Scale for Local Scour Downstream of Parallel Sluice Gates. Journal of Irrigation and Drainage Engineering. 2023;149(10). 10.1061/jidedh.ireng-10012
32. Roth A, Hager WH. Underflow of standard sluice gate. Exp Fluids. 1999;27(4):339–50. 10.1007/s003480050358
33. Abdellateef M. Energy dissipation DS low head irrigation structures using bed roughness. Ph D Thesis, Ain Shams University, Cairo, Egypt. 1984
34. Aboulatta N. Study of the effect of location and length of roughened beds on flow characteristics in stilling basins. Ph D Thesis, Ain Shams University, Cairo, Egypt. 1986
35. Abdelsalam W. Optimum Height of Bed Roughness in Stilling Basins. Ain Shams University, Engineering Bulletin. vol. 1988; 1(22): 59-73.
36. Raudkivi AJ. Loose boundary hydraulics. CRC Press; 2020. 10.1201/9781003077800
37. Das BM. Advanced soil mechanics. CRC press; 2019. 10.1201/9781351215183
38. Chow VT. Open-channel hydraulics mcgraw-hill book company, 1959. ISBN 07-010776-9; 1959.
39. Aamir M, Ahmad Z. Effect of apron roughness on flow characteristics and scour depth under submerged wall jets. *Acta Geophysica.* 2021;1-17. 10.1007/s11600-021-00672-9
40. Khalili Shayan H, Farhoudi J, Vatankhah A. Analysis of sequent depth ratio and length of sudden expanding hydraulic jump under symmetrical and asymmetrical developments. Journal of Hydraulics. 2020;15(1):75–95. 10.30482/jhyd.2020.208837.1420
41. Bremen R. Expanding stilling basin. Ph.D Thesis, Ecole Polytechnique Federale de Lausanne (EPFL), Lausanne, Switzerland, 1990
42. Sauida MF. Reverse flow downstream multi-vent regulators. Ain Shams Engineering Journal. 2013;4(2):207–14. 10.1016/j.asej.2012.09.002
43. Sauida MF. Prediction of hydraulic jump length downstream of multi-vent regulators using Artificial Neural Networks. Ain Shams Engineering Journal. 2016;7(2):819–26. 10.1016/j.asej.2015.12.005

© 2025 by the authors. Licensee SCU, Ahvaz, Iran. This article is an open access article distributed under the terms and conditions of the Creative Commons Attribution 4.0 International (CC BY 4.0 license) (http://creativecommons.org/licenses/by/4.0/).

Variation in Effluent Quality of Household Water Treatment Systems Over Time: A Case Study in Ahvaz

Seyedeh Tooba Mirsalari[1] ,Hossein Sasani[*,1] ,Mohammad Azizipour[2] , Neematollah jaafarzadeh[3]

1. Department of Environmental Engineering, Faculty of Civil Engineering and Architecture, Shahid Chamran University of Ahvaz, Ahvaz, Iran.
2. Civil Engineering Department, Faculty of Engineering, Shahid Chamran University of Ahvaz, Ahvaz, Iran.
3. Environmental technologies research center, Ahvaz jundishapur university of medical sciences, Ahvaz, Iran.

***Corresponding Author:**
Hossein Sasani,

Email: h.sasani@scu.ac.ir
Received: 2025.05.02
Accepted: 2025.05.29
J. Hydraul. Struct., 2025; 12(1):69-83
DOI: 10.22055/jhs.2025.49748.1353

ABSTRACT

In certain regions, increased salinity in surface water and the aging of urban water distribution networks have led many citizens to rely on household water purification systems. However, if the filters in these systems are not replaced on time, the quality of the treated water can deteriorate. This study evaluated the performance of three household water purifiers over a one-year period in Ahvaz, Iran. Parameters such as Total Dissolved Solids (TDS), pH, turbidity, and total coliforms were measured monthly at both the inlet and outlet of the systems. In addition, weekly visual inspections were conducted to monitor changes in the appearance of the first-stage filters. The results confirmed the absence of coliforms in all effluent samples. However, in the first month following the installation of the first filter, the turbidity of its output exceeded the acceptable limit. Notably, significant color change in the first filter occurred by the second month. Furthermore, it was observed that two years after membrane installation, regular monitoring of output TDS is essential. If the TDS exceeds permissible levels, membrane replacement is necessary. Additionally, when the membrane is new, the TDS of the treated water may drop below 50 mg/L, increasing the risk of acidification. In such cases, adjusting the pH through a mixing valve or replacing the sixth-stage filter is recommended to ensure water quality and safety.

KEYWORDS

household water purifiers, TDS, Turbidity, pH, Coliforms.

1. Introduction

Providing access to safe drinking water is one of the core responsibilities of public authorities. To achieve this objective, a comprehensive infrastructure is developed, including water intake systems, treatment facilities, storage reservoirs, transmission pipelines, and distribution networks. The selection of a suitable treatment process, tailored to the characteristics of the raw water, along with careful attention to both design and operational standards, is essential for delivering water that meets safety and quality benchmarks. According to the latest revisions of national standards 1053 and 1011 by the Institute of Standards and Industrial Research of Iran (ISIRI), and consistent with the guidelines of the World Health Organization (WHO, 2011), water quality assessment is categorized into three main components: physical, chemical, and microbial. Each category includes defined permissible and maximum contaminant limits for various parameters. Nonetheless, challenges such as declining raw water quality due to prolonged drought and the influx of untreated wastewater into surface water sources have resulted in treated water from some conventional systems failing to meet safe drinking standards.

In addition, the aging and deteriorating condition of distribution network pipelines increases the likelihood of secondary contamination entering the water supply, thereby jeopardizing its safety at the point of use. This risk is further aggravated by external stressors such as extreme weather events, which can inflict significant damage on water treatment and distribution systems, adversely affecting both the availability and quality of drinking water[1]. Under such circumstances, consumers may become vulnerable to waterborne illnesses [2]. Simply having access to tap water does not ensure its safety, as contamination may arise at multiple stages—including the source, within the distribution network, or during the collection, transport, and storage of water. As a result, in many regions, the lack of reliable access to safe drinking water has driven populations to adopt alternatives like bottled water and Point-of-Use (POU) treatment methods [3]. The processes of purifying and safely storing water at the household level are collectively termed "household water treatment and safe storage" (HWTS), or more broadly, POU treatment (WHO, 2013). Until treated piped water becomes universally accessible, POU interventions represent a practical and cost-effective means of protecting public health in underserved communities [4]. Consequently, Point-of-Use (POU) drinking water treatment technologies are gaining widespread adoption due to their effectiveness in removing a wide range of contaminants and mitigating associated health risks. Numerous studies have demonstrated the considerable efficiency of household water treatment systems in reducing pollutant levels in drinking water. However, these systems are not without limitations [5]. A key concern is the unintentional removal of essential minerals during the treatment process, which may lead to nutritional deficiencies and an increased risk of bone-related disorders with prolonged consumption of demineralized water [6]. Additionally, the relatively high upfront costs of these systems, along with the recurring expenses for maintenance—particularly filter replacement—can be economically burdensome. In systems employing Reverse Osmosis (RO) technology, water is separated into purified and concentrated waste streams, the latter of which is discharged, often increasing overall water consumption. Consequently, the use of such systems is typically recommended only in regions where the drinking water is characterized by high salinity or elevated nitrate levels [7]. A reduction in fluoride concentration in treated water can adversely affect long-term dental and skeletal health. As such, it is crucial to educate both users and operators of Point-of-Use (POU) systems on water-related health issues and the potential consequences of improper usage. Regular and timely replacement of system filters is also essential to maintain the quality of treated water and to ensure continued protection against contaminants [5]. In a study by Angela D. Coulliette and colleagues examining the effectiveness of household water purification systems in developing nations, the findings indicated a substantial decrease in the risk of infectious diseases following water treatment [8]. Nevertheless, other research presents contrasting evidence, suggesting that water purified by such systems may still harbor various bacterial contaminants [9-12]. For instance, a study conducted in Sari, Iran, revealed a significant relationship between filter age and the presence of heterotrophic bacteria as well as residual chlorine levels in treated water, highlighting the importance of proper maintenance [10]. A study conducted in Turkey reported that coliform concentrations at the outlet of certain household water treatment devices were higher than at the inlet. This phenomenon was attributed to several factors, including aging municipal water distribution networks, diminished chlorine efficacy due to prolonged water retention times, poorly maintained building water storage tanks, and delays in filter replacement [9]. Another investigation

found that RO filters outperformed Ultrafiltration (UF) systems in removing organic contaminants and reducing turbidity. However, while household water purifiers are designed to lower microbial risks, under certain conditions they may inadvertently increase them. The most frequently detected bacteria within membrane pores were Escherichia coli and Pseudomonas aeruginosa. Therefore, to minimize microbial contamination, filters must be replaced or backwashed before reaching saturation, and integrating a UV-LED disinfection step at the final stage of treatment is recommended [12]. imilarly, a study on water purifiers in Ahvaz (Iran) revealed that the heterotrophic plate count (HPC) at the device outlet exceeded that at the inlet, underscoring the importance of timely filter maintenance [11]. A review of studies assessing the performance of household water treatment devices in Iran indicates that delayed filter replacement leads to a deterioration in the microbial quality of treated water. Specifically, the average concentrations of heterotrophic plate count (HPC) and total coliforms in the effluent have been reported at 436 and 36 colony-forming units per 100 mL, respectively [5]. These findings underscore the critical need for proper maintenance to ensure that the treated water remains within international drinking water quality standards. Timely replacement of filters is essential to consistently produce safe and potable water. Although numerous studies have evaluated the microbial quality of water produced by these devices, there remains a gap in the literature regarding how the effluent quality evolves over a defined period following filter installation. This highlights the need for longitudinal studies to better understand the temporal dynamics of water quality in household treatment systems. Accordingly, this study investigates the year-long performance of household water purification devices in the city of Ahvaz, with the aim of identifying trends in the quality of treated water over time. A key objective is to determine the point at which water quality parameters begin to exceed the acceptable thresholds defined by drinking water standards, thereby establishing the optimal interval for filter replacement. Given the findings of prior studies, maintaining these devices through proper and timely filter changes is critical to ensuring that the treated water remains safe for consumption. Despite extensive research on the output quality of household water purifiers, there remains a lack of longitudinal data assessing how their performance changes over time. This study seeks to address that gap by monitoring variations in water quality throughout a one-year period, ultimately aiming to recommend an evidence-based schedule for filter replacement to consistently achieve standard-compliant water quality.

2. Materials and methods

2.1 Study area

Ahvaz, is situated in the southwestern region of Iran. The city’s primary water supply is derived from surface water sources, which undergo conventional treatment processes prior to distribution through the municipal network. Despite these treatments, residents frequently experience issues such as elevated turbidity, as well as unpleasant taste and odor in tap water. As a result, many consumers turn to POU water purification systems to enhance the quality of their drinking water.



Figure 1. Location of studied systems in Ahvaz city

2.2. Selection of POU Systems

For this study, three POU water purification systems were selected from different residential areas within Ahvaz city (Fig. 1). All systems, produced by comparable manufacturers, shared similar specifications, with a daily treatment capacity of 10 to 12 liters. Each unit incorporated a six-stage filtration process designed to maximize purification efficiency. The first three stages functioned as pretreatment filters. The first stage included a microfilter, primarily responsible for removing total suspended solids (TSS) and reducing turbidity. The second and third stages featured granular activated carbon (GAC) and block activated carbon (BAC) filters, respectively, which were employed to remove free chlorine and residual organic compounds. Notably, the GAC filter contains larger particles, offering a higher flow rate but lower contaminant removal efficiency. Conversely, the BAC filter is composed of much finer particles—approximately 5 to 20 times smaller—which allow for more thorough contaminant removal at the expense of flow rate [13]. In the fourth stage of filtration, each system utilizes a horizontally mounted reverse osmosis (RO) membrane to effectively remove dissolved minerals and other impurities from the water. To support this process, a pump delivering pressure between 6 and 7 bar is employed, ensuring sufficient force for water to pass through the semipermeable membrane. A key distinction among the three selected POU systems is the age of their RO membranes. In Device (1), a new membrane was installed at the beginning of the sampling period. Device (2) was fitted with a membrane that had been in use for one year, while Device (3) featured a membrane with a two-year usage history. This variation in membrane lifespan provides valuable insight into the long-term performance and efficiency of the systems under real-world operating conditions. The fifth and sixth stages are dedicated to post-treatment processes. The fifth stage includes a taste-enhancing filter designed to improve the palatability of the RO-treated water, which often tastes flat due to the removal of both contaminants and beneficial ions. The sixth stage incorporates a remineralization filter that reintroduces essential minerals, thereby enhancing both the nutritional value and overall acceptability of the water. Table 1 presents a detailed summary of the characteristics and functions of each filtration stage, offering a clear understanding of their specific contributions to the overall purification process.

Table 1. Specifications of the filters installed in the household water purifier

Filter Location	Filter Name	Filter material	Performance	Reference
First stage	Microfiltration	Polypropylene	Turbidity removal	[14, 15]
Second stage	Granular activated carbon	Coal	Chlorine and organic matter removal	[15]
Third stage	Carbon block	Coal	Chlorine and organic matter removal	[16]
Fourth stage	Membrane	polyamide	demineralization	[1]
Fifth stage	Post carbon	Coal	Regulation of taste and odor	[15]
Sixth stage	Remineralization	Minerals	Returning minerals to water	[17]

2.3. Sampling method

This study was conducted over a one-year period, from July 2021 to June 2022. Three residential units located in different districts of Ahvaz—Golestan, Kian Pars, and Koye Mellat—were selected as sampling sites, as illustrated in Figure 1. All three POU devices were configured with identical filter arrangements, detailed in Figure 2, ensuring consistency in system design across sampling locations. Water samples were collected from three distinct points within each POU system: before filtration, after the RO membrane, and at the final output. As summarized in Table 2, a total of 102 samples were obtained throughout the study period. It is important to note that sampling from Device (3) commenced in the third month of the study, resulting in fewer total samples from that unit. Furthermore, the first-stage filter (microfilter) featured a transparent housing, allowing for regular visual inspection of its condition. To assess potential clogging, this filter was removed from its housing and examined on a weekly basis.

Table 2. Specifications of sampling points and sampling frequency

Row	Parameter	Input	First filter output	System output	Sampling frequency
1	pH	✓	–	✓	Monthly
2	TDS	✓	–	✓	Monthly
3	Turbidity	✓	✓	–	Monthly
4	Total Coliforms	✓	–	✓	Monthly
5	visual Inspection	✓	✓	✓	Weekly



Figure 2. The studied household water purifier

2.4. Test method

The parameters of pH, turbidity, and total TDS were analyzed using potentiometric, nephelometric, and gravimetric techniques, respectively, at the laboratory of Khuzestan Water and Wastewater Engineering Services Company. The equipment employed included an analytical balance (AND GF-3000, Japan) with a maximum capacity of 3100 grams and a precision of 0.01 grams, a pH meter (HACH Sension3, USA), and a turbidity meter (HACH 2100AN, USA). TDS measurements were conducted using filter paper with a pore size less than 0.2 micrometers. Total coliform bacteria were detected through the Presence/Absence (PA) test method applied to the water samples. Concurrently, the first-stage filter of each device was photographed weekly to monitor any visual changes. All sampling and analyses followed the relevant water and wastewater testing standards[18]. Finally, the obtained results were evaluated in comparison to the World Health Organization (WHO) guidelines and the drinking water quality standards established by Iran.

3. Results and discussion

3.1. Turbidity

To assess the efficacy of the first filter in turbidity removal, two methods (photographing the filter and a turbidity test) were employed. Typically, the first filter in each system is housed in a transparent container, allowing visual observation of its color change from white to brown, indicating the need for replacement. Over a two-month period, the clogging depth of this filter was monitored weekly, comparing the results of turbidity tests and filter clogging depth. Most membrane manufacturers recommend that water entering the membrane should have a turbidity of less than 1 NTU. Hence, surpassing this value in the output turbidity was established as the criterion for replacing the first filter. Fig. 3 illustrates changes in output turbidity for the first filter of System 1, while Fig. 6 depicts the weekly color change procedure over three months. Replacements were carried out in September, January, and June based on the appearance color of the filter. Fig. 6 highlights significant color changes on the filter surface after two months of installation. Fig. 4 showcases variations in the turbidity of the inlet and outlet water of the first filter of System 2, and Fig. 7 displays its color change procedure. Replacements occurred in October, January, and April based on appearance color, with the output turbidity exceeding 1 NTU about two months after the first filter replacement, as indicated in Fig. 4. Fig. 7 demonstrates color changes starting one month after filter installation, progressing to the inner layers by the end of the second month. Fig. 5 and Fig.8 depict changes in the color of the first filter in System 3 and variations in raw water turbidity and the first filter's output turbidity. Replacements took place in October, January, April, and July, guided by appearance color. An increase in output turbidity was observed approximately one month after filter installation, while raw water turbidity averaged 1.1 NTU during the sampling period, often exceeding 1 NTU. Fig.7 indicates that the color change on the filter surface began one week after installation. Thus, signs of first filter clogging manifested about one month after installation, reaching a potential maximum within second months.

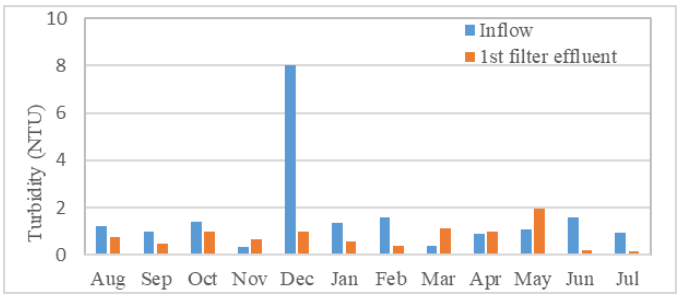


Figure 3. Changes in the input and output turbidity of system 1 during the sampling period

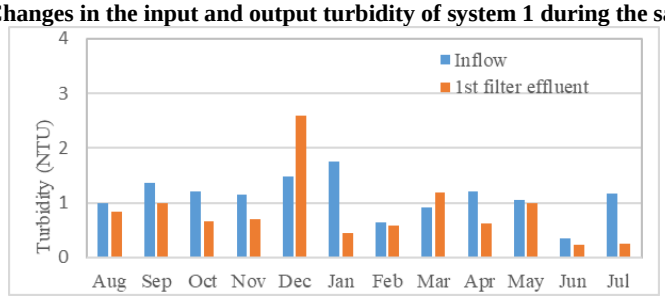


Figure 4. Changes in the input and output turbidity of system 2 during the sampling period

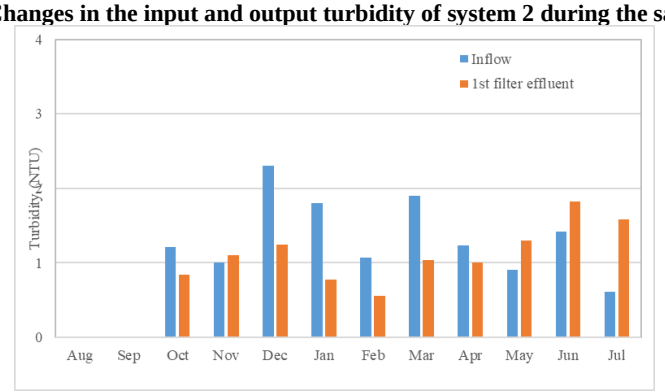


Figure 5. Changes in the input and output turbidity of system 3 during the sampling period

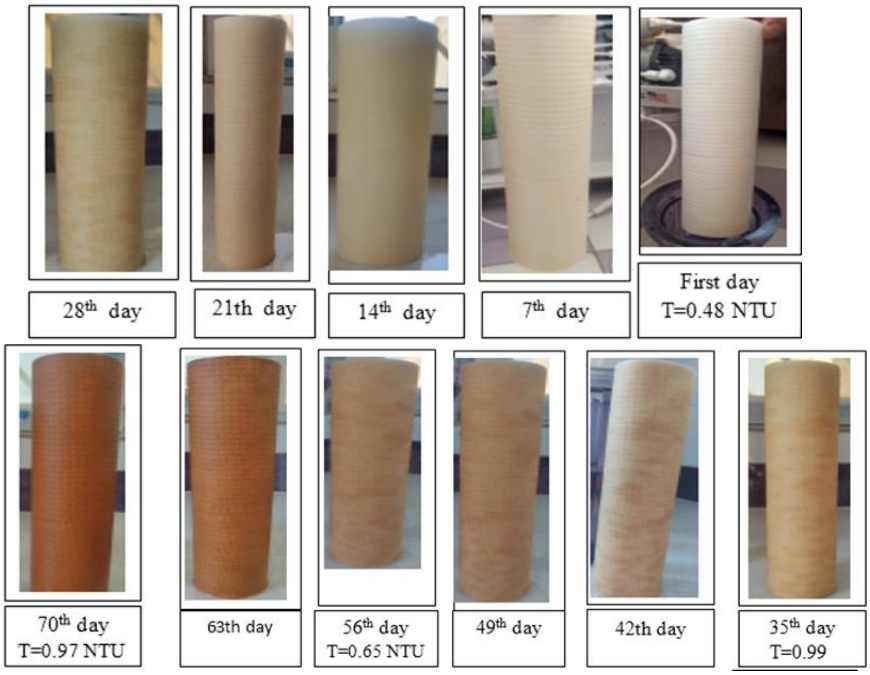


Figure 6. Appearance changes of the first filter of the system 1

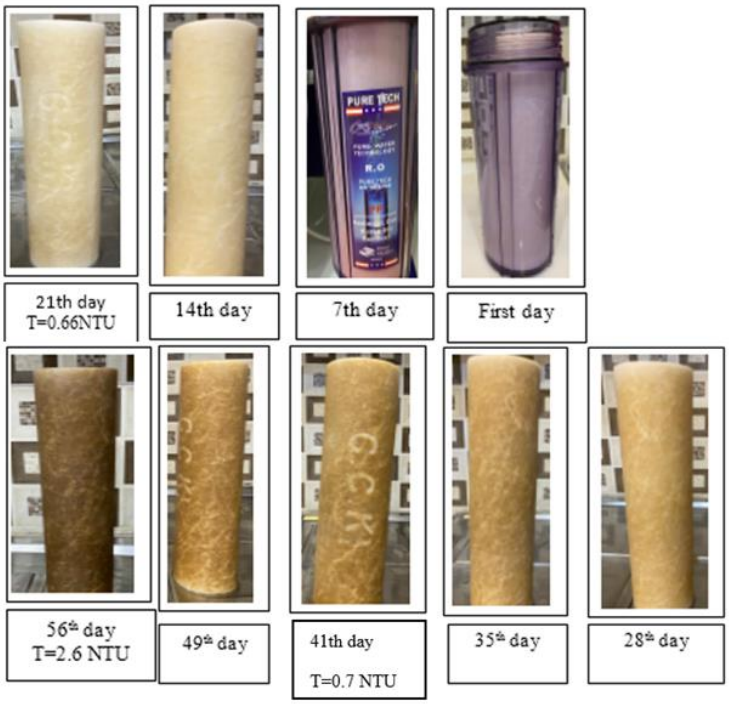


Figure 7. Appearance changes of the first filter of system2

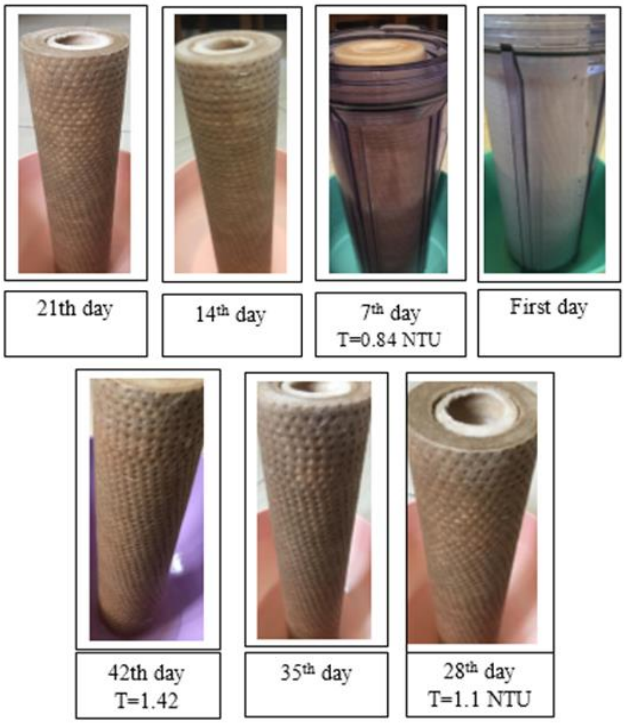
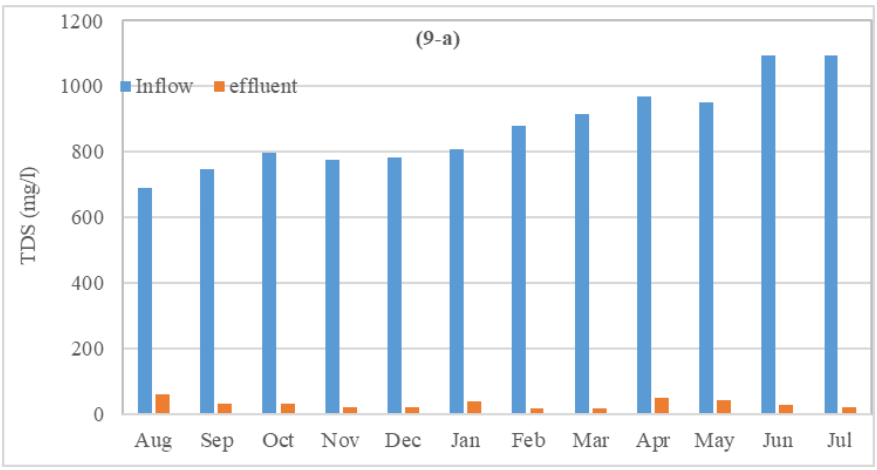


Figure 8. Appearance changes of the first filter of system3

3.2. TDS

Figure 9-a shows the fluctuations in input and output TDS for System 1 over the duration of one year. The input TDS values ranged from 700 to 1100 mg/L, while the output TDS consistently stayed below 100 mg/L. This level complies with the acceptable limits set by both ISIRI (1000 mg/L) and WHO (600 mg/L). However, an

output TDS below 100 mg/L may suggest the excessive removal of important dissolved minerals such as calcium, magnesium, and fluoride, which are beneficial for human health but tend to be largely removed by the membrane [19, 20]. Figure 9-b illustrates the TDS changes for System 2 during the year following membrane installation. The input TDS fluctuated between 700 and 1100 mg/L, and output TDS ranged from 100 to 200 mg/L. Similar to System 1, the output TDS was within recommended limits, although it was approximately 100 mg/L higher than System 1's output. This increase might be related to the longer membrane lifespan in System 2. Figure 9-c depicts the input and output TDS variations for System 3 across one year. The membrane in this device had been installed two years before sampling began. Input TDS ranged from 800 to 1300 mg/L, while output TDS was between 300 and 500 mg/L. In the final month of the sampling period, the membrane was replaced, causing output TDS to drop to 50 mg/L. Despite the TDS levels being within acceptable standards, consumers found the water's taste unsatisfactory, prompting filter replacement roughly three years after installation. Comparing the three systems indicates that during the first year of membrane use, output TDS consistently remained below 100 mg/L. In the second year, the output TDS levels increased to approximately 200 mg/L, and by the third year, they approached the upper permissible limits set by the WHO. It is important to be cautious about very low TDS concentrations, as water with insufficient mineral content may pose health risks, such as cardiovascular issues, impaired thyroid function, and a higher likelihood of diseases like osteoporosis and cancer. Consequently, in addition to following standards that specify maximum allowable levels, it is recommended to also consider minimum thresholds for essential minerals to protect human health during the use of these purification devices (see Table 3) [21, 22]). The study by Sediq et al. [23] reported output TDS values below 100 mg/L, which corresponds closely to the TDS levels observed in System 1 of the current research. Similarly, Bonnélye et al. [24] developed a seven-stage treatment process that included a Reverse Osmosis (RO) system to reduce TDS in Curacao's drinking water, achieving a final TDS concentration below 150 mg/L—comparable to the TDS output recorded for System 2 in this study. Dinarello et al. [25] reported an output TDS around 500 mg/L, aligning with the values seen for System 3 in the last month of sampling here. However, none of these studies specified the membrane lifespans used during their experiments.



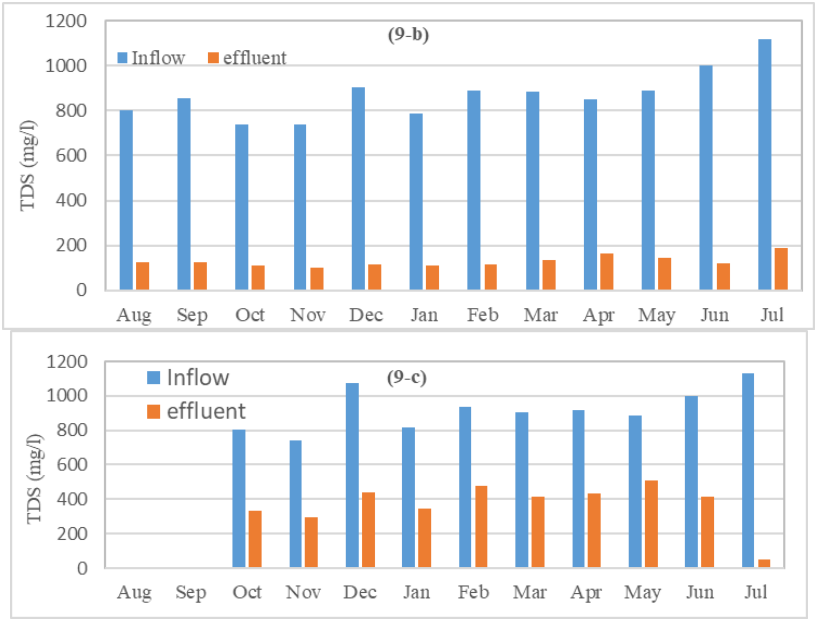


Figure 9. Changes in input and output TDS of systems 1(a), 2(b) and 3(c)

3.3. pH

As shown in Figure 10, the pH levels of all three systems decreased throughout the sampling period, reaching acidic values of 5.8, 6.7, and 6.5 for Systems 1, 2, and 3, respectively. This acidification is mainly due to the removal of alkalinity components, such as carbonate and bicarbonate ions, by the membranes. The extraction of these ions disturbs the balance between hydrogen (H^+) and hydroxide (OH^-) ions, causing the water to become more acidic, as noted by the WHO[26]. The WHO recommends a minimum pH of 6.5 for drinking water, and Figure 14 reveals that the pH of the effluent from all three systems occasionally reached this lower limit or even dropped below it, indicating acidity. Therefore, it is crucial to monitor and address this acidification because consuming acidic water over the long term may have adverse health impacts. Moreover, acidified water can cause unpleasant taste and heightened corrosiveness, which is particularly problematic near metal pipes [27]. Research by Rezaeinia et al. [27] and Saini [28] suggests that the intake of acidic water and beverages can disrupt the mineral balance in the human body. This is especially significant for cancer patients who often suffer from electrolyte imbalances such as hyponatremia, hypokalemia, hypocalcemia, and hypomagnesemia, emphasizing the importance of maintaining adequate mineral content in drinking water [21]. Although adjusting the pH of membrane-treated water by mixing it with other sources to increase TDS is possible, this method is not advisable for long-term use in Ahvaz due to the risk of sediment buildup and clogging in mixer taps. In System 3 (Figure 10-c), replacing the fourth filter in July led to a decrease in TDS from 400 to 50 mg/L and a corresponding pH drop from 7 to 6.5. Despite these fluctuations, continuous monitoring of pH in the treated water is recommended. Other studies, such as those by Yari et al. [29-31], have also confirmed the acidification of membrane-treated water, although their focus was more on the effects rather than the pH variation patterns. Conversely, some research has consistently found that output pH remained within acceptable standards, likely due to the effective functioning of the fourth and sixth filters during the sampling period [14, 25, 27, 32-35].

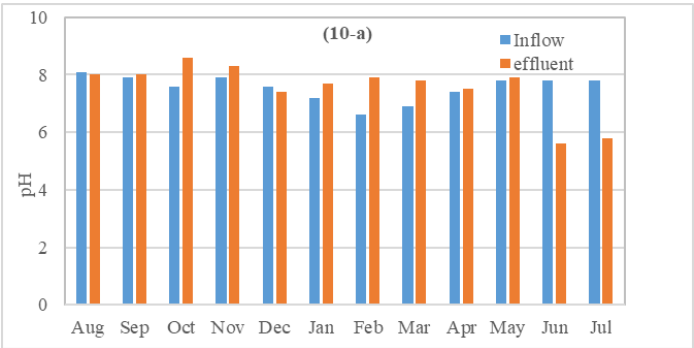
Table 3. Suggested suitable ranges for drinking water nutrients (Rosborg & Kozisek., 2019)

Parameter	Range	Unit
pH	7-8.5	-
Calcium	30-80	mg/l
Magnesium	10-50	mg/l
Bicarbonate	100-300	mg/l
Sulphate	25-100	mg/l
Fluoride	0.5-1	mg/l
Chloride	20-50	mg/l
TDS	100-500	mg/l

Figure 11 presents the relationship between pH and TDS for both the inlet and outlet water across all three systems. In these graphs, the TDS values are plotted in ascending order, with corresponding pH values shown for each data point. Figures 11-a, 11-c, and 11-e illustrate that the TDS levels of the input water consistently exceeded 690 mg/L, while the pH values remained within the acceptable range of 6.5 to 8.5, as per drinking water standards. In contrast, Figures 11-b, 11-d, and 11-f, which depict the treated water from each system, show several instances where the pH dropped below the minimum recommended limit of 6.5. Notably, these drops in pH coincided with very low TDS levels, often below 50 mg/L. This pattern points to a potential risk of water acidification as TDS decreases. Supporting this observation, Rosborg and Kozisek [21] have recommended a minimum TDS concentration of 100 mg/L in drinking water to ensure adequate mineral content and avoid associated health risks.

3.4. Microbial quality

During the sampling period, total coliforms were monitored in both the influent and effluent water. The findings showed that coliforms were detected in only three of the input water samples, while none were found in the treated water from any of the systems. This result is consistent with previous studies conducted by Dehghani et al. [36] and Twanger et al. and Twanger et al. [6]. In contrast, some studies, including those by Yari et al. [29] and Ebrahimi et al. [37] eported the presence of coliforms in the outlet water. These instances were often associated with delayed membrane replacement, during which microbial leakage could occur due to membrane fatigue or degradation [6]. Lin et al. [6]. Lin et al. [12] also observed coliform contamination in the treated water and suggested that to ensure microbial safety, either timely membrane replacement or the incorporation of a UV disinfection unit at the final treatment stage is necessary.



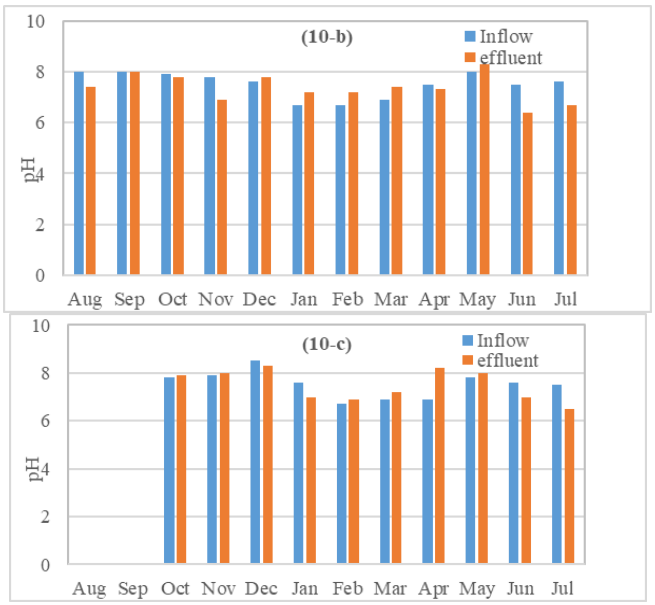


Figure 10. Changes in input and output pH of systems 1(a), 2(b) and 3(c)

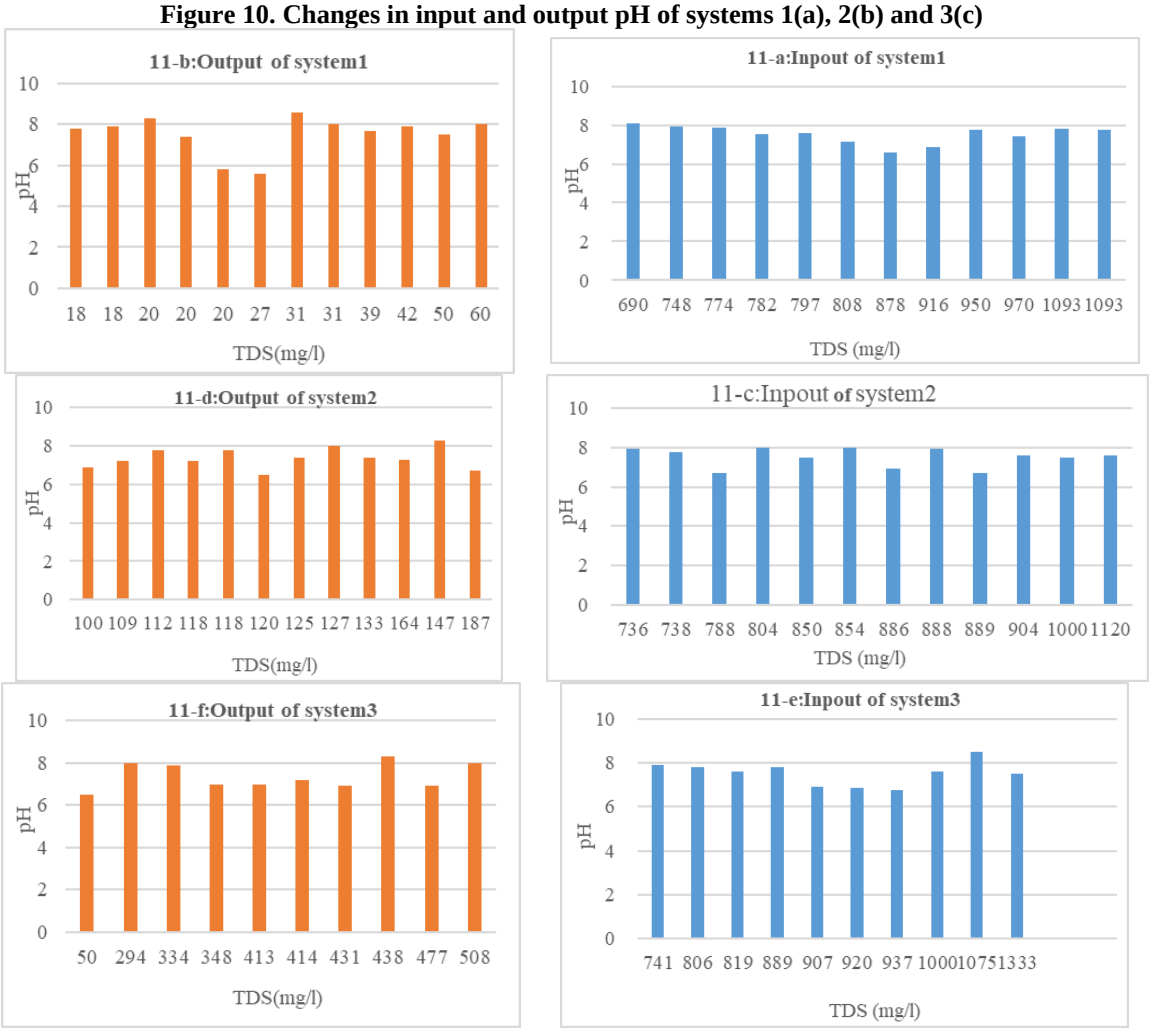


Figure 11. The impact of TDS on the pH levels of input water in the first (a), second (c), and third (e) systems, as well as the pH levels of output water in the first (b), second (d), and third (f) systems.

4. Conclusion

This study assessed the performance of three household water purifiers over a one-year period in Ahvaz, focusing on variations in effluent quality as a function of time and filter lifespan. The results revealed that the first-stage filters experienced significant clogging approximately one month after installation, with turbidity in the output water exceeding acceptable thresholds by the second month. These findings highlight the need for users to visually inspect and replace the first filter every 1–2 months to maintain water clarity and protect the downstream filters. Regarding the reverse osmosis membranes, the devices showed consistent removal of TDS within the first two years of operation. However, by the third year, TDS concentrations in the effluent increased notably, nearing the maximum acceptable limits. This gradual rise indicates a decline in membrane performance over time and underscores the importance of replacing the membrane after two years of continuous use to maintain water quality and system efficiency. Interestingly, after membrane replacement, output TDS dropped below 50 mg/L in one system, causing the pH to fall below the acceptable limit of 6.5. This observation demonstrates a potential for water acidification when the mineral content is excessively reduced. It suggests that maintaining a balance between adequate contaminant removal and essential mineral retention is critical. Monitoring and, if needed, adjusting the pH after membrane replacement—through mixing valves or remineralization filters—are important practices for ensuring the long-term safety of treated water. Also, Microbial analysis showed the consistent absence of total coliforms in all effluent samples throughout the year, indicating the effective performance of the RO membranes in removing microbial contaminants under regular maintenance conditions. While these findings provide valuable insights into the operational lifespan and quality outcomes of household water purifiers, further research is recommended to build upon and enhance these results:

-Future studies should include a larger number of devices across a broader demographic and geographic range to improve the statistical power of the findings and their generalizability.

-Testing a variety of brands and models will help assess the variability in system design and performance.

-Detailed evaluations of the second and third filters—typically granular and block activated carbon—are needed to better understand their efficiency in removing chlorine, organic matter, and undesirable taste or odor.

-In-depth investigations of the fifth (post-carbon) and sixth (mineral) filters will also be essential to assess their specific contributions to taste improvement, remineralization, and pH stabilization.

Such comprehensive research will contribute to more informed recommendations for users and manufacturers, ensuring that household water purification systems deliver safe, palatable, and mineral-balanced water over time.

Acknowledgements

This research was supported by the Water and Wastewater Company of Ahvaz and the Faculty of Civil Engineering and Architecture at Shahid Chamran University of Ahvaz. The authors gratefully acknowledge their valuable support and contributions throughout the course of this study.

Declarations

The authors declare that they have no competing interests.

References

1. Wang, Y.-N. and R. Wang, Reverse osmosis membrane separation technology, in Membrane separation principles and applications. 2019, Elsevier. p. 1-45.
2. Pooi, C.K. and H.Y. Ng, Review of low-cost point-of-use water treatment systems for developing communities. npj Clean Water, 2018. 1(1): p. 11.
3. Mulhern, R., et al., User experience of point-of-use water treatment for private wells in North Carolina: Implications for outreach and well stewardship. Science of the Total Environment, 2022. 806: p. 150448.
4. Fiebelkorn, A.P., et al., Systematic review of behavior change research on point-of-use water treatment interventions in countries categorized as low-to medium-development on the human development index. Social Science & Medicine, 2012. 75(4): p. 622-633.
5. Mirsalari, S.T., et al., Evaluation of effluent quality changes of household water purifiers: A case study of Ahvaz city. 2024.
6. Morris, R.W., et al., Hard drinking water does not protect against cardiovascular disease: new evidence from the British Regional Heart Study. European Journal of Preventive Cardiology, 2008. 15(2): p. 185-189.
7. Malakootian, M., et al., Performance evaluation of household water treatment systems used in Kerman for removal of cations and anions from drinking water. Applied Water Science, 2017. 7: p. 4437-4447.
8. Coulliette, A.D., et al., Risk reduction assessment of waterborne Salmonella and Vibrio by a chlorine contact disinfectant point-of-use device. International Journal of Hygiene and Environmental Health, 2013. 216(3): p. 355-361.
9. Aydin, R., Evaluation of household water treatment systems in terms of physicochemical and microbiological parameters, Adana Province (Turkey) example. Desalination and Water Treatment, 2019. 149: p. 209-227.
10. Gholami-Borujeni, F., et al., Heterotrophic Bacteria Count Index in Drinking Water and Possibility of Biofilm Formation in Household Drinking Water Treatment Devices in Sari, Iran. Journal of Mazandaran University of Medical Sciences (In Persian), 2021. 30(192): p. 118-125.
11. Talepour, N., et al., Isolation, identification and reviewing the health effect of HPC bacteria in household point-of-use (PoU) water treatment devices: a case study, Ahvaz, Iran. Journal of Environmental Health Science and Engineering, 2021. 19: p. 59-69.
12. Lin, W., et al., Analysis of microbial contamination of household water purifiers. Applied Microbiology and Biotechnology, 2020. 104: p. 4533-4545.
13. Labhasetwar, P.K. and A. Yadav, Membrane based point-of-use drinking water treatment systems. 2023: IWA Publishing.
14. Al-Jayyousi, O.R. and M.S. Mohsen, Evaluation of small home-use reverse osmosis units in Jordan. Desalination, 2001. 139(1-3): p. 237-247.
15. Hoslett, J., et al., Surface water filtration using granular media and membranes: A review. Science of the Total Environment, 2018. 639: p. 1268-1282.
16. Wu, J., et al., A critical review of point-of-use drinking water treatment in the United States. NPJ Clean Water, 2021. 4(1): p. 40.
17. Michel, M.M., et al., Mineral materials coated with and consisting of MnOx—characteristics and application of filter media for groundwater treatment: a review. Materials, 2020. 13(10): p. 2232.
18. Rice, E.W., et al., Standard methods for the examination of water and wastewater. 2012.
19. Warsinger, D.M., et al., A review of polymeric membranes and processes for potable water reuse. Progress in polymer science, 2018. 81: p. 209-237.
20. Bellona, C., et al., Factors affecting the rejection of organic solutes during NF/RO treatment—a literature review. Water research, 2004. 38(12): p. 2795-2809.
21. Rosborg, I. and F. Kozisek, Drinking water minerals and mineral balance. Springer International Pu, 2016. 1(1): p. 175.
22. Cotruvo, J.A., 2017 WHO guidelines for drinking water quality: first addendum to the fourth edition. Journal-American Water Works Association, 2017. 109(7): p. 44-51.

23. Sadigh, A., et al., Investigating the efficiency of home water treatment systems to reduce or eliminate water quality parameters in the city of Ardabil in 1392. J Health (In Persian), 2015. 6(4): p. 458-69.
24. Bonnélye, V., et al., Curacao, Netherlands Antilles: A successful example of boron removal on a seawater desalination plant. Desalination, 2007. 205(1-3): p. 200-205.
25. Dindarloo, K., et al., Drinking water quality: comparative study of tap water, drinking bottled water and point of use (PoU) treated water in Bandar-e-Abbas, Iran. Desalination and water treatment, 2016. 57(10): p. 4487-4493.
26. Team, W., Guidelines for Drinking water Quality, ed. t. edition. 2017.
27. Rezaeinia, S., et al., Qualitative and health-related evaluation of point-of-use water treatment equipment performance in three cities of Iran. Journal of Environmental Health Science and Engineering, 2018. 16: p. 265-275.
28. Saini, R.D., Health risks from long term consumption of reverse osmosis water. International journal of applied chemistry, 2017. 13(2): p. 293-301.
29. Yari A R, S.M., Hadadian L, Babakhani M H, Physical, Chemical and Microbial Quality of Treated Water in Qom s Desalination Plants. Qom University of Medical Sciences Journal (In Persian), 2016. 1(1): p. 45-54.
30. Miranzadeh, M.B. and D.K. Rabbani, Chemical quality evaluation for the inlet and outlet water taken from of the desalination plants utilized in Kashan during 2008. Feyz Medical Sciences Journal (In Persian), 2010. 14(2): p. 120-125.
31. Jafaripour, M., et al., Health, sanitary and economic evaluation of Home-like systems of water treatment (Reverse Osmosis, RO) in Qom city. Journal of Water and Wastewater; Ab va Fazilab (in persian), 2011. 22(2): p. 15-21.
32. babaei A, g.z.F., normoradi H, ahmadi angali K, moslemnia M, salimi J, Investigation on the Microbial Quality of Water Treatment centers in Abadan City. Journal of Ilam University of Medical Sciences (In Persian), 2014. 22(4): p. 132-140.
33. Tavangar A, N.N., Alizade H, Tavakoli Ghochani H, Ghorbanpour R, Evaluation of water treatment systems' performance available in Bojnurd ciry during 2013. North Khorasan University of Medical Sciences (In Persian), 2013. 5(5): p. 1107-1119.
34. Naghipour, D., et al., Data on microbial and physiochemical characteristics of inlet and outlet water from household water treatment devices in Rasht, Iran. Data in brief, 2017. 16: p. 1005.
35. Zhang, Z., et al., Evaluating the efficacy of point-of-use water treatment systems using the water quality index in rural southwest China. Water, 2020. 12(3): p. 867.
36. Deghani M, N.H., Hashemi , H, Azimi A A, Doleh M, Vafaee R, An evaluation of physical, chemical and biological quality of influent and effluent water obtained by reverse osmosis and multistage flash processes for drinking consumption. Research in Medicine, 2013. 36(5): p. 36-42.
37. Ebrahimi, S.M., et al., Bacteriological quality of water produced by household water treatment devices. Journal of Mazandaran University of Medical Sciences (In Persian), 2015. 25(130): p. 8-18.

© 2026 by the authors. Licensee SCU, Ahvaz, Iran. This article is an open access article distributed under the terms and conditions of the Creative Commons Attribution 4.0 International (CC BY 4.0 license) (http://creativecommons.org/licenses/by/4.0/).

Efficiency Improvement of Piano Key Weirs Using Numerical Simulation

Behnam Taheri [1], Ehsan Fadaei-Kermani [*,1] , Mahnaz Ghaeini-Hessaroeyeh [1]

1. Department of Civil Engineering, Faculty of Engineering, Shahid Bahonar University of Kerman, Kerman, Iran.

***Corresponding Author:**
Ehsan Fadaei-Kermani,

Email: e.fadaei@uk.ac.ir
Received: 2025.03.01
Accepted: 2025.07.01
J. Hydraul. Struct., 12(1):84-99
DOI: 10.22055/jhs.2025.49154.1342

ABSTRACT

Water management and conveyance have been crucial aspects throughout the development of human civilization. One of the significant methods of water storage is the construction of dams. Dams require spillways to pass excess water safely. Piano key weirs, as a type of non-linear spillway with specific geometry, have a higher discharge capacity and have thus attracted researchers' attention. The use of piano key weirs is proposed as an alternative solution to improve dam performance. In this research, the performance of piano key weirs was studied using numerical simulations in the Flow 3D software. After evaluating the accuracy of the numerical model results with the experimental results and ensuring the high accuracy of the numerical model, the development and optimization of the numerical model to enhance the spillway's performance in passing flow begins. Based on earlier research, a notable drawback of these spillways is the decrease in the discharge coefficient as the upstream volume flow rate increases, which causes an increase in flow head before the spillway. Therefore, in this research, geometric modifications to the spillway model, including sloping the sidewalls of the spillway by 5, 7, 10 and 12 degrees, were examined. The numerical modeling results indicated an 11% to 15% increase in the discharge capacity of the piano key weir with 5-degree sloped walls, an 8% to 19% increase in the discharge capacity with 7-degree sloped walls, and a 7% to 11% increase in the discharge capacity with 10-degree sloped walls compared to the simple spillway at various upstream volume flow rates. However, in the model constructed with a wall slope of 12 degrees, no increase in the discharge coefficient was observed, and the flow head upstream of the spillway increased.

KEYWORDS

Dam, Piano key weir, Numerical modeling, Discharge coefficient, Flow 3D software.

1. Introduction

Climate change and torrential rainfall worldwide have prompted the International Commission on Large Dams (ICOLD) to issue a statement calling for a review and reassessment of the performance of existing dam spillways. Actions should be taken to rebuild, expand, or strengthen these spillways if needed. According to studies and assessments conducted by the (ICOLD), about 30% of the world's dams face insufficient spillway capacity during floods, which poses a significant and dangerous threat [1]. The mismatch between spillway discharge capacity and incoming floodwaters reduces the spillway's efficiency. As a result, this elevates the burden on the dam. Continuing this cycle can lead to severe problems, including the failure and collapse of dams, causing irreparable damages and costs.

Therefore, given the importance and critical role of spillways, these structures must be robust, reliable, and highly efficient, ensuring they are always at the highest level of readiness to manage excess water and floods. Today, the most advanced type of non-linear spillway is the piano key weir (PKW) 2]. One of the main advantages of piano key weirs is their reduced construction space requirement and smaller dimensions [3]. This results in a reduction in the amount of concrete used and finally reduces costs [4]; in addition, Toulis (2013), in comparing piano key weirs with ogee spillways, has highlighted the economic advantages and lower maintenance costs of piano key weirs. Another significant advantage of piano key weirs is their ability to manage higher flow rates than other spillway types, which can significantly contribute to the dam's safety [5]. The results and analysis by Blancher et al. (2011) demonstrated that the flow capacity of this spillway is at least four times greater than that of a linear spillway (5). Additionally, the unique geometry of piano-key weirs allows them to be installed on the crests of many existing dams, making them one of the most suitable options for upgrading existing spillways 6]. However, optimizing the performance of piano key weirs remains a crucial issue. Researchers have been concentrating on enhancing the discharge coefficient as upstream flow rates increase and minimizing the flow head before the weir. Ribeiro et al. (2009) investigated the impact of parapet walls on the hydraulic efficiency of piano key weirs. These researchers augmented the height of the weir without extending the length of the slopes and obtained that a 12.30% increase in weir height leads to a 15% improvement in its hydraulic efficiency [7]. Anderson (2011), by examining various geometries of piano key weirs and comparing them, concluded that the discharge coefficient of the weir increases as the ratio of the inlet to outlet cycle increases 8]. Machiels et al. (2012) investigated the flow rate through piano key weirs. They concluded that, considering a constant total head on the piano key weir, increasing the slope of the inlet key with the presence of a perimeter wall (parapet wall) results in better performance compared to increasing the slope of the inlet key without the perimeter wall on the weir [9]. Anderson and Tullis (2013), in their study on piano key weirs, discovered that the weir's discharge capacity increases as the ratio of the inlet key width to the outlet key width increases [10]. Falvey (2003) introduced Equation (1), which was previously used for calculating the pass discharge through sharp-crested weirs, as a formula for determining the discharge through piano key weirs [11].

$$Q = C_d \frac{2}{3} L H^{\frac{3}{2}} \sqrt{2g} \quad (1)$$

where Q is the discharge through the weir, Cd represents the weir discharge coefficient, L is the width of the weir, g is the acceleration due to gravity, and H is the flow height over the weir crest. Bremmer and Ortel (2017) demonstrated through numerical simulations that the thickness of the walls of piano key weirs affects the flow discharge coefficient [12]. Al-Baghdadi and Khasaf (2018) examined the impact of varying the crest length of piano key weirs on their discharge capacity. They observed that increasing the crest length significantly affects the discharge capacity of this weir model [13]. Bekheet et al. (2022), through experimental modeling and analysis of the hydraulic behavior of trapezoidal, rectangular, and triangular piano key weirs, concluded that the trapezoidal weir exhibited better hydraulic performance compared to the other shapes, while the triangular weir had the weakest performance. In another part of their study, they used numerical modeling to study the effect of the inlet-to-outlet critical width ratio. Their findings indicated that increasing the inlet-to-outlet critical width ratio to 1.25 resulted in up to a 15% increase in the discharge coefficient [14]. In

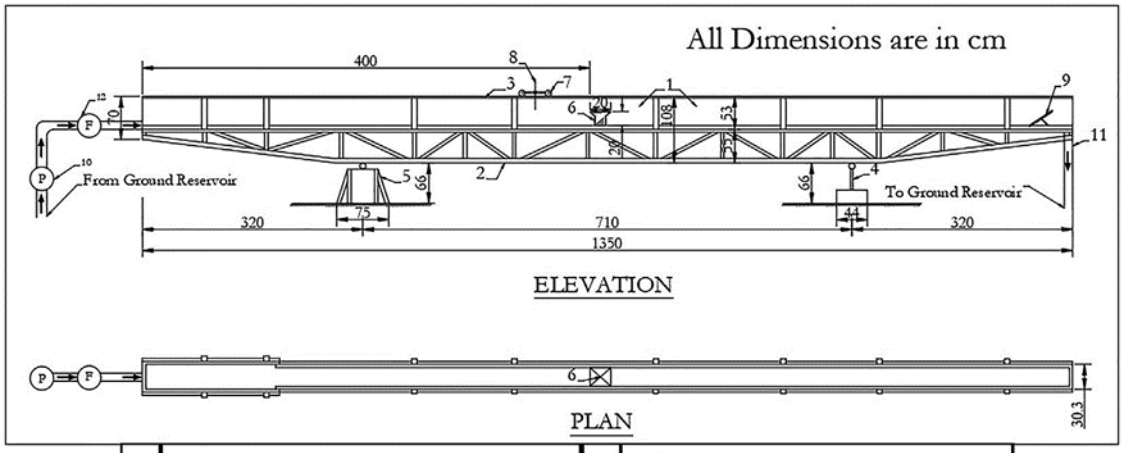
a study by Eltarabily et al. (2025), for different types of piano key weirs, the hydraulic parameters, including water surface profile, flow regimes, and nappes interference, were numerically investigated for different flow rates. The results agreed well, in addition, an empirical equation was proposed for energy dispersion rate prediction in the case of different discharges [15]. Yang et al. (2023) employed numerical simulations to show that geometric modifications can significantly improve PKW discharge efficiency and capacity. These modifications applied the cross-section of each key as a downward semicircle. [16]. Selim et al. (2024) compared PKWs with trapezoidal labyrinth weirs and found that PKWs provide better energy dissipation and discharge performance under free flow conditions [17]. Alizadeh et al. (2023) conducted laboratory tests on A-type triangular PKWs, confirming good discharge capacity and highlighting the potential for further geometric optimization. In their study, the stage–discharge relationship, discharge coefficient, and flow regime were examined [18].

A study by Jin et al. (2025) found that a novel composite Piano Key Weir, featuring both trapezoidal and rectangular sections, dramatically boosts discharge capacity. Numerical tests demonstrated an improvement of up to 16% over conventional trapezoidal designs [19].

Based on earlier research, a notable drawback of these spillways is the decrease in the discharge coefficient as the upstream volume flow rate increases, which causes an increase in flow head before the spillway. However, the present study aims to enhance the discharge efficiency of piano key weirs through geometric modification, specifically by investigating the effects of inclined sidewalls using a numerical approach. To achieve this, the study begins with a comprehensive review of previous research to gather relevant information and select a reliable experimental model for validation. Numerical simulations based on computational fluid dynamics (CFD) are then conducted to model the flow behavior over piano key weirs, with a focus on simulating the spillway geometry and applying the governing flow equations under specified initial and boundary conditions. The numerical model is calibrated and validated using laboratory data to ensure its accuracy. The main novelties of this research include the integration of previous design principles to propose a refined weir geometry and the use of geometric modifications, such as inclined sidewalls, to improve the weir's performance. By enhancing the discharge coefficient and flow capacity, this study provides reasonable insights into improving piano key weir design for greater hydraulic efficiency and better performance under varying flow conditions.

2. Methodology

At first, an appropriate experimental model for developing the numerical model was selected. This case utilizes the experimental model developed by Bekheet et al. (2022) [14]. The experimental setup consisted of an inclined laboratory flume measuring 13.5 meters in length, 0.30 meters in width, and 0.50 meters in depth. The sidewalls were constructed from 10 mm-thick glass panels, reinforced with vertical supporting frames spaced at 1.50-meter intervals. The flume's bed was fabricated from continuous steel sheets spanning its full length. A comprehensive illustration of the flume's structural configuration, including detailed dimensions and design features, is provided in Fig. 1.



1	Flume side walls	7	Rolling carriage
2	Supporting steel truss	8	Point gauge
3	Two rails for the needle gauge	9	Tailgate
4	Tilting support	10	Pump
5	The other support	11	Outlet Pipe
6	PKW position	12	Flowmeter

Figure 1. Layout, details, and dimensions of the flume [14]

In the present research, the rectangular piano key weir model is considered to be in alignment with the research objectives. Fig. 2 shows the rectangular piano key weir experimental model [14]. The geometric specifications of a rectangular weir are provided in Fig. 3. Moreover, Table 1 represents the dimensions of the rectangular piano key weir model considered in this study.

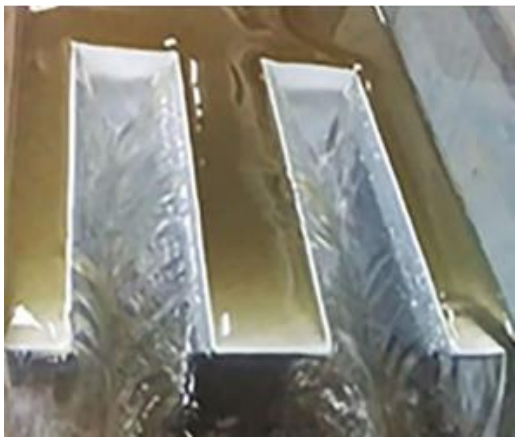


Figure 2. Rectangular PKW model in laboratory [14]

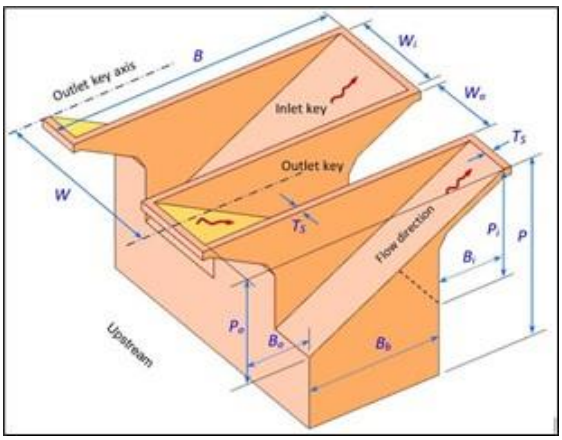


Figure 3. Geometric specifications of PKW [16]

Table 1. The dimensions of the PKW model used in the experimental study (cm) [14].

PKW model's shape	W	L	P	W_i	W_o	B_i=B_o	B	T_s
Rectangular	30.3	151.5	20	6.5	8.25	7.575	30.3	0.2

Subsequently, numerical modeling of the flow over the rectangular piano key weir was performed using Flow-3D software, a powerful tool for numerical simulation and computational fluid dynamics (CFD) [20]. One crucial aspect of numerical modeling is the time required to achieve stable conditions. This study employed a simulation duration of 15 seconds for all models under different conditions and characteristics. After this period, the piano key weir model's flow conditions were stabilized, and the flow characteristics remained consistent. Additionally, the physical conditions for modeling the flow over the piano key weir include a gravitational acceleration of 9.81 m/s2, and the fluid is considered Newtonian. The standard k–ε turbulence model was employed to simulate turbulent flow behavior. A variable time-step size was used in the simulations, automatically adjusted to ensure the Courant number remained within an acceptable range throughout the simulation. In the end, the time-step size was stabilized at 0.15 seconds. Pressure–velocity coupling was handled using the PISO (Pressure Implicit with Splitting of Operators) algorithm, which is an iterative method used to solve the Navier Stokes equations in the numerical modeling. The PISO algorithm improves the stability and accuracy of the solution by performing multiple correction steps for pressure and velocity fields within each time step. At the beginning of the modeling process, a mesh with 400,000 cells specifically for the weir geometry and a 0.01-meter grid size for the weir channel was created (Fig. 6). The optimal mesh dimensions will be determined as the simulation progresses. The PKW geometry was designed using AutoCAD software and exported in the stereolithographic (STL) format. The STL file was then directly imported into Flow-3D for further analysis. Fig. 4 shows the rectangular piano key weir model created in Flow-3D.

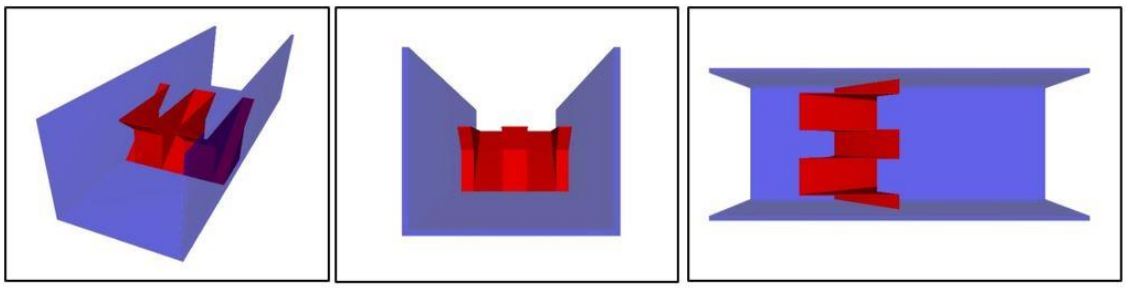


Figure 4. The PKW numerical model created in Flow 3D

3. Results and Discussion

In order to validate the numerical model, a flume replicating the experimental setup used in the laboratory study by Bekheet et al. (2022) was modeled in Flow-3D. The rectangular piano-key weir geometry was constructed based on the exact specifications of the physical experimental model. Boundary conditions matching the experimental setup were applied to the numerical model, including an inlet with a flow rate of 38.89 m^3/h and a flow surface height of 0.225 meters. The flow surface height over the weir crest was then analyzed and quantitatively compared with the experimental results. Figure 1 represents the boundary conditions applied to the numerical model, and the mesh system is shown in Error! Reference source not found.. The boundary conditions have been applied as wall (W), symmetry (S), inlet flow discharge (Q), and outflow (O) to the model.

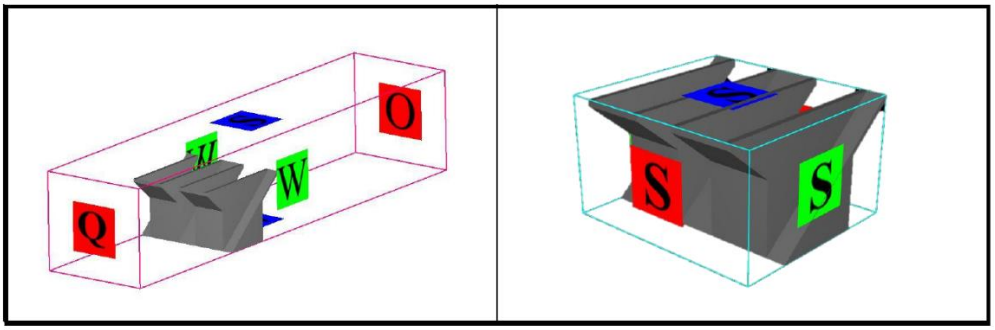


Figure 1. The boundary conditions applied to the numerical model.

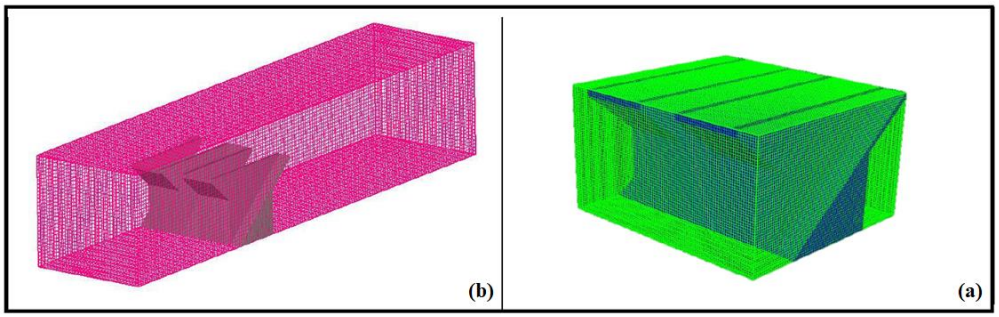


Figure 6. The mesh system applied to the model: (a) weir geometry, (b) the channel.

The model was run in three stages with different mesh sizes including 0.5 cm, 1.0 cm, and 1.5 cm.

Table 1 to Table 3 show the comparison of the results from the experimental model and the numerical modeling. In these Tables, (X_o) represents the distance from the beginning of the weir, (X) denotes the distance from the start of the channel, (B) is the side width of the weir, and (Y) indicates the flow head. Error represents the calculated absolute relative error between the numerical results and the experimental data.

Table 1. Comparison of the experimental data and the numerical results (Mesh size = 0.5 cm)

Mesh 0.5cm	X_o(m)	X(m)	X/B	Y_o(m)	Y(m)	Y/P	Error
Numerical Result	0	0.37425	0	0.02531	0.22531	0.12657	0.14%
Experimental Data			0	0.025	0.225	0.125	
Numerical Result	0.0606	0.43485	0.2	0.02113	0.22113	0.10563	0.30%
Experimental Data			0.2	0.0218	0.2218	0.109	
Numerical Result	0.1212	0.49545	0.4	0.02183	0.22183	0.10915	0.08%
Experimental Data			0.4	0.022	0.222	0.11	
Numerical Result	0.1818	0.55605	0.6	0.02139	0.22139	0.10694	0.28%
Experimental Data			0.6	0.022	0.222	0.11	
Numerical Result	0.2424	0.61665	0.8	0.02157	0.22157	0.10783	0.11%
Experimental Data			0.8	0.0218	0.2218	0.109	
Numerical Result	0.303	0.67725	1	0.01791	0.21791	0.08955	0.42%
Experimental Data			1	0.017	0.217	0.085	

Table 2. Comparison of the experimental data and the numerical results (Mesh size = 1 cm)

Mesh 1cm	X_o(m)	X(m)	X/B	Y_o(m)	Y(m)	Y/P	Error
Numerical Result	0	0.37425	0	0.02742	0.22742	0.13710	1.08%
Experimental Data			0	0.025	0.225	0.125	
Numerical Result	0.0606	0.43485	0.2	0.02372	0.22372	0.11860	0.87%
Experimental Data			0.2	0.0218	0.2218	0.109	
Numerical Result	0.1212	0.49545	0.4	0.02373	0.22373	0.11863	0.78%
Experimental Data			0.4	0.022	0.222	0.11	
Numerical Result	0.1818	0.55605	0.6	0.02341	0.22341	0.11703	0.63%
Experimental Data			0.6	0.022	0.222	0.11	
Numerical Result	0.2424	0.61665	0.8	0.02204	0.22204	0.11020	0.11%
Experimental Data			0.8	0.0218	0.2218	0.109	
Numerical Result	0.303	0.67725	1	0.02068	0.22068	0.10338	1.69%
Experimental Data			1	0.017	0.217	0.085	

Table 3. Comparison of the experimental data and the numerical results (Mesh size = 1.5 cm)

Mesh 1.5 cm	X_o(m)	X(m)	X/B	Y_o(m)	Y(m)	Y/P	Error
Numerical Result	0	0.37425	0	0.04391	0.243912	0.21956	8.41%
Experimental Data			0	0.025	0.225	0.125	
Numerical Result	0.0606	0.43485	0.2	0.02558	0.225584	0.127921	1.71%
Experimental Data			0.2	0.0218	0.2218	0.109	
Numerical Result	0.1212	0.49545	0.4	0.00686	0.206862	0.034308	6.82%
Experimental Data			0.4	0.022	0.222	0.11	
Numerical Result	0.1818	0.55605	0.6	0.00912	0.209122	0.045611	5.80%
Experimental Data			0.6	0.022	0.222	0.11	
Numerical Result	0.2424	0.61665	0.8	0.0086	0.208604	0.043022	5.95%
Experimental Data			0.8	0.0218	0.2218	0.109	
Numerical Result	0.303	0.67725	1	1E-06	0.200001	5E-06	7.83%
Experimental Data			1	0.017	0.217	0.085	

The model with a 0.5 cm mesh size, the small dimensions of cells, and their exact alignment with the weir model's meshing led to highly accurate numerical results compared to the experimental model. As a result, the error between the two models was at most 0.42%. However, this fine mesh size considerably increased the computation time, extending it to 36 hours, which is a notable drawback.

The numerical results for the 1.0 cm mesh model showed acceptable accuracy relative to the experimental data, with a maximum error of 1.69% between the two. Additionally, this mesh size significantly reduced computational time compared to the 0.5 cm mesh model.

The larger cell dimensions and mesh size in the model with a 1.5 cm mesh size resulted in a relatively higher error rate between the numerical and experimental models. Based on the review and evaluation

of the results from the numerical models and considering the primary objectives of the modeling, the model with a 1.0 cm mesh size was selected as the reference model, and subsequent calculations were performed with this mesh size.

Unlike numerous previous studies that validated their numerical models at only a single point on the weir crest, this study conducted validation at six locations along the crest. Using a 5 mm mesh, the maximum error was only 0.42%, indicating good precision. Even with a 10 mm mesh, the error remained low at 1.69%. In contrast, the reference study (Bekheet et al. 2022) used for validation reported a 6.77% error at the upstream point of the weir under similar conditions. The present model, at the same location and with a 10 mm mesh, achieved a much lower error of 1.69%, demonstrating the reasonable accuracy of the current numerical approach.

3.1. Evaluation of the reference model at various upstream flow rates

This study aims to improve the hydraulic efficiency of the piano key weir, particularly by increasing the discharge coefficient. Therefore, the performance of the reference weir model was evaluated at various upstream flow rates. The initial upstream flow rate of 38.89 cubic meters per hour, used for model validation, was incrementally increased by 25% and then 40%, leading to new flow rates of 48.612 and 54.446 cubic meters per hour, respectively. Fig. 7 presents a general overview of the analyzed models and their corresponding names.

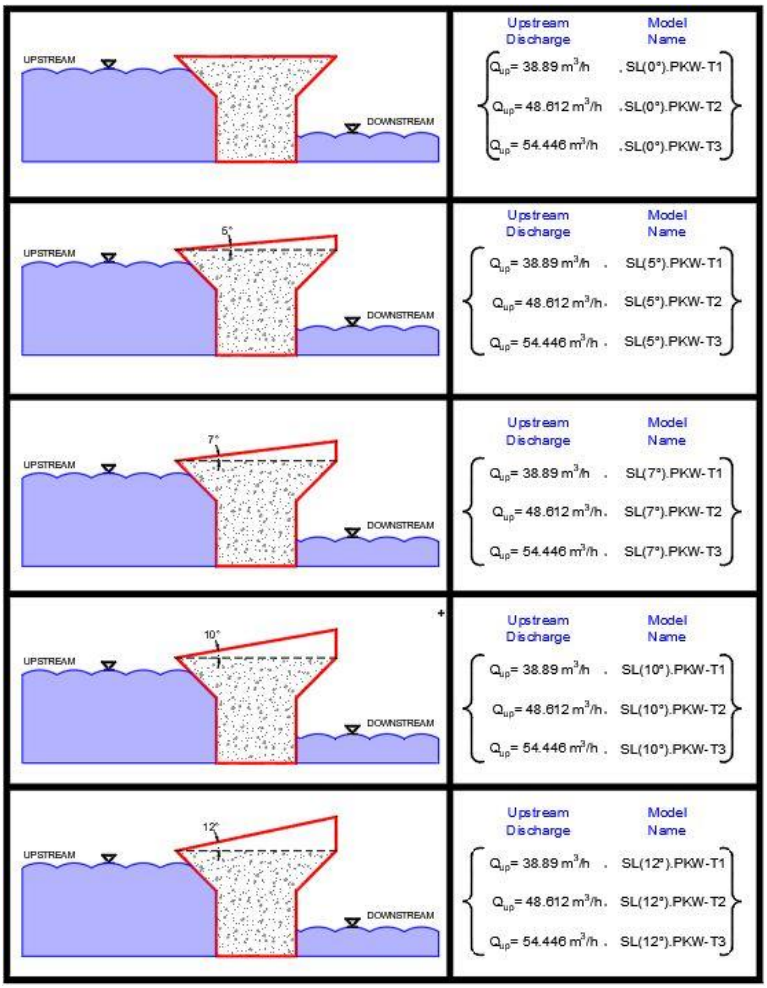


Figure 7. General overview of the analyzed models and their corresponding names.

Table 4 details the numerical results, which outline the models' performance with increasing upstream flow rate to the weir. Figure 2 shows each model's discharge coefficient plotted against H/P. Additionally two charts showing flow discharge through the weir and free surface profile have been presented in Figure 3 and Figure 4 to further illustrate and substantiate the analysis.

Table 4. Comparison of the data from the analysis of the three PKW models at different flow rates

Model name	(H/P)	Weir height (P)	Flow head on weir (H)	Discharge (Q)	Discharge coefficient (C_d)
(SL(0°).PKW-T1)	0.137875	0.2 m	0.027575 m	0.0095 m^3/s	2.1091
(SL(0°).PKW-T2)	0.153825	0.2 m	0.030765 m	0.012090 m^3/s	2.2649
(SL(0°).PKW-T3)	0.167255	0.2 m	0.033451 m	0.01372 m^3/s	2.2664

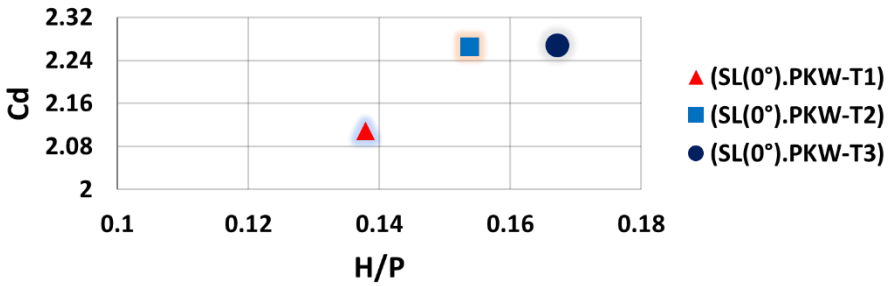


Figure 2. Discharge coefficient plotted against H/P for each of the three models

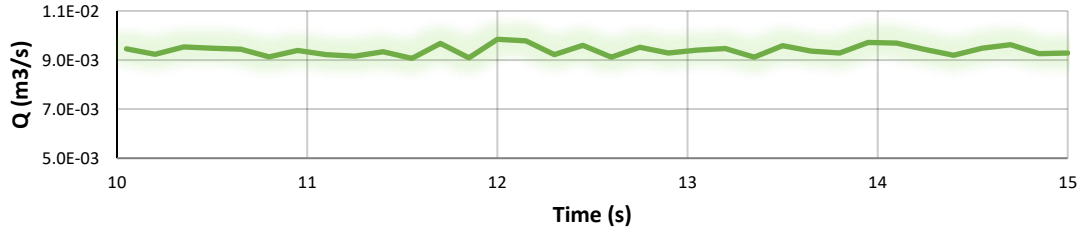


Figure 3. Flow discharge through the weir - (SL(0°).PKW-T1)

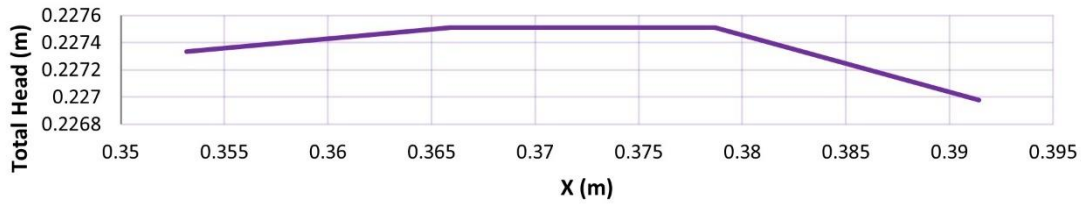


Figure 4. Free surface profile (head) of the flow upstream of the weir - (SL(0°).PKW-T1)

Based on the results and the chart presented in Table 5 and Fig. 8, it is observed that with increasing upstream flow rate, the discharge coefficient in the model (SL(0°).PKW-T2) has increased compared to the model (SL(0°).PKW-T1), and the flow head before the weir has also risen. In the model (SL(0°).PKW-T3), despite the increase in upstream flow rate to the weir and the rise in upstream flow head, the discharge coefficient has not changed compared to the model (SL(0°).PKW-T2). This indicates that with higher flow rates, this particular geometry and model of the weir cannot pass more flow, and the flow head before the weir will continue to increase.

The results indicate that the simple piano

key weir with flat walls experiences reduced discharge efficiency as the upstream flow rate increases and leading to a rise in the flow head before the weir. To enhance the performance of these weirs under high flow conditions, the design of a modified weir with wall slopes of 5, 7, 10 and 12 degrees relative to the horizontal was evaluated and analyzed.

3.2. Evaluation of the performance of the PKW with a 5-degree wall slope at various upstream flow rates

Table 6 presents the numerical results, illustrating the models' performance under increasing upstream flow rates at the weir. Fig. 11 shows each model's discharge coefficient plotted against H/P. Additionally two charts showing flow discharge through the weir and free surface profile have been presented in Fig. 12 and Fig. 13 to further illustrate and substantiate the analysis.

Table 5. Comparison of the data from the analysis of the three PKW models at different flow rates.

Model name	(H/P)	Weir height (P)	Flow head on weir (H)	Discharge (Q)	Discharge coefficient (C_d)
(SL(5°).PKW-T1)	0.08224	0.2128 m	0.0175 m	0.01098 m^3/s	4.7942
(SL(5°).PKW-T2)	0.06824	0.2128 m	0.014521 m	0.01342 m^3/s	7.7532
(SL(5°).PKW-T3)	0.066114	0.2128 m	0.014069 m	0.01537 m^3/s	9.3126

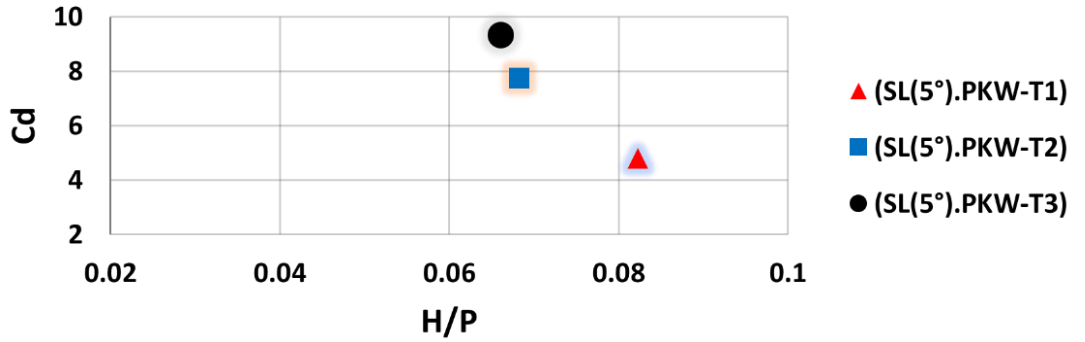


Figure 5. Discharge coefficient plotted against H/P for each of the three models

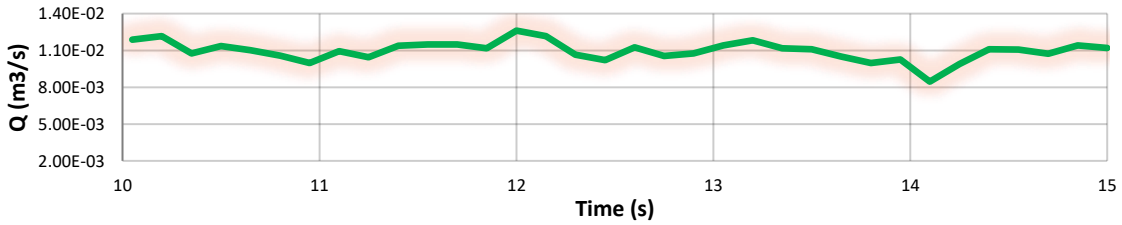


Figure 6. Flow discharge through the weir - (SL(5°).PKW-T1)

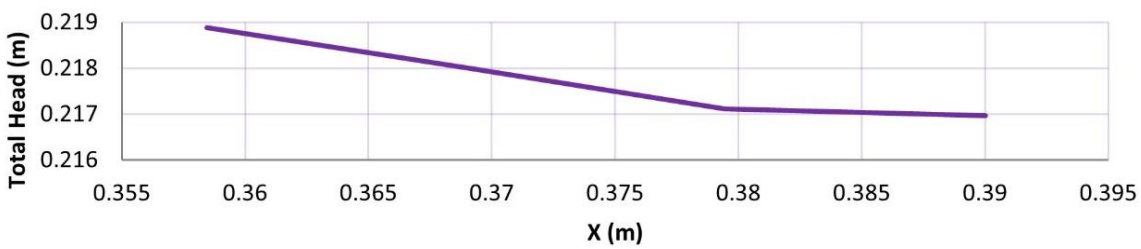


Figure 7. Free surface profile (head) of the flow upstream of the weir - (SL(5°).PKW-T1)

The results and data indicate that the weir with a 5-degree wall slope allows a significantly higher flow rate passed as the upstream inflow increases. The weir's discharge coefficient rises in line with the increasing volume of incoming flow. Additionally, the flow head before the weir decreases as the discharge coefficient improves.

3.3. Evaluation of the performance of the PKW with a 7-degree wall slope at various upstream flow rates

Table 6 presents the numerical results, illustrating the models' performance under increasing upstream flow rates at the weir. Figure 8 shows each model's discharge coefficient plotted against H/P. Additionally two charts showing flow discharge through the weir and free surface profile have been presented in Figure 9 and Figure 10 to further illustrate and substantiate the analysis.

Table 6. Comparison of the data from the analysis of the three PKW models at different flow rates.

Model name	(H/P)	Weir height (P)	Flow head on weir (H)	Discharge (Q)	Discharge coefficient (C_d)
(SL(7°).PKW-T1)	0.09541	0.218 m	0.0208 m	0.01033 m^3/s	3.4802
(SL(7°).PKW-T2)	0.09334	0.218 m	0.02035 m	0.01366 m^3/s	4.7581
(SL(7°).PKW-T3)	0.08738	0.218 m	0.01905 m	0.01626 m^3/s	6.2507

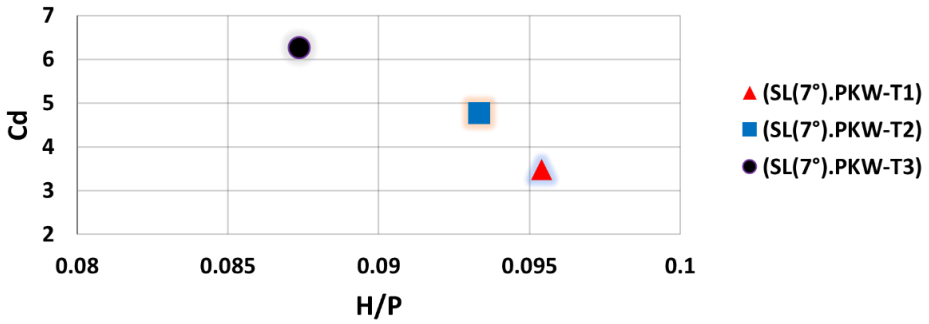


Figure 8. Discharge coefficient plotted against H/P for each of the three models

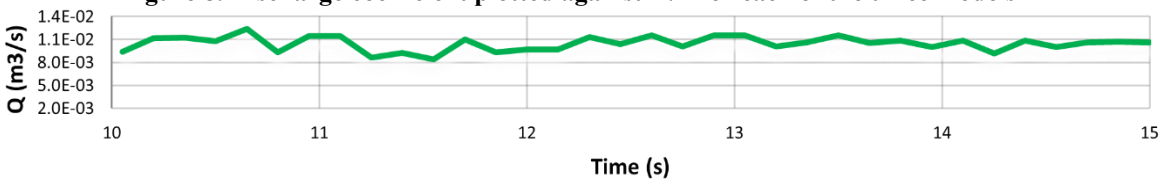


Figure 9. Flow discharge through the weir - (SL(7°).PKW-T1)

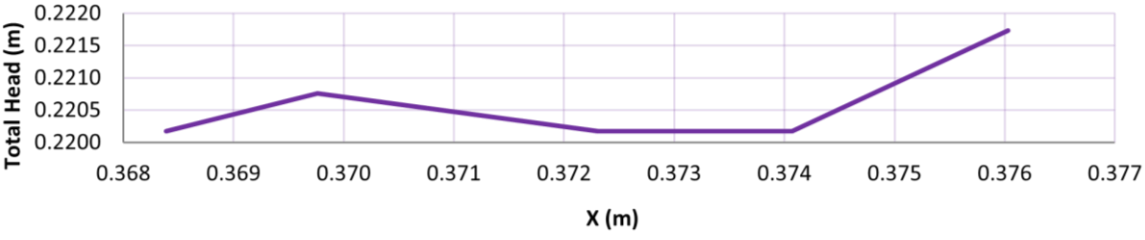


Figure 10. Free surface profile (head) of the flow upstream of the weir - (SL(7°).PKW-T1)

The results and data indicate that the weir with a 7-degree wall slope allows a significantly higher flow rate passed as the upstream inflow increases. The weir's discharge coefficient rises in line with the increasing volume of incoming flow. Additionally, the flow head before the weir decreases as the discharge coefficient improves.

3.4. Evaluation of the performance of the PKW with a 10-degree wall slope at various upstream flow rates

Table 7 presents the numerical results, illustrating the models' performance under increasing upstream flow rates at the weir. Figure 11 shows each model's discharge coefficient plotted against H/P. Additionally two charts showing flow discharge through the weir and free surface profile have been presented in Figure 12 and Figure 13 to further illustrate and substantiate the analysis.

Table 7. Comparison of the data from the analysis of the three PKW models at different flow rates.

Model name	(H/P)	Weir height (P)	Flow head on weir (H)	Discharge (Q)	Discharge coefficient (C_d)
(SL(10°).PKW-T1)	0.136816	0.2264 m	0.031 m	0.01051 m^3/s	1.94451
(SL(10°).PKW-T2)	0.14687	0.2264 m	0.0333 m	0.01297 m^3/s	2.15799
(SL(10°).PKW-T3)	0.059932	0.2264 m	0.01359 m	0.01522 m^3/s	9.71876

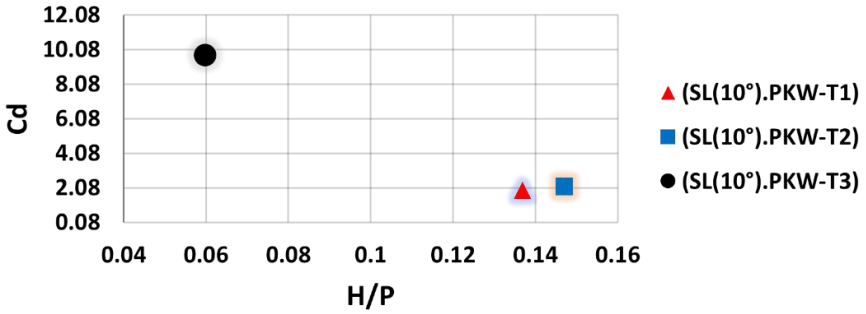


Figure 11. Discharge coefficient plotted against H/P for each of the three models

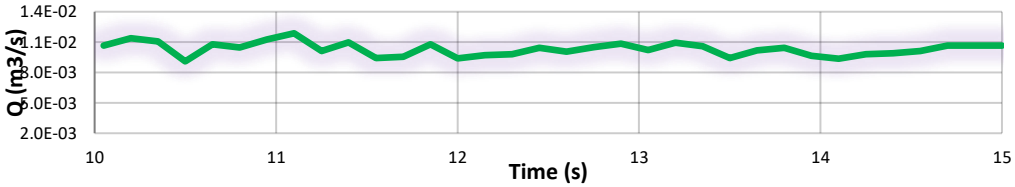


Figure 12. Flow discharge through the weir - (SL(10°).PKW-T1)

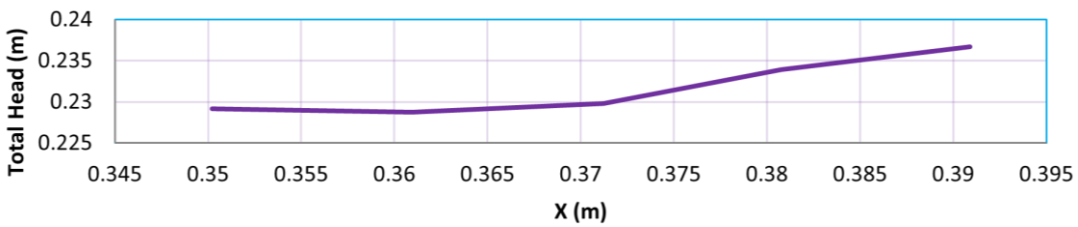


Figure 13. Free surface profile (head) of the flow upstream of the weir - (SL(10°).PKW-T1)

In the piano key weir with a 10-degree wall slope, the results show that while increasing the upstream flow rate from 38.89 to 48.612 cubic meters per hour (25% increase). This only leads to an 11% rise in the discharge coefficient. However, a 40% increase in inflow causes a significant improvement in the discharge coefficient as the weir begins to discharge the flow effectively. This results in a noticeable reduction in the flow head before the weir.

3.5. Evaluation of the performance of the PKW with a 12-degree wall slope at various upstream flow rates

Table 8 presents the numerical results, illustrating the models' performance under increasing upstream flow rates at the weir. Figure 14 shows each model's discharge coefficient plotted against H/P. Additionally two charts showing flow discharge through the weir and free surface profile have been presented in Figure 15 and Figure 16 to further illustrate and substantiate the analysis.

Table 8. Comparison of the data from the analysis of the three PKW models at different flow rates.

Model name	(H/P)	Weir height (P)	Flow head on weir (H)	Discharge (Q)	Discharge coefficient (C_d)
(SL(12°).PKW-T1)	0.0954	0.2311 m	0.043 m	0.01043 m^3/s	1.181
(SL(12°).PKW-T2)	0.2076	0.2311 m	0.048 m	0.01319 m^3/s	1.2683
(SL(12°).PKW-T3)	0.2228	0.2311 m	0.0515 m	0.01469 m^3/s	1.271

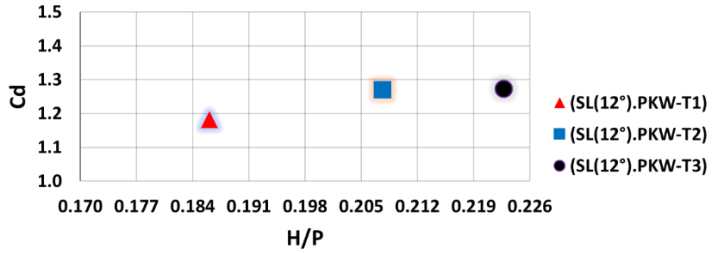


Figure 14. Discharge coefficient plotted against H/P for each of the three models

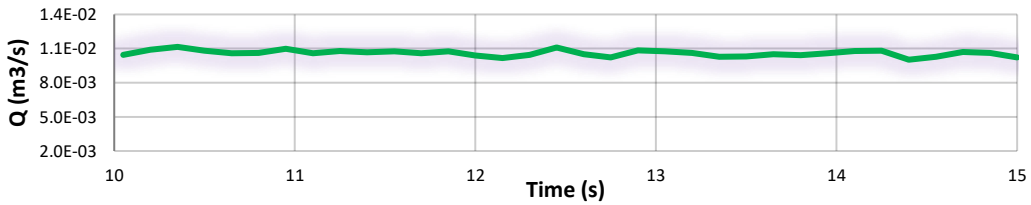


Figure 15. Flow discharge through the weir - (SL(12°).PKW-T1)

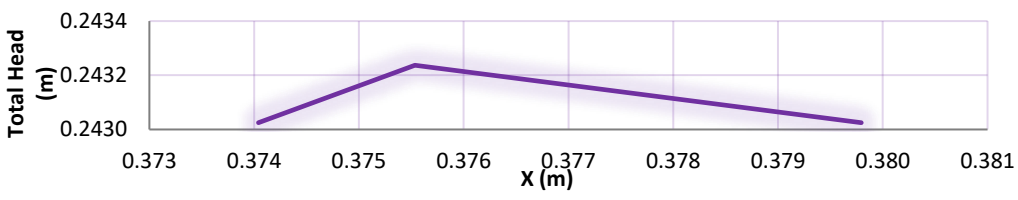


Figure 16. Free surface profile (head) of the flow upstream of the weir - (SL(12°).PKW-T1)

In the piano key weir with a 12-degree wall slope, as indicated by the results, there is no significant increase in the discharge coefficient as the upstream flow rate to the weir increases from 38.89 to 48.612 cubic meters per hour. Additionally, as the upstream flow rate to the weir increases, this geometry is unable to pass the additional flow, leading to an increase in the upstream head of the flow before the weir.
Finally, the results of the discharge coefficients from the numerical simulations for all models were presented in Figure 17 and
Table 9. According to the presented results, the improved models, including weirs with sloping sidewalls, demonstrated a significant increase in discharge rate compared to simple piano key weirs with flat sidewalls. Furthermore, the modified geometries exhibited a marked improvement in the discharge coefficient.

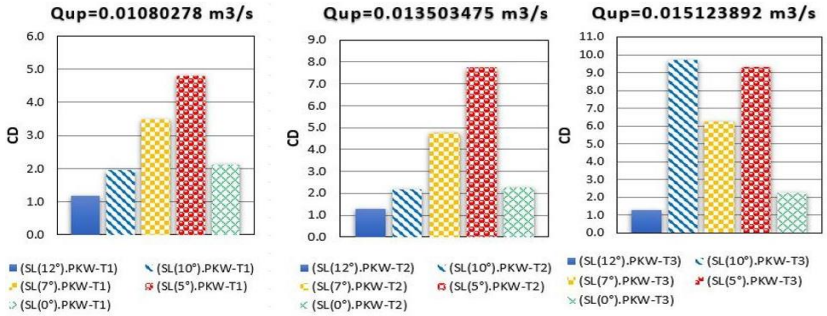


Figure 17. Comparison of the discharge coefficients of the analyzed models.

Table 9. Comparison of the increase in flow discharge rate across the analyzed weirs.

Upstream Volume of Flow Rate = 38.89 m3/hr					
Model Name	**Flow Discharge Through Weir**	**Increase in Flow Discharge Rate**	**Model Name**	**Flow Discharge Through Weir**	**Increase in Flow Discharge Rate**
(SL(0°).PKW-T1)	34.39	15%	(SL(0°).PKW-T1)	34.39	10%
(SL(5°).PKW-T1)	39.52		(SL(10°).PKW-T1)	37.826	
(SL(0°).PKW-T1)	34.39	8%	(SL(0°).PKW-T1)	34.39	9%
(SL(7°).PKW-T1)	37.18		(SL(12°).PKW-T1)	37.534	
Upstream Volume of Flow Rate = 48.612 m3/hr					
Model Name	**Flow Discharge Through Weir**	**Increase in Flow Discharge Rate**	**Model Name**	**Flow Discharge Through Weir**	**Increase in Flow Discharge Rate**
(SL(0°).PKW-T2)	43.525	11%	(SL(0°).PKW-T2)	43.525	7%
(SL(5°).PKW-T2)	48.315		(SL(10°).PKW-T2)	46.693	
(SL(0°).PKW-T2)	43.525	13%	(SL(0°).PKW-T2)	43.525	9%
(SL(7°).PKW-T2)	49.2		(SL(12°).PKW-T2)	47.5	
Upstream Volume of Flow Rate = 54.446 m3/hr					
Model Name	**Flow Discharge Through Weir**	**Increase in Flow Discharge Rate**	**Model Name**	**Flow Discharge Through Weir**	**Increase in Flow Discharge Rate**
(SL(0°).PKW-T3)	49.38	12%	(SL(0°).PKW-T3)	49.38	11%
(SL(5°).PKW-T3)	55.343		(SL(10°).PKW-T3)	54.812	
(SL(0°).PKW-T3)	49.38	19%	(SL(0°).PKW-T3)	49.38	7%
(SL(7°).PKW-T3)	58.53		(SL(12°).PKW-T3)	52.9	

4. Conclusion

The present study investigates the effects of sidewall slope variation on the discharge capacity of Piano Key Weirs (PKWs) through numerical modeling. The numerical simulation results demonstrated acceptable accuracy of the model compared to experimental data. The baseline PKW configuration, with a 0° sidewall slope, was analyzed in three stages under different flow rates to determine its discharge capacity. Subsequently, the weir's discharge performance was compared to the baseline model after modifying the sidewall slope to 5°, 7°, 10°, and 12°.

In the simple piano key weir with a 0-degree wall slope, it was observed that increasing the upstream flow rate decreases its discharge efficiency and leads to a rise in the flow head before the weir. To enhance the performance of the piano key weir, this study simulated and analyzed four different weir geometries with wall slopes of 5, 7, 10 and 12 degrees relative to the horizontal. By comparing the discharge coefficients of these models at identical upstream flow rates, a significant increase in the discharge coefficient was observed for the weirs with sloped walls.

As demonstrated by the numerical model results, the simple piano key weir exhibits a decrease in flow discharge performance as the upstream flow rate increases, leading to a rise in flow head before the weir and a corresponding reduction in the discharge coefficient. However, a significant increase in the discharge coefficient and flow rate can be achieved by sloping the weir's sidewalls. This improvement is due to the increased effective crest length and the stepwise discharge mechanism created by the sloped walls. This geometric modification can also be easily applied to existing simple piano key weirs.

Statements and Declarations:

Author Contributions

All authors contributed to the study conception and design. Material preparation, data collection and analysis were performed by all authors. The first draft of the manuscript was written by the first author (Behnam Taheri), and all authors commented on previous versions of the manuscript (Ehsan Fadaei-Kermani, Mahnaz Ghaeini-Hessaroeyeh). The final revisions have been applied by Ehsan Fadaei-Kermani and Mahnaz Ghaeini-Hessaroeyeh. Moreover, all authors have read and approved the final manuscript.

Funding

The authors declare that no funds, grants, or other support were received during the preparation of this manuscript.

Data Availability

The paper models and data can be available from the corresponding author upon request.

Competing Interests

The authors have no relevant financial or non-financial interests to disclose.

Conflict of Interest

There are no conflicts of interest related to this work.

Consent for Publication

The authors declare their consent to publication of the manuscript by the "journal of Hydraulic Structures".

Consent to Participate

The authors give their consent to take part in this project.

References

1. Rajabzadeh V, Hekmatzadeh AA, Shourijeh PT, Haghighi AT. Introducing a probabilistic framework to measure dam overtopping risk for dams benefiting from dual spillways. Reliability Engineering & System Safety. 2023 Mar 1;231:109030.
2. Ehsanifar A, Ghodsian M. Experimental and Numerical study of piano key weir with upstream nose and semicircular section at the outlet. Journal of Hydraulics. 2020 Jul

22;15(2):31-45.
3. Leite Ribeiro M, Bieri M, Boillat JL, Schleiss A, Delorme F, Laugier F. Hydraulic capacity improvement of existing spillways–design of a piano key weirs. InProceedings (on CD) of the 23rd Congress of the Int. Commission on Large Dams CIGB-ICOLD 2009 (Vol. 2, pp. 100-118).
4. Rezaei Ahvanooei A, Mousavi SF, Karami H. Improvement of hydraulic performance of nonlinear piano-key weirs in plan. Modares Civil Engineering journal. 2019 Nov 10;19(4):71-82.
5. Paxson G, Tullis B, Hertel D. Comparison of Piano Key Weirs with labyrinth and gated spillways: Hydraulics, cost, constructability and operations. InProceedings of the Second International Workshop on Labyrinth and Piano Key Weirs II 2013 Oct 21 (pp. 123-130).
6. Blancher B, Montarros F, Laugier F. Hydraulic comparison between Piano Key Weirs and labyrinth spillways. InProc. Int. Conf. Labyrinth and Piano Key Weirs Liège B 2011 May 10 (pp. 141-150).
7. Leite Ribeiro M, Bieri M, Boillat JL, Schleiss A, Delorme F, Laugier F. Hydraulic capacity improvement of existing spillways–design of a piano key weirs. InProceedings (on CD) of the 23rd Congress of the Int. Commission on Large Dams CIGB-ICOLD 2009 (Vol. 2, pp. 100-118).
8. Anderson RM. Piano key weir head discharge relationships. Utah State University; 2011.
9. Machiels O, Erpicum S, Archambeau P, Dewals B, Pirotton M. On the Piano Key Weir hydraulics. In2nd IAHR Europe Conference 2012.
10. Anderson RM, Tullis BP. Piano key weir hydraulics and labyrinth weir comparison. Journal of Irrigation and Drainage Engineering. 2013 Mar 1;139(3):246-53.
11. Falvey HT. Hydraulic design of labyrinth weirs. Reston, VA: ASCE Press (American Society of Civil Engineers); 2003 Jan.
12. Bremer FL, Oertel M. Numerical investigation of wall thickness influence on Piano Key Weir discharge coefficients: A preliminary study. InLabyrinth and Piano Key Weirs III 2017 Apr 11 (pp. 101-108). CRC Press.
13. Al-Baghdadi MB, Khassaf SI. Evaluation of crest length effect on piano key weir discharge coefficient. International Journal of Energy and Environment. 2018 Sep 1;9(5):473-80.
14. Bekheet AA, AboulAtta NM, Saad NY, El-Molla DA. Effect of the shape and type of piano key weirs on the flow efficiency. Ain Shams Engineering Journal. 2022 May 1;13(3):101620.
15. Eltarabily MG, Kamal Hamed A, Elkiki M, Selim T. Hydraulic assessment of different types of piano key weirs. ISH Journal of Hydraulic Engineering. 2025 Jan 1;31(1):8-31.
16. Yang J, Li S, Helgesson A, Skepparkrans E, Ansell A. Geometric modification of piano key weirs to enhance hydraulic performance and discharge capacity. Water. 2023 Jan;15(23):4148.
17. Selim T, Hamed AK, Elkiki M, Eltarabily MG. Numerical investigation of flow characteristics and energy dissipation over piano key and trapezoidal labyrinth weirs under free-flow conditions. Modeling Earth Systems and Environment. 2024 Feb;10(1):1253-72.
18. Alizadeh Sanami F, Ghaderi A, Alizadeh Sanami F, Mirkhorli P, Di Francesco S. Laboratory study of the hydraulic performance of the A-type triangular piano key weir. Water. 2023 Jun 2;15(11):2124.
19. Jin S, Shen X, Oertel M. Discharge Efficiency of an Innovative Composite Piano Key Weir. Water. 2025 Mar 21;17(7):921.
20. Fadaei-Kermani E, Barani GA. Numerical simulation of flow over spillway based on the CFD method. Scientia Iranica. Transaction A, Civil Engineering. 2014 Feb 1;21(1):91.



© 2025 by the authors. Licensee SCU, Ahvaz, Iran. This article is an open access article distributed under the terms and conditions of the Creative Commons Attribution 4.0 International (CC BY 4.0 license) (http://creativecommons.org/licenses/by/4.0/).

Journal of Hydraulic Structures

Volume 12 – Issue 1 – January 2026

Contents:

01 Investigation of discharge coefficient and energy dissipation in free-flowing Quarter-Circular Gates

Abbas Parsaie; AmirHamzeh Haghiabi

09 A Hybrid AHP-AI Framework for Assessing and Mitigating Tunneling Impacts on Confined Spring Discharge

Saeed Samiei; Ali Aalianvari

20 River Behavior and Morphological Analysis of a Meandering Channel in the Ganga River System, India

Kuldeep Pareta; Upasana Pareta

50 Effect of bed roughness shape on mitigating scour the downstream of parallel sluice gates

Iman Akbari; Mohammad Hemmati; Sung-Uk Choi; Yousef Ramezani; Babak Mahmoudi

69 Variation in Effluent Quality of Household Water Treatment Systems Over Time: A Case Study in Ahvaz

Hossein Sasani; Seyedeh Tooba Mirsalari; Mohammad Azizipour; Neematollah jaafarzadeh

84 Efficiency Improvement of Piano Key Weirs Using Numerical Simulation

Behnam Taheri; Ehsan Fadaei-Kermani; Mahnaz Ghaeini-Hessaroeyeh

Shahid Chamran University of Ahvaz